THREE-DIMENSIONAL MODELLING OF IMPULSE FORCES AND TORQUES ON A GAS TURBINE BLADE DUE TO NOZZLE EXCITATIONS

SUNIL AGARWAL

THREE-DIMENSIONAL MODELLING OF IMPULSE FORCES AND TORQUES ON A GAS TURBINE BLADE DUE TO NOZZLE EXCITATIONS

By

© Sunil Agarwal (B. E.)

A thesis submitted to the School of Graduate Studies

in partial fulfilment of the

requirements for the degree of

Master of Engineering

Faculty of Engineering and Applied Sciences

Memorial University of Newfoundland

October 1995

St. John's Newfoundland Canada

ISBN 0-612-13877-1

ABSTRACT

The efficiency of turbines depends to a large extent on the forces developed on rotor blades. The blades, while they pass by nozzles, are subjected to gas forces. It is quite important to understand the development of these forces to do any useful turbomachine work. The understanding of these forces and torques would also be quite helpful in designing the bearing supports.

The rotor as well as the nozzle system can be defined in an inertial frame at any instant of time. In this frame, the fluid-flow through the nozzles can be described as a vector in three dimensions. Similarly, the position and the velocity of any point on the rotor blade can also be specified at any instant of time. Using transformation matrices, one can calculate the change in momentum of gases as they impinge on the blade surfaces and get reflected. The resulting forces, then, can be expressed in the inertial frame, and one can calculate the three-dimensional forces and torques.

The thesis brings forth an analytical model to calculate the impulse forces, and the resulting torques on the rotating blade due to nozzle excitations. The results obtained by the present method are compared with those used by conventional method to establish the validity of the model and the underlying principle. The modelling principle is quite general in nature and can be used for various rotating machines.

ACKNOWLEDGEMENTS

With sincere appreciation and gratitude I would like to thank Dr. Anand M. Sharan for his direction and support during this research work. His encouragement to apply new ideas for engineering applications, and excellent supervision has been major inspiration for the present work. Working with him has been a great professional experience.

I would also like to extend my thanks to the school of Graduate Studies and the Faculty of Engineering and Applied Sciences for their financial support through this period. I sincerely thank Dr. J. Malpas, Dean of Graduate Studies, Dr. R. Seshadri, Dean of Faculty of Engineering and Applied Sciences, Dr. J. Sharp, Associate Dean of Engineering for their support during my graduate work. I would like to thank the staff at the Centre for Computer Aided Engineering for their support and timely advice at various stages of the work.

I enjoyed working in Faculty of Engineering at MUN. The camaraderie of my fellow grad-students, the enthusiasm of the faculty has made the work quite pleasant and enjoyable. Finally, my acknowledgement is due to everyone who, directly or indirectly, has been inspiring me during this work.

October 1995 *Sunil Agarwal*

TABLE OF CONTENTS

CHAPTER 3

VERIFICATION AND ANALYSES OF THE MODEL

LIST OF FIGURES

LIST OF TABLES

NOMENCLATURE

^{A}P	position vector of point A
$\{S_{k,l}\}$	blade finite surface vector drawn from node l to k
$\{\hat{n}\}$	vector normal to the blade finite element surface
$\{V_1\}$	absolute velocity vector at nozzle exit point
α_0	flow angle at nozzle exit point
α_1	flow angle at the blade entrance (at the leading edge) in the conventional model
α_2	flow angle at the blade exit (at the trailing edge) in the conventional model
β_1	blade angle at the leading edge in the conventional model
β_2	blade angle at the trailing edge in the conventional model
c	blade chord
{U}	tangential velocity of an elemental layer of blade
$\{W_1\}$	incoming relative flow velocity on blade surface
$\{W_2\}$	reflected relative flow velocity from blade surface
ω	instantaneous rotor speed
θ	angular movement of the rotor
d	diameter of the rotor wheel

ε_h	height of the centroid of finite layer of the blade from blade root
γ_i	angle of flow incidence measured from the normal to the finite surface
γ_r	angle of flow reflection measured from the normal to the finite surface
γ	magnitude of the angle of incidence or reflection
θ_R	angle of rotation about local z - axis on finite blade surface
K	velocity loss factor in blade passage
ΔA	absolute area of the finite blade surface
ΔA_n	projected area of the finite blade surface normal to the incoming relative flow
$\Delta \dot{m}_n$	elemental mass flow normal to incoming relative velocity
θ_p	pitch angle of nozzle, and blade
θ_N	nozzle angle
ρ	fluid density
$\{\Delta F\}$	impulse force on a finite surface
$\{F\}$	net resultant impulse force on a blade
x_c, y_c, z_c	geometric centroid of the surface of the blade finite element

X_c, Y_c, Z_c	point of application of the net resultant impulse force on the blade
$\{R_d\}$	position vector of the point of application of net resultant impulse force
$\{T\}$	torque about the rotor centre due net resultant gas forces
α	angular acceleration of the single blade rotor system
${}^{B}(I_{xx})_b$	mass moment of inertia of a single blade in frame B
${}^{G}(I_{xx})_b$	mass moment of inertia of a single blade in global frame
${}^{G}(I_{xx})_d$	mass moment of inertia of the rotor disc in global frame
${}^{G}(I_{xx})$	mass moment of inertia of a single blade and rotor in global frame
G	notation for global frame
B	notation for blade frame
N	notation for nozzle frame
L	notation for local frames
n_b	number of total blades or nozzles

θ_n	nozzle angle
α_o	angle of incidence of gases
α	apparent angle of incidence of gases

Matrices

{ }	column matrix or a vector
$[R_z]$	rotation matrix about z - axis
$[R_x]$	rotation matrix about x - axis
${}^{A}_{B}[R]$	rotation matrix describing the orientation of frame 'B' relative to frame 'A' in three - dimension
${}^{A}_{B}[T]$	transformation matrix describing the orientation, and translation of frame 'B' relative to frame 'A' in three - dimension

Superscripts

s	suction side of the blade
p	pressure side of the blade
ϕ	surface of the blade finite element

CHAPTER 1

INTRODUCTION AND LITERATURE SURVEY

1.1 INTRODUCTION

Gas Turbines are well known for their application in Industry. There have been widely increasing demands for gas turbines in the power sector generation, and the jet propulsion over the past few decades. Fig. 1.1 shows the major components of a gas turbine used in aircrafts. As can be seen from this figure, the air is let in through an air-inlet or a diffuser, it is then compressed and led to combustor where the temperature, and pressure of air is increased. The air-fuel mixture is then injected through the nozzles of the gas turbine chamber onto the turbine blades. The air, as it hits the rotor blade, imparts its kinetic energy to the blades by change of momentum of the directed gases. This produces mechanical power, which is then used to drive the propeller attached to the turbine shaft.

As is evident, the exchange of momentum is quite significant from the point of view of power generation. This exchange of momentum depends on the profile of the rotor blade, and the orientation of the blade surfaces with respect to the interacting gas flow from the nozzle. Hence, it is quite crucial to have a fairly accurate estimate of the flow exchange as the rotor blade passes by the fixed nozzle. Furthermore, the blades experience dynamic loading due to nozzle excitations as they pass by a finite nozzle.

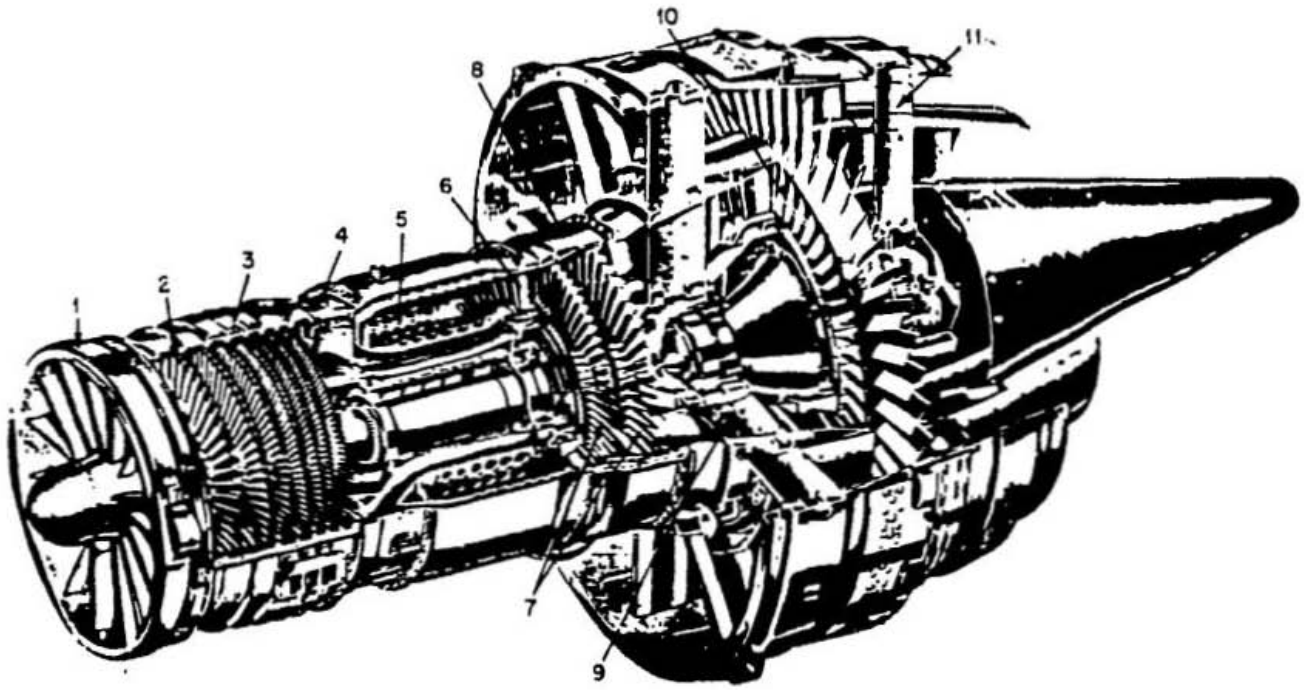

1 FORWARD FRAME
2 EIGHT-STAGE AXIAL-FLOW COMPRESSOR ROTOR
3 COMPRESSOR CASING
4 MAIN FRAME
5 COMBUSTOR
6 TURBINE NOZZLE
7 TWO-STAGE AXIAL-FLOW TURBINE
8 TURBINE CASING
9 FAN FRONT FRAME
10 BUCKETS
11 FAN REAR FRAME

Fig. 1.1 A CUT AWAY VIEW OF THE GENERAL ELECTRIC CF700 GAS TURBINE SHOWING MAJOR COMPONENTS [TREAGER, 1970]

The dynamic loading is exhibited in terms of instantaneous alternating impulsive forces and moments due to the nozzle excitations onto the moving blade. These loads are known to be the major cause of vibration, and the blade failure due to fatigue. Hence it is quite important to understand the nature of these forces in a sufficiently accurate manner to take suitable preventive measures against the blade failure.

1.2 LITERATURE SURVEY

The major source of excitations, in normal operating conditions in turbomachines, arises out of the interaction between the moving blade rows and stationary blade rows. Basic work relating to this field comes from Karman and Sears(1938) who presented an analysis for airfoil theory for non uniform motion by replacing the airfoil by vortex sheet and by assuming the flow to be potential and two-dimensional. Kemp and Sears(1953) applied this theory to calculate unsteady lifts and moments on elementary turbo-machine stage. Osborne(1971) extended the work of Kemp and Sears to the case of compressible flow. Increased attention has been directed towards determining the nature and magnitude of blade dynamic loads in recent years to focus on the larger problem of designing blades to suit the real environment for stress and failures. For example, Rao and Rao (1987) generalized the theory of flow interference between the stator and rotor rows by including both the upwash and downwash effects of a stage with generalized camber blades in subsonic compressible flow.

It is not only difficult to have a definite quantitative assessment of the unsteady forces in a turbomachine blade stage directly but also very expensive, even if a suitable method is devised. Classical hydraulic analogy has been extensively used to study the gas flow in qualitative manner. Loh(1959) has summarized the two-dimensional steady flow equations and one-dimensional non-steady equations of this analogy. Hoyt(1962) has reviewed the hydraulic analogy literature. Rieger(1975) has obtained the two-dimensional non steady analogy equations in generalized coordinates. However, the classical analogy has its own inherent limitations because the analogy is valid for a hypothetical gas of specific heat ratio equal to 2, which no real gas possesses. This is a serious limitation which has to be taken into account before relating the simulated flow results with those obtained from dynamic gas solution. Rao(1980) made extensive studies and established a modified analogy for gases with any specific heat ratio. This analogy was used by Rao et al. (1985) to build a rotating water table to determine the non-steady forces in a turbine stage.

When the blades are thick, thin airfoil theories may become inadequate and numerical techniques involving computational model becomes necessary. Most of the researchers in this area used the conditions that (a) the blade surface is impermeable, (b) the relative velocity over the blade profile is tangential, and they set up a system of equations and obtained steady pressure field using Euler's equation. Yet another approach to study the rotor-stator interaction is to solve the unsteady thin layer Navier-Stokes equations using a system of patched and overlaid grids [Rai(1985); Gundy-Burlet et al(1990)]. They derived the necessary equations for an accurate transfer of information

between the several grids and developed an iterative implicit algorithm. The computational time was, however, enormous in this case, and was seemingly unjustifiable.

The procedure used in design and off-design analysis was based on a quasi-three-dimensional flow model whose origin could be traced back to late forties and early fifties [e.g. Wu(1952); Smith(1966)]. This model required calculations to be executed on two orthogonal surfaces within a blade row passage of a multistage configuration. One of these surfaces was an axi-symmetric surface of revolution whose interaction with a blade row defined a cascade. The flow field relative to this cascade was assumed to be steady in time. McFarland(1982) used panel method of discretizing the blade surface into several panels to investigate the plane cascade flow over the blade foil. Two three-dimensional flow models were proposed for the simulations and analysis of multiple blade row flow. The first [Denton(1979); Adamczyk(1984); Ni(1987)], referred to as the average flow modelled by Adamczyk (1986), simulating the time-averaged flow field within a typical passage of the blade row. The second simulated the unsteady deterministic flow field with the machine. Although a number of simulations have been reported, the computational time, and effort required in all the cases became enormous.

Though, there have been significant developments in computational models and design of turbomachine over the past few decades, the three-dimensional analysis of the forces, and the torque on gas turbine blade is still a cause of concern to engineers. To simulate three-dimensional blade dynamics and the actual flow interaction with the blade, and to develop a significantly appropriate model is still a challenging subject matter. The

survey of literature reveals that the problems of flow interaction from stator rows to the rotor have been addressed by considering streamline flow and laying out the grid patterns. Based on these grid patterns the Navier Stokes equation is solved. As already discussed, the relative flow over the blade foil is considered to be tangent to the blade surface. Moreover, the blade is assumed to be in complete fluid continuum (refer Fig. 1.2). These idealization, however, do not represent the true flow interaction with turbomachine blade.

From Fig. 1.3, the representative arrangement of the nozzles, and the blades (shown cut-out portions) in an axial gas turbine unit can be understood. From the figure, it is evident that during the transient conditions, i.e both at start-up, and shut-down conditions, the blade velocity changes its magnitude and direction with time. Therefore, the incident relative velocity, $\{W_1\}$, which is given by the difference of the absolute flow velocity and the blade velocity (refer to Fig. 1.4), also changes its magnitude and direction with time. Even during steady-state period, while rotor attains a constant angular speed, the direction of the blade velocity always changes in radial plane. This gives rise to a continuously varying relative velocity vector. Hence the angle of attack of the flow with the blade surface continuously changes in both the transient and steady state. Also, in practice, the flow within the blade passage is highly disturbed due to presence of casing and a radial flow arising due to interaction with the blade surface. Thus, the assumptions of smooth streamline flow using ideal boundary conditions of flow being tangent to the blade surface, and complete immersion of the blade in the gas are not achievable in the actual systems.

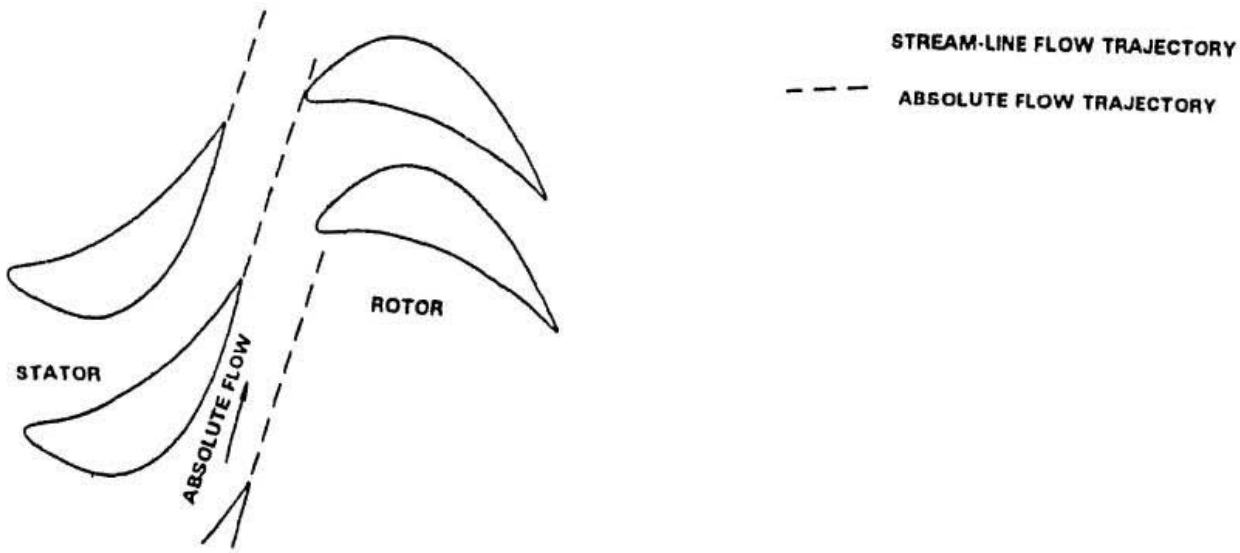

FIG. 1.2 STATOR - ROTOR INTERACTION (FLOW TRAJECTORIES)

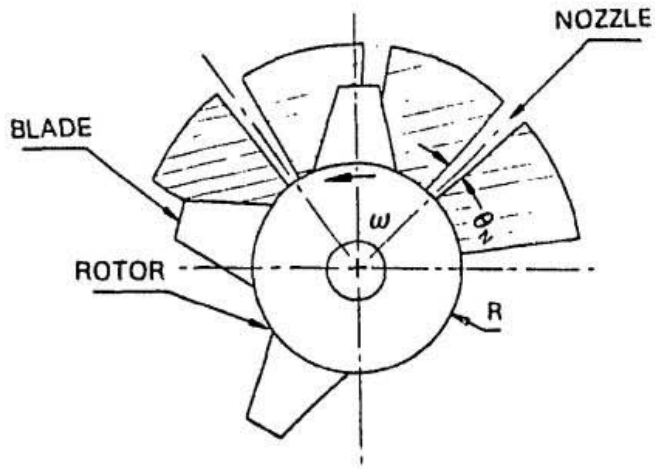

FIG. 1.3 SCHEMATIC OF NOZZLE, BLADE CONFIGURATION

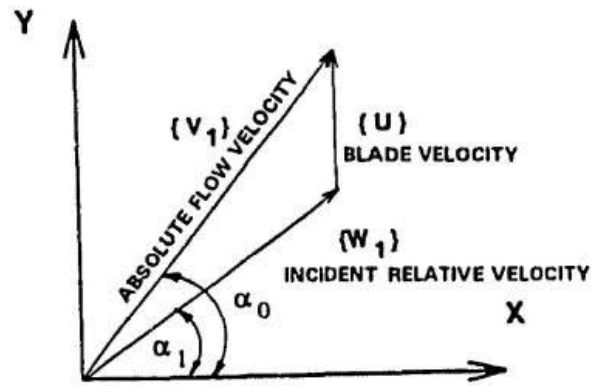

FIG. 1.4 INCIDENT RELATIVE VECLOCITY DIAGRAM

It is worth mentioning here that the fluid dynamics models were mainly adopted from flight models where aircrafts fly into more or less undisturbed fluid continuum. However, in the case of turbomachinery, the flow is highly disturbed by the rotation of the blades. Therefore, the assumptions which were valid for calculations of lift in case of aircrafts are not applicable in turbomachines even if similar blade profiles were assumed. In view of these facts, there is a need of other approaches considering the realistic conditions of flow incidence with the blade surface and the corresponding impulsive forces.

In order to deploy a general model of the gas turbine stage, one needs the basic understanding of the various geometrical as well as the functional aspects of the gas turbines. These can be studied through a number of literature and sources [Kerrebrock(1977); Boyce(1982); Jennings and Rogers(1953); Vincent(1963); Csanady(1964); Dzung(1970); Harman (1981); Rao (1991)].

1.3 OBJECTIVES OF THE THESIS

We have seen in the last few sections that the forces and torques on the turbine blade arising due to instantaneous flow interaction are quite significant from both utility, and life management (fatigue life) point of views. Therefore, a need is felt to develop an analytical model which could be able to present the state of forces without exhaustive computational cost and effort, as in the case in most of the fluid continuum models. Hence, based on the review of the literature, the following objectives were set up:

1. to develop a three-dimensional analytical model to represent the dynamics of a single blade of a gas turbine, and to determine the gas excitation forces, and torques over the blade.
2. to study the force distribution on a single blade due to the variation in the nozzle geometry.
3. to study the difference in the distribution of forces acting on a straight and tapered blade.
4. to study the force distribution on a single blade due to the variation in the absolute velocity of the gases.
5. to study the force variation at different angular positions of the blade.
6. to determine the total forces and torques due to summation of forces on all the blades.

In Chapter 2, an analytical method has been discussed for the impulse analysis of the turbine blade due to nozzle excitations. The stage is modelled considering the blade discretization, and vectorization of each finite element surface. The dynamics of the blade, and the flow have been modelled, and a methodology is developed for calculation of forces, and the torques acting on the three dimensional model. Finally, the equation for angular acceleration has been derived considering the inertia of a single blade-rotor system.

In Chapter 3, the mathematical model developed in the Chapter 2 is compared against a conventional impulse model. The effect of the geometrical, and operating parameters are studied. The results obtained for the nozzle excitations on two different blade types, a straight blade, and a tapered blade are put forth for a comprehensive and comparative studies. A formulation is developed for multi blade-rotor system, and the forces and the torques due to impulse action of the fluid flow are analyzed for the entire system.

Finally, the conclusions and recommendations for future work are presented in Chapter 4.

CHAPTER 2

MODELLING OF THE NOZZLE EXCITATION ON GAS TURBINE BLADE

2.1 INTRODUCTION

Since the very beginning of the development of turbines, the danger of a general failure of rotor blades has remained practically unpredictable with sufficient accuracy. The reason is - very little is known about the excitations on the rotating blade due to gas forces in three-dimensions for the overall range viz. both at design and off-design conditions of operation. Analysis of these excitations on rotating blade is very complicated because the geometry of nozzle and the blade are quite intricate and involved. Moreover, it is extremely difficult to accurately analyze the gas interaction within the blade passage due to relative motion between the stator and rotor. However, understanding such mechanism is quite crucial to the efforts to calculate sufficiently accurate nature of the exciting forces over a range of performance, and to improve the current turbomachinery design.

The present chapter deals with the analytical modelling of the nozzle excitations on the moving blades under transient condition. The modelling approach is suggested for a single stage of a partial-admission, axial-gas turbine. The nozzle and the blade geometry, the gas flow, and the dynamics of the turbine wheel have been defined by using several

inertial frames and the vector algebra. A mathematical formulation has been suggested for the analysis of the impulse force over the whole blade profile as gases impinge on the blade. The modelling also takes care of the three-dimensionality of the gas flow in the blade stage, periodicity of flow admission due to discrete nozzle, and relative motion between the stator and rotor rows.

2.2 MATHEMATICAL FORMULATION

2.2.1 FRAME DESCRIPTION

Fig. 2.1(a) shows an axial gas turbine unit. Blades, B, are mounted on a wheel rotating with the shaft. Nozzles, N, are mounted on an annular disc co-axially placed to the blade wheel. The gases at high temperature and pressure are directed on to the turbine blade, which in turn cause the wheel to rotate. The dynamics of blade and the gas flow can be modelled by considering three basic frames of reference as shown in Fig. 2.1(b).

A global reference frame (stationary) is considered at the rotor axis about which the whole rotor and the blade assembly rotate. The X - axis is defined along the shaft axis. The entities, such as vectors etc., in this frame are referred by G.

A second reference frame has been considered at the centroid of the root of the turbine blade. The orientation of this frame is exactly similar to the global frame. ${}^{G}P_{BORG}$

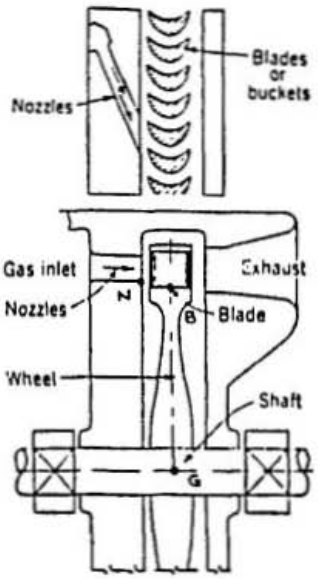

(a)

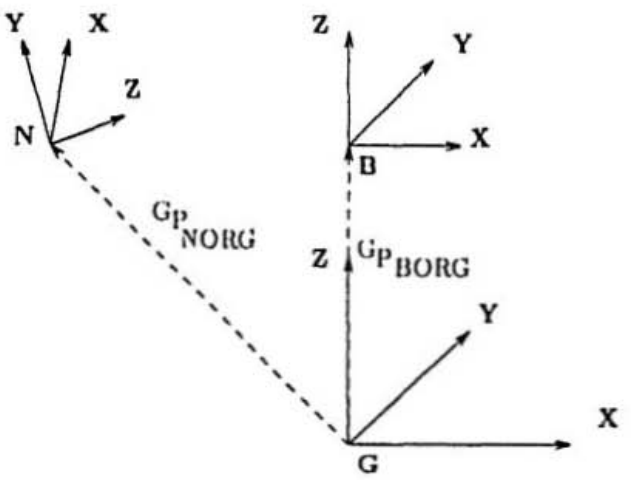

(b)

Fig. 2.1 (a) SCHEMATIC OF AN AXIAL GAS TURBINE STAGE; (b) BASIC FRAMES OF REFERENCE

shows the position vector of this frame relative to the global frame. The geometry of the blade has been represented in this frame. The frame is denoted by B. The third reference frame has been considered at the nozzle exit. The X-Y plane of this frame is perpendicular to the relative velocity of the flow at the nozzle exit. This will be dealt with detail in later section. ${}^{G}P_{NORG}$ shows the position vector of this frame relative to the global frame. The frame is denoted by N. The position vector of the origin of the blade frame is denoted by ${}^{G}P_{NORG}$.

In addition, several local frames of references have been used at the blade surfaces to represent the interaction of the gas with the blade surfaces. These frames will also be discussed in later sections.

In most of the cases, the computations are carried out by transforming vectors into the global frame, G. The transformation of a vector from one frame to another can be achieved by premultiplying the vector by a transformation operator. The transformation operator, [T], is a 4 x 4 homogeneous matrix [Craig, 1989] which takes care of translation as well as the orientation of the frames relative to each other. A general description of the frame transformation is given in the Appendix A.

The quantities to be computed are the forces on the blade elemental surface, their resultant, the driving torque, and the angular acceleration of the rotor at any instant of its angular position.

2.2.2 BLADE MODELLING

2.2.2.1 FINITE ELEMENT DISCRETIZATION OF THE BLADE

To investigate the gas flow interaction and the resulting excitation forces over the entire blade profile, it is convenient to discretize the blade by using finite element technique. Fig. 2.2 shows a representative three-dimensional finite element model of the blade. A total of 35 elements are used to describe the blade with 7 elements across the cross-section and 5 layers along the height [Bahree, 1988]. The elements used are curved, solid, C^0 continuity, serendipity, twenty-noded, isoparametric finite elements. This type of element is chosen because of its versatility in accurately mapping the complex three-dimensional geometry of the turbine blade. Figs. 2.3(a), and 2.3(b) show one such finite element including the local coordinate system (ξ, η, ζ), and the global coordinate system (X, Y, Z).

The following geometric properties were calculated using a finite element software package called ANSYS :

i) Centroid of the area of the finite surfaces (both suction, and pressure side)

ii) Centroid of the volume of each elemental layer across the blade height, and the entire blade

iii) The volume of the blade

iv) The moment of inertia of volume of each elemental layer across the blade height, and the entire blade about the origin of the blade frame, B.

Description of the program prepared in ANSYS is given in Appendix B.

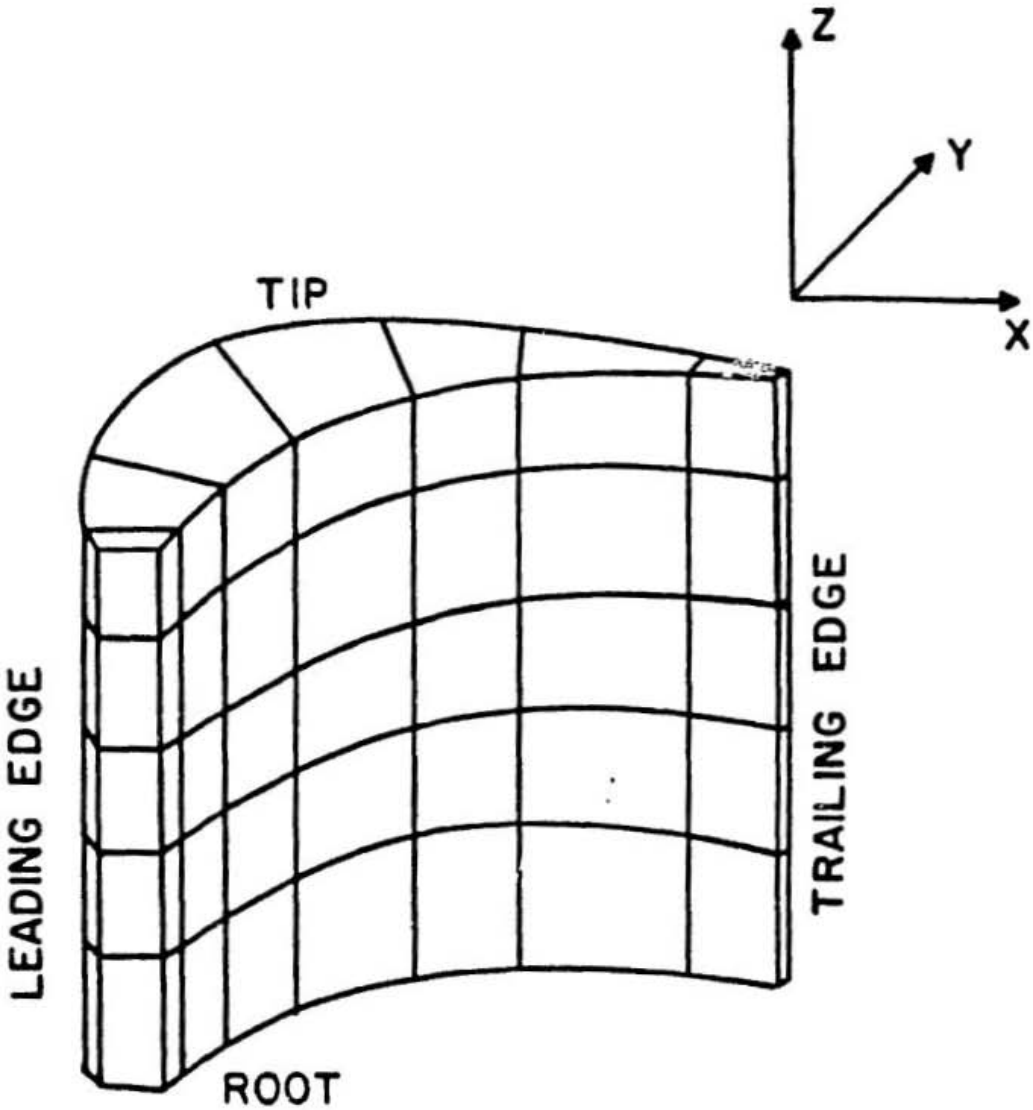

Fig. 2.2 THREE-DIMENSIONAL FINITE ELEMENT MODEL OF A TURBINE BLADE

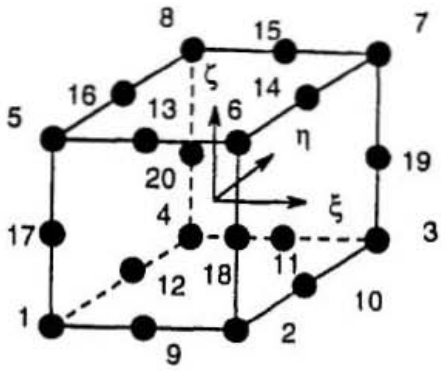

(a)

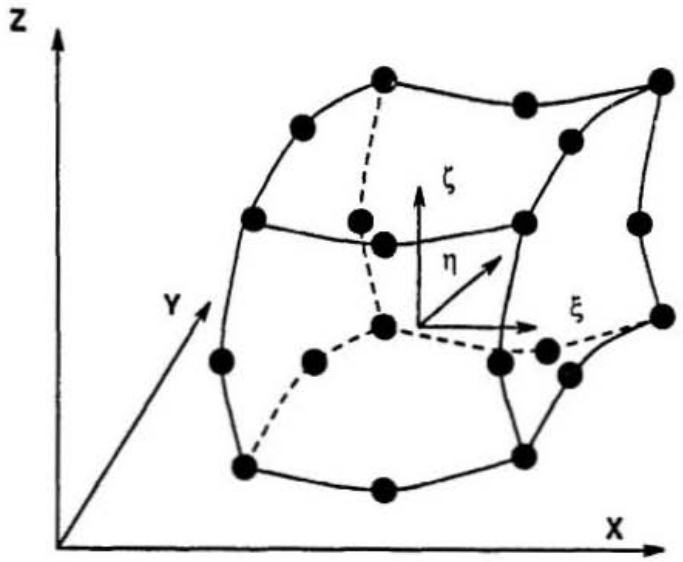

(b)

Fig. 2.3 SOLID ISOPARAMETRIC, SERENDIPITY, C° CONTINUITY, 20-NODED ELEMENT (a) LOCAL COORDINATE SYSTEM ; (b) GLOBAL COORDINATE SYSTEM

2.2.2.2. BLADE KINEMATICS

Fig. 2.4 shows an instantaneous position of the blade represented by angular movement of the turbine shaft, about the global X - axis by an angle θ. The position vector of any point ${}^{B}P$ given by ${}^{B}\{x, y, z\}^{T}$ on the blade surface in the frame 'B' can be given in global frame as follows:

$$ {}^{G}\begin{Bmatrix} x \\ y \\ z \\ 1 \end{Bmatrix} = \left[\begin{array}{c|c} {}^{G}_{B}[R] & {}^{G}P_{BORG} \\ \hline 0 \;\; 0 \;\; 0 & 1 \end{array}\right]_{4\times 4} {}^{B}\begin{Bmatrix} x \\ y \\ z \\ 1 \end{Bmatrix} \qquad \textbf{(2.1)} $$

where ${}^{G}P_{BORG}$ is the position vector of the blade frame with respect to global frame, and ${}^{G}_{B}[R]$ is a 3 x 3 rotation matrix required to describe the rotation about X - axis of the global frame. The rotation matrix [R] can be given as:

$$ {}^{G}_{B}[R] = [R_x(\theta)] = \begin{bmatrix} 1 & 0 & 0 \\ 0 & \cos(\theta) & -\sin(\theta) \\ 0 & \sin(\theta) & \cos(\theta) \end{bmatrix}_{3\times 3} \qquad \textbf{(2.2)} $$

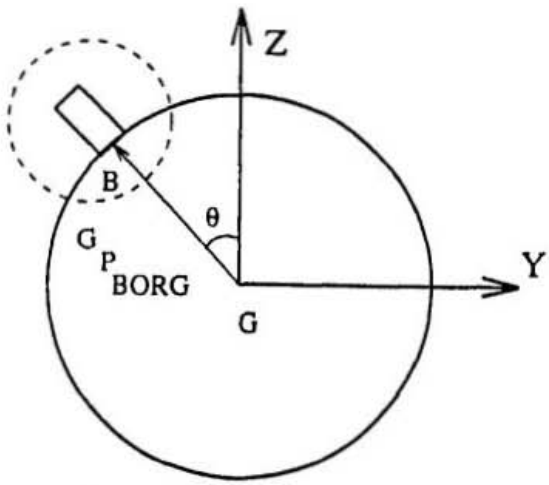

GLOBAL FRAME

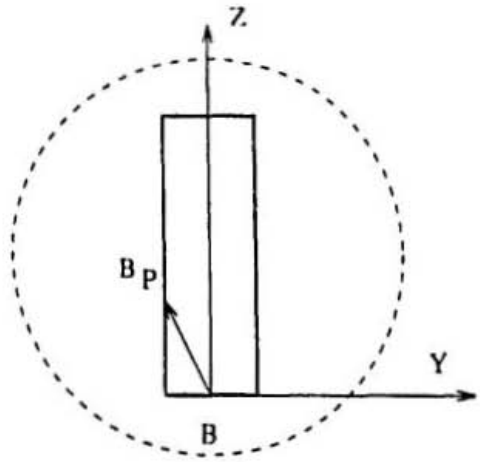

BLADE FRAME

Fig. 2.4 INSTANTANEOUS POSITION OF ANY POINT ^{B}P ON THE BLADE

2.2.2.3 VECTOR DESCRIPTION OF THE BLADE FINITE ELEMENT SURFACE

It is convenient to define the blade element in terms of vectors in order to investigate the dynamics in three-dimensional frame. Finite element surfaces are described in terms of vectors along **cross-section** and the **blade height.**

Fig. 2.5(a) shows the vector layout of the blade along the blade cross-section. Using only the corner nodes of each finite element, the vectors are drawn from the trailing edge to the leading edge along both pressure and suction surfaces in such a way that the tip of the vectors face the nozzle. The nozzle is on the left of the leading edge (not shown). A vector can be given by the difference of the coordinate of the two adjacent corner nodes of the element on each side respectively as shown below:

$$ {}^{G}\{S_{k,l}\}^{\phi} = {}^{G}\begin{Bmatrix} x_k - x_l \\ y_k - y_l \\ z_k - z_l \end{Bmatrix}^{\phi} \qquad (2.3) $$

where the subscripts k, and l refer to the adjacent corner nodes of elemental surface along the blade cross section. ${}^{G}\{S_{k,l}\}$ represents the vector drawn from the node l to node k, and its corresponding unit vector is denoted by ${}^{G}\{\hat{S}_{k,l}\}$. The superscript ϕ stands for a finite surface in consideration and is denoted by s, p for suction, and pressure surfaces

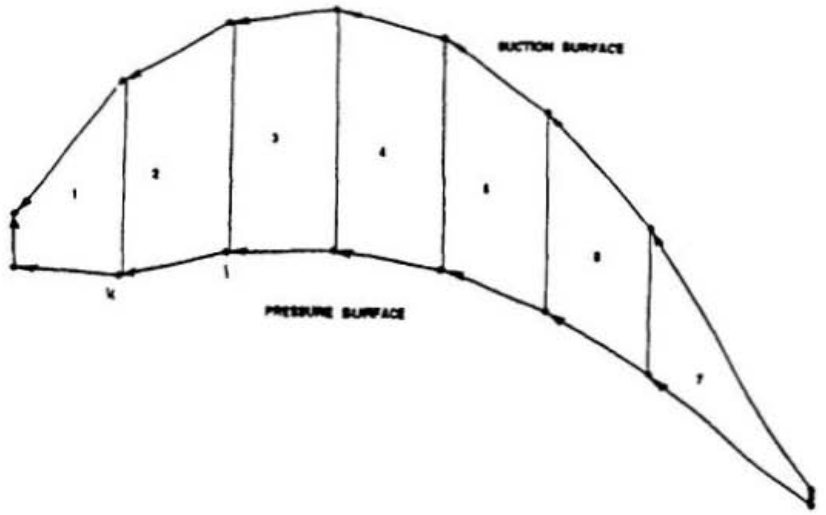

(a)

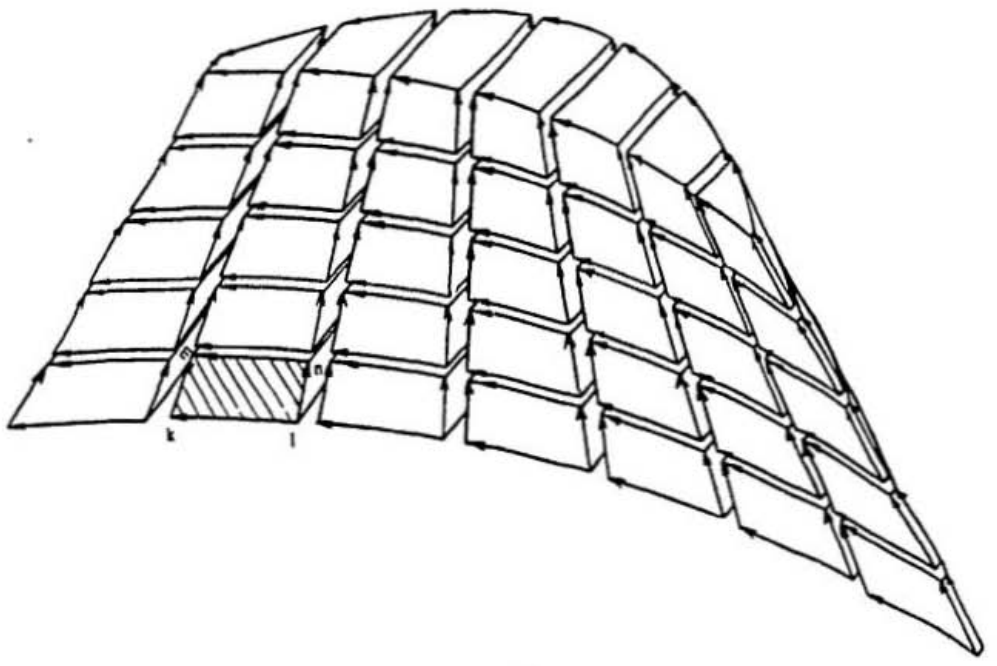

(b)

FIG. 2.5 VECTOR DESCRIPTION OF THE BLADE FINITE ELEMENT ALONG

(a) CROSS-SECTION ; (b) BLADE HEIGHT

respectively.

Fig. 2.5(b) shows the layout of the vectors along the whole surface the blade in three-dimension. The hatched area shows a representative blade finite surface with corner nodes l, k, m, and n respectively. The vectors along blade height are drawn from the bottom layer to the adjacent top layer. Thus, one can define a height vector, ${}^{G}\{S_{k,m}\}$, by the co-ordinate difference of the corner nodes k, m respectively using an equation similar to Eq. (2.3).

From Figs. 2.5(b) and 2.6(a), it is evident that a blade finite element surface can be represented by two vectors along the cross-section of the adjacent layers, and two vectors along the height from adjacent corner nodes. Also, it can be assumed that all the vectors defining a finite surface lie in a plane provided the blade twist angle is negligible or small. The orientation of finite surface area can be represented by a unit vector normal to it as shown in Fig. 2.6(a). The unit vectors normal to the suction and pressure surfaces can be defined as:

$$
\begin{aligned}
{}^{G}\{\hat{n}\}^{s} &= {}^{G}\{\hat{S}_{k,l}\}^{s} \times {}^{G}\{\hat{S}_{m,k}\}^{s} \\
{}^{G}\{\hat{n}\}^{p} &= {}^{G}\{\hat{S}_{m,k}\}^{p} \times {}^{G}\{\hat{S}_{k,l}\}^{p}
\end{aligned}
\qquad (2.4)
$$

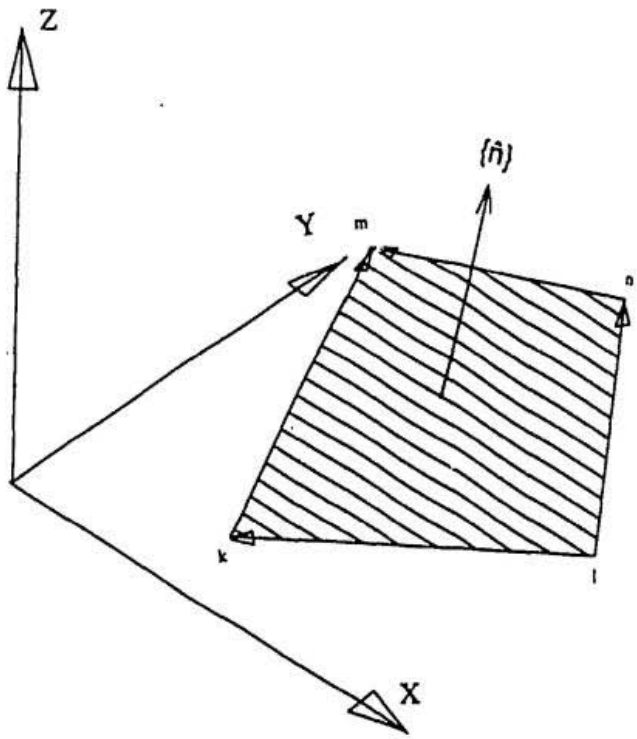

(a)

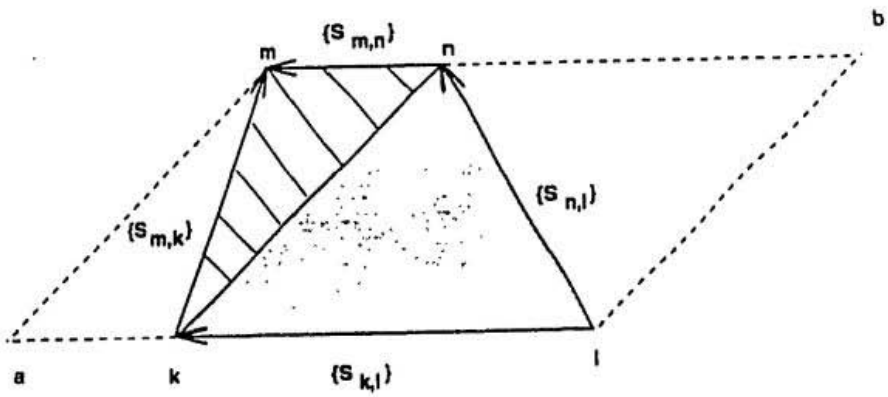

(b)

Fig. 2.6 (a) VECTOR LAYOUT OF A BLADE FINITE ELEMENT SURFACE ;

(b) CALCULATION OF THE BLADE FINITE ELEMENT SURFACE AREA

While taking the cross product, one should be careful to select the vectors such that the normal vectors ${}^{G}\{\hat{n}\}^{s}$, and ${}^{G}\{\hat{n}\}^{p}$ always point outwards to the respective surface.

One can also calculate the surface area (ΔA) of a finite surface with the combination of the vectors along cross section and height (refer to Fig. 2.6(b)) as follows:

$$\{\Delta A\}^{\phi} = \frac{1}{2}\left(\left| {}^{G}\{S_{k,l}\} \times {}^{G}\{S_{n,l}\} \right| + \left| {}^{G}\{S_{m,k}\} \times {}^{G}\{S_{m,n}\} \right| \right)^{\phi} \qquad (2.5)$$

Geometrically, as shown in Fig. 2.6(b), the first term in the right hand side of the above equation represents the area of the parallelogram klbn. Its corresponding half is represented by shaded area kln. Similarly, the second term corresponds to parallelogram aknm, and the corresponding half is represented by the hatched area knm. The total surface area ΔA is, thus, given by the sum of the two halves as shown in the figure.

Thus the blade geometry can be completely defined in terms of the finite elemental surfaces, and the vectors described for each such finite elemental surface.

2.2.3. FLOW MODELLING

The fluid flow from the nozzle strikes the exposed finite element surfaces and gets reflected by the impermeable blade surfaces causing a change in the direction of the flow

velocity, thus changing the momentum of the flow. The change of momentum results in an instantaneous impulsive force on the blade surface. The tangential component of the net impulse forces thus causes the wheel to rotate. However, the dynamics of the flow interaction with the moving blade is quite complicated phenomenon and is highly dependent on several flow parameters, geometric constraints and the rotation of the blade. The following assumptions have been made in order to model the gas flow:

i) the velocity remains uniform across the nozzle,

ii) the absolute efflux at nozzle is parallel to the global X-Y plane,

iii) the flow is incompressible, and non-viscous,

iv) partial-admission (i.e. a nozzle covers only a fraction of the blade annulus circumferential area) of flow is assumed by considering several equiangular discrete nozzle blocks on an annular disk, and

v) identical number of nozzles and rotor blades have been used.

2.2.3.1 FLOW MODELLING AT NOZZLE EXIT

Fig. 2.7(a) shows the planar layout of a representative stage of a gas turbine. The corresponding velocity diagram at nozzle exit point, in global X-Y frame, can be seen in Fig. 2.7(b). The absolute velocity of efflux, ${}^{G}\{V_1\}$, subtends an angle of α_0 (refer to Fig. 1.4 for the nomenclature) with the axial direction and can be represented in global frame as:

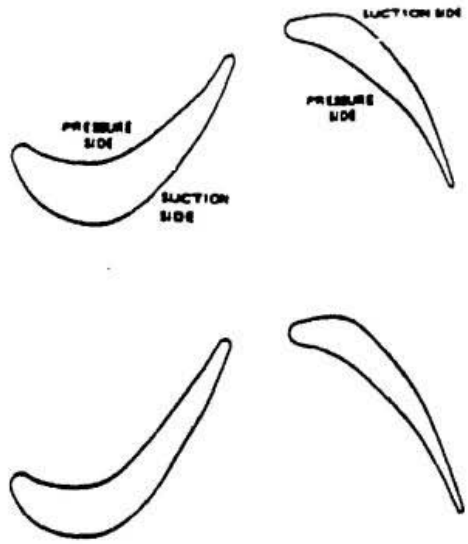

(a)

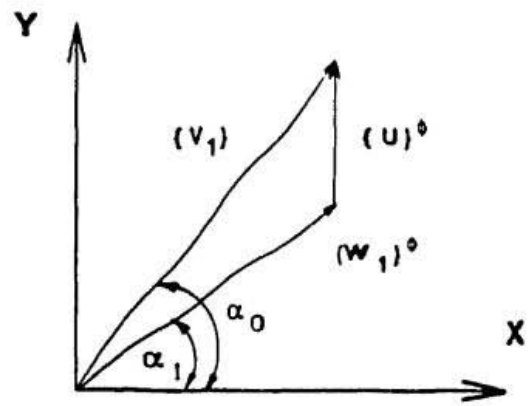

(b)

Fig. 2.7 (a) SCHEMATIC OF PLANAR LAYOUT OF A GAS TURBINE STAGE ;

(b) VELOCITY DIAGRAM AT NOZZLE EXIT POINT IN GLOBAL X-Y PLANE

$$ {}^{G}\{V_1\} = \left| {}^{G}\{V_1\} \right| \begin{Bmatrix} \cos(\alpha_0) \\ \sin(\alpha_0) \\ 0 \end{Bmatrix} \tag{2.6} $$

The relative velocity of the incoming flow on a finite surface of the elemental layer can be given as (the superscript ϕ is used to indicate the surface which can be *p* (pressure) or *s* (suction) :

$$ {}^{G}\{W_1\}^{\phi} = {}^{G}\{V_1\}^{\phi} - {}^{G}\{U\}^{\phi} \tag{2.7} $$

where ${}^{G}\{U\}^{\phi}$ is the tangential velocity of the blade element in the elemental layer under consideration. It is a function of instantaneous rotor speed, ω, and the height of the centroid of the elemental layer, ε_h, in consideration from the root of the blade. The mathematical expression of this vector is given by:

$$ {}^{G}\{U\}^{\phi} = \begin{Bmatrix} 0 \\ \dfrac{2\pi\omega\left(R - e_h\right)}{60} \\ 0 \end{Bmatrix} \tag{2.8} $$

2.2.3.2 FLOW INTERACTION WITH MOVING BLADE SURFACES

The interaction of the flow with the blade element can be modelled by a simple reflection process as shown in the Fig. 2.8. The flow ${}^{G}\{W_1\}$ strikes the exposed finite surface lkmn of the moving blade and gets reflected from the surface. The change in the direction of the flow causes a change in the flow momentum at the blade surface, resulting in an instantaneous impulse force. In order to calculate the momentum change, one needs to know the direction and the magnitude of the incident and reflected flow velocities.

The orientation of the ${}^{G}\{W_1\}$ with the finite surface lkmn is given by the angle of incidence to the surface as expressed below:

$$(\gamma_i)^{\Phi} = \cos^{-1}\left({}^{G}\{\hat{W}_1\}^{\Phi} \cdot {}^{G}\{\hat{n}\}^{\Phi} \right) \qquad (2.9)$$

where ${}^{G}\{\hat{W}_1\}^{\Phi}$, and ${}^{G}\{\hat{n}\}^{\Phi}$ are the unit relative velocity vector of incidence at the surface and unit vector representing normal to the surface (discussed in Section 2.2.2.3) in consideration.

Fig. 2.9 explains the flow reflection process in the plane of reflection over the blade surfaces. $(\gamma_i)^{\Phi}$, as explained earlier, represents the angle of incidence and $(\gamma_r)^{\Phi}$ represents the angle of reflection measured from the normal to the surface in consideration. The orientation of the reflected velocity can be achieved by rotating the unit incident relative

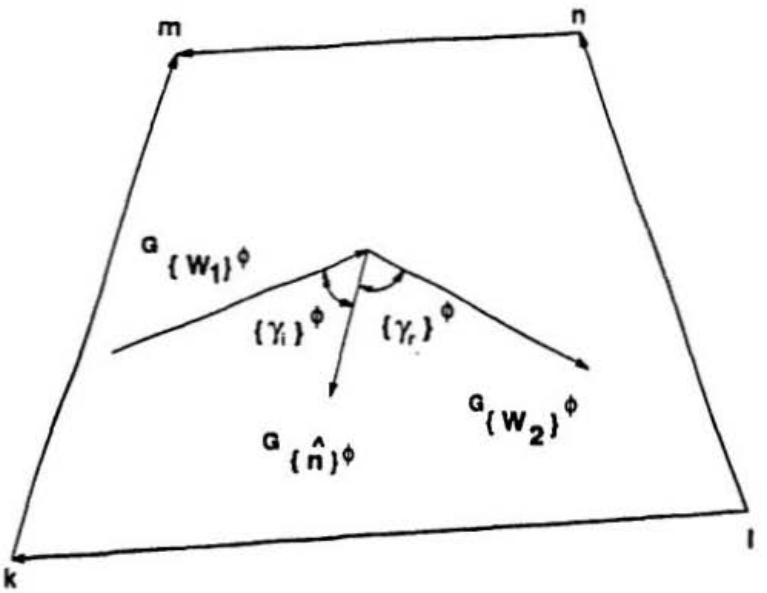

Fig. 2.8 SCHEMATIC OF FLOW INTERACTION WITH THE BLADE FINITE ELEMENT SURFACE

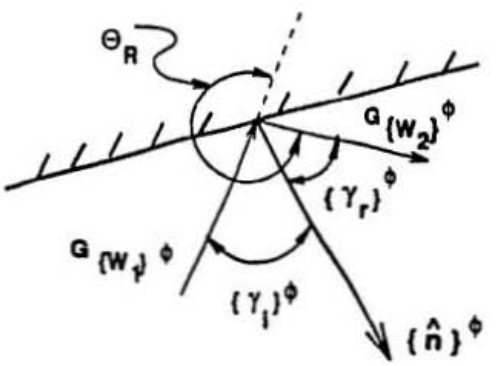

Fig. 2.9 FLOW INTERACTION WITH THE BLADE SURFACE IN THE PLANE OF REFLECTION

velocity ${}^{G}\{\hat{W}_1\}^{\phi}$ by an angle θ_R about an axis parallel to the surface, and perpendicular to the plane of reflection so that the angle of reflection from normal to the surface is exactly the same as angle of incidence from it. The angle θ_R will be explained later. However, in order to rotate the vector, it is convenient to use a local frame at the point of incidence of the flow on the surface. Fig. 2.10 explains one such local frame at the finite surface of the blade element.

Now, our objective is to obtain the vector ${}^{G}\{W_2\}^{\phi}$ having known the angle γ_i, ${}^{G}\{W_1\}^{\phi}$, and ${}^{G}\{\hat{n}\}^{\phi}$. This can be done in the following steps [Sharan and Agarwal (1996)]:

Step 1. Obtain ${}^{G}\{\hat{z}_L\}^{\phi}$ using the following equation:

$$ {}^{G}\{\hat{z}_L\}^{\phi} = \frac{{}^{G}\{\hat{W}_1\}^{\phi} \times {}^{G}\{\hat{n}\}^{\phi}}{\left| {}^{G}\{\hat{W}_1\} \times {}^{G}\{\hat{n}\}^{\phi} \right|} \qquad (2.10) $$

One should ensure that the unit vector describes the positive z - direction in the local frame.

Step 2. Define ${}^{G}\{\hat{x}_L\}^{\phi}$ along ${}^{G}\{\hat{n}\}^{\phi}$ such that

$$ {}^{G}\{\hat{x}_L\}^{\phi} = {}^{G}\{\hat{n}\}^{\phi} \qquad (2.11) $$

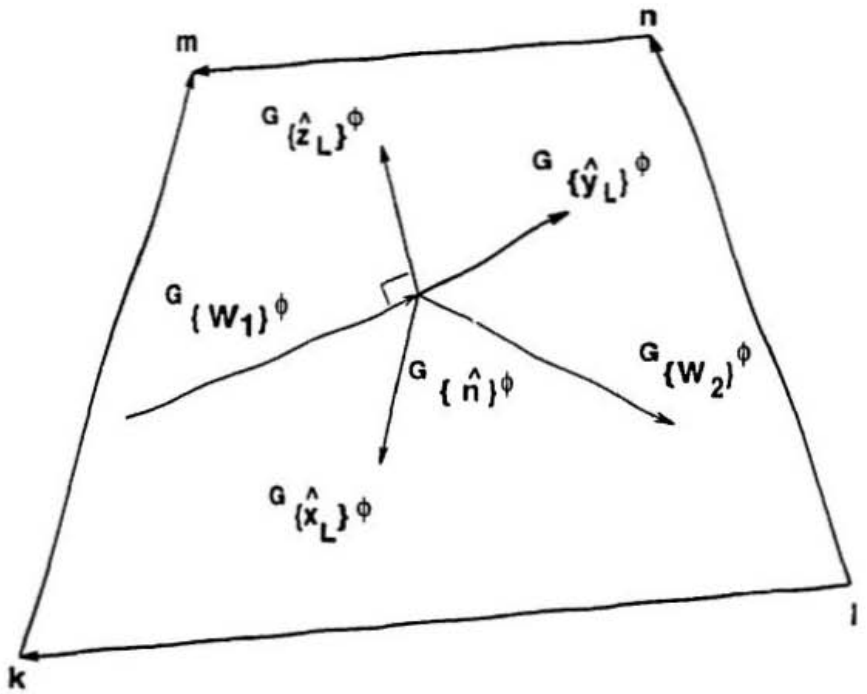

Fig. 2.10 LOCAL FRAME AT THE FINITE ELEMENT SURFACE OF THE BLADE

Step 3. Compute ${}^{G}\{\hat{y}_L\}^{\phi}$ using the cross product of ${}^{G}\{\hat{z}_L\}^{\phi}$, and ${}^{G}\{\hat{x}_L\}^{\phi}$ as given in the equation below:

$$ {}^{G}\{\hat{y}_L\}^{\phi} = {}^{G}\{\hat{z}_L\}^{\phi} \times {}^{G}\{\hat{x}_L\}^{\phi} \tag{2.12} $$

Step 4. Obtain ${}^{L}\{W_1\}^{\phi}$ using the following equation

$$ {}^{L}\{W_1\}^{\phi} = {}^{L}_{G}[R]^{\phi} \; {}^{G}\{W_1\}^{\phi} \tag{2.13} $$

where,

$$ {}^{L}_{G}[R]^{\phi} = \left[{}^{G}_{L}[R]^{\phi} \right]^{-1} = \left[{}^{G}_{L}[R]^{\phi} \right]^{T} \tag{2.14} $$

and,

$$ {}^{G}_{L}[R]^{\phi} = \underset{3 \times 3}{\left[{}^{G}\{\hat{x}_L\}^{\phi} \; {}^{G}\{\hat{y}_L\}^{\phi} \; {}^{G}\{\hat{z}_L\}^{\phi} \right]} \tag{2.15} $$

Here, G corresponds to the global frame and L corresponds to the local frame at the finite surface of the blade.

Step 5. Obtain a vector ${}^{L}\{W_2^R\}^{\phi}$ by rotating ${}^{L}\{W_1\}^{\phi}$ counterclockwise about ${}^{Q}\{\hat{z}_L\}^{\phi}$ by angle θ_R. This is mathematically represented as follows:

$$ {}^{L}\left\{W_2^R\right\}^{\phi} = {}^{L}[R_z(\theta_R)]^{\phi}\ {}^{L}\{W_1\}^{\phi} \tag{2.16} $$

where ${}^{L}[R_z(\theta_R)]$ is the rotation matrix representing a counterclockwise rotation by θ_R about Z-axis of the local triad. It is given by [Craig, 1989]:

$$ {}^{L}[R_z(\theta_R)] = \begin{bmatrix} \cos(\theta_R) & -\sin(\theta_R) & 0 \\ \sin(\theta_R) & \cos(\theta_R) & 0 \\ 0 & 0 & 1 \end{bmatrix} \tag{2.17} $$

3×3

where θ_R is the angle of rotation by which the incident relative velocity vector is rotated about the local z-axis to obtain the direction of reflected relative velocity. The mathematical expression for θ_R is given as (refer to the Fig. 2.10)

$$ (\theta_R)^{\phi} = \pi + 2(\gamma)^{\phi} \tag{2.18} $$

where $(\gamma)^{\phi}$ is the magnitude of the angle of incidence or reflection of flow measured from the normal to the surface in consideration.

Thus ${}^{L}\{W_2^R\}^{\phi}$ represents a vector which is equal in magnitude to the incident relative velocity, and is oriented in the direction of the reflected relative velocity. To include the frictional losses, one can write an equation with $K < 1$ such that the reflected relative velocity is given by:

$$ {}^{L}\{W_2\}^{\phi} = K \; {}^{L}\{W_2^R\}^{\phi} \tag{2.19} $$

Once the reflected velocity vector is obtained in the local frame, it can be expressed in global frame by multiplying with the global-local rotation matrix as defined in Eq. (2.15) as follows:

$$ \{W_2\}^{\phi} = {}^{G}\{W_2\}^{\phi} = {}^{G}_{L}[R]^{\phi} \; {}^{L}\{W_2\}^{\phi} \tag{2.20} $$

Now the vector difference of the relative velocity is given by:

$$ {}^{G}\{\Delta W\}^{\phi} = {}^{G}\{W_1\}^{\phi} - {}^{G}\{W_2\}^{\phi} \tag{2.21} $$

2.2.3.3 SELECTION OF ACTIVE SURFACES OF BLADE FINITE ELEMENT AND CALCULATION OF MASS FLOW IMPINGING ON THE FINITE SURFACES

There are three important state variables to analyze the flow and its interaction with the blade surface. They are - the flow orientation from the nozzle, the geometry of the blade and the nozzle, and the blade rotation. One should consider all these factors in order to select the active surfaces that receive the instantaneous flow, and to calculate the magnitude of the flow impingement on a particular finite blade surface as the blade passes across the nozzle.

The scheme for the selection of the active surface can be led out in two successive steps:

Step 1. Select surfaces based on flow vector and the orientation of the elemental surface as described by the blade vectors.

Fig. 2.11 shows any arbitrary position of flow vector and the blade geometry as represented by vectors. The unit normal vectors extend outwards to the surfaces of the blade element. Depending on the vector orientation of the blade surfaces and the relative incident velocity, a surface that would make a contact with the flow can easily be determined. The criterion of the surface selection should be that if the condition given below

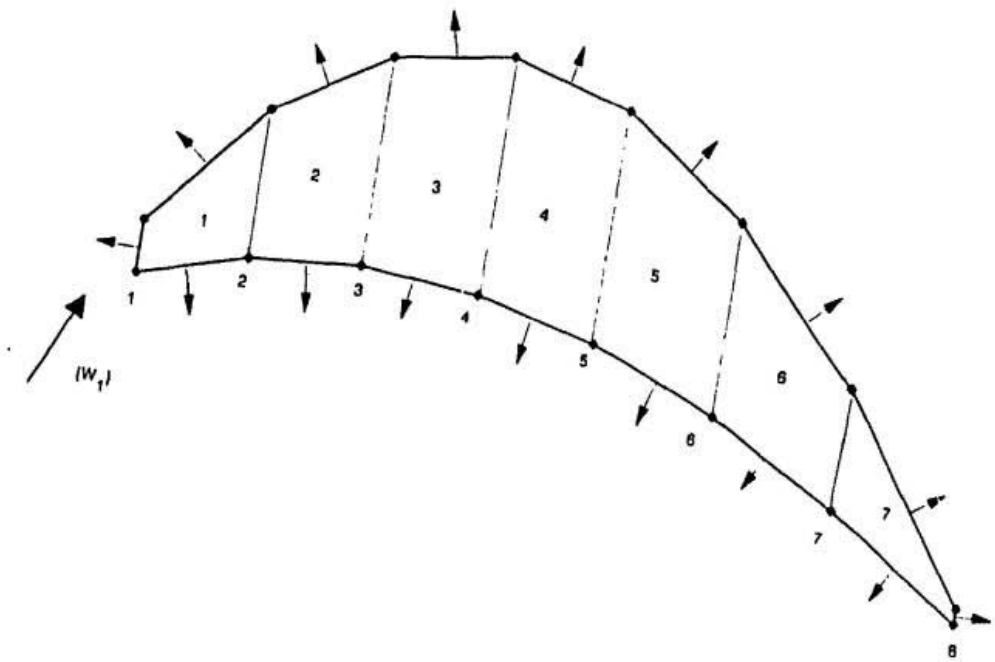

Fig. 2.11 SCHEMATIC OF FLOW VECTOR AND THE BLADE SURFACE VECTORS

$$\left(\{\hat{W}_1\}^{\phi} \cdot \{\hat{n}\}^{\phi} \right) < 0 \qquad (2.22)$$

is satisfied. The area, then, has to be considered as the active surface. The condition holds good for both pressure and suction surfaces. A surface is discarded when the dot product is positive.

Step 2. Select surfaces considering the flow bounded by nozzle geometry, and the orientation of the element surfaces with rotor movement.

Fig. 2.12 represents the schematic of a nozzle, turbine blade, and the rotor configuration. As it is evident from the figure that the moving blade is momentarily excited upon by the impingement of gases while it gets exposed to the discrete nozzle. However, this instantaneous excitation is a function of the geometry of the nozzle, the blade, the axial spacing between the two, at a given instant of time.

In order to estimate the surfaces that are exposed to the flow, one needs to have the projection of finite surface area of the blade, and the nozzle cross-section at outlet on a common plane perpendicular to the relative incident velocity, $\{W_1\}$. This can be done by establishing a local triad denoted by frame N (as pointed out in Section 2.2.1) at one of the points of the nozzle cross section at exit. Fig. 2.13 shows the nozzle cross-section at exit in a global frame. $\{W_1\}$ shows the relative velocity at the nozzle exit. N_1,

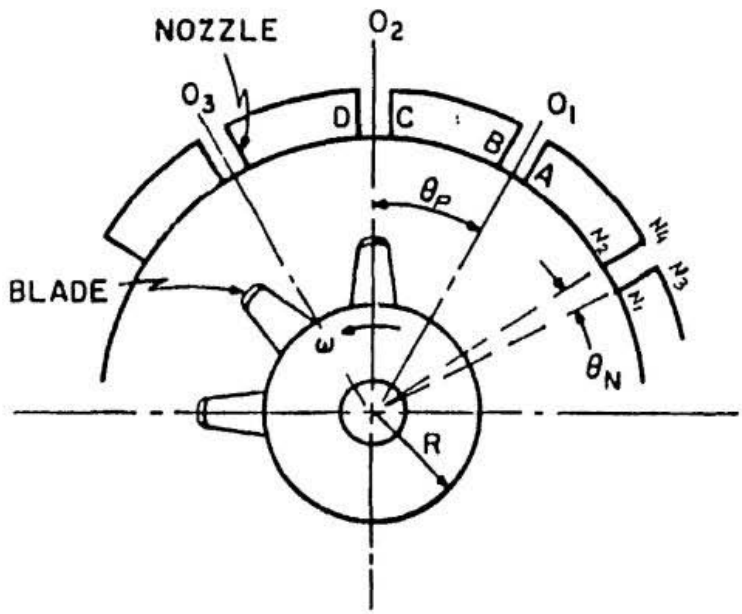

Fig. 2.12 SCHEMATIC OF NOZZLE, BLADE AND ROTOR CONFIGURATION

[BAHREE, 1988]

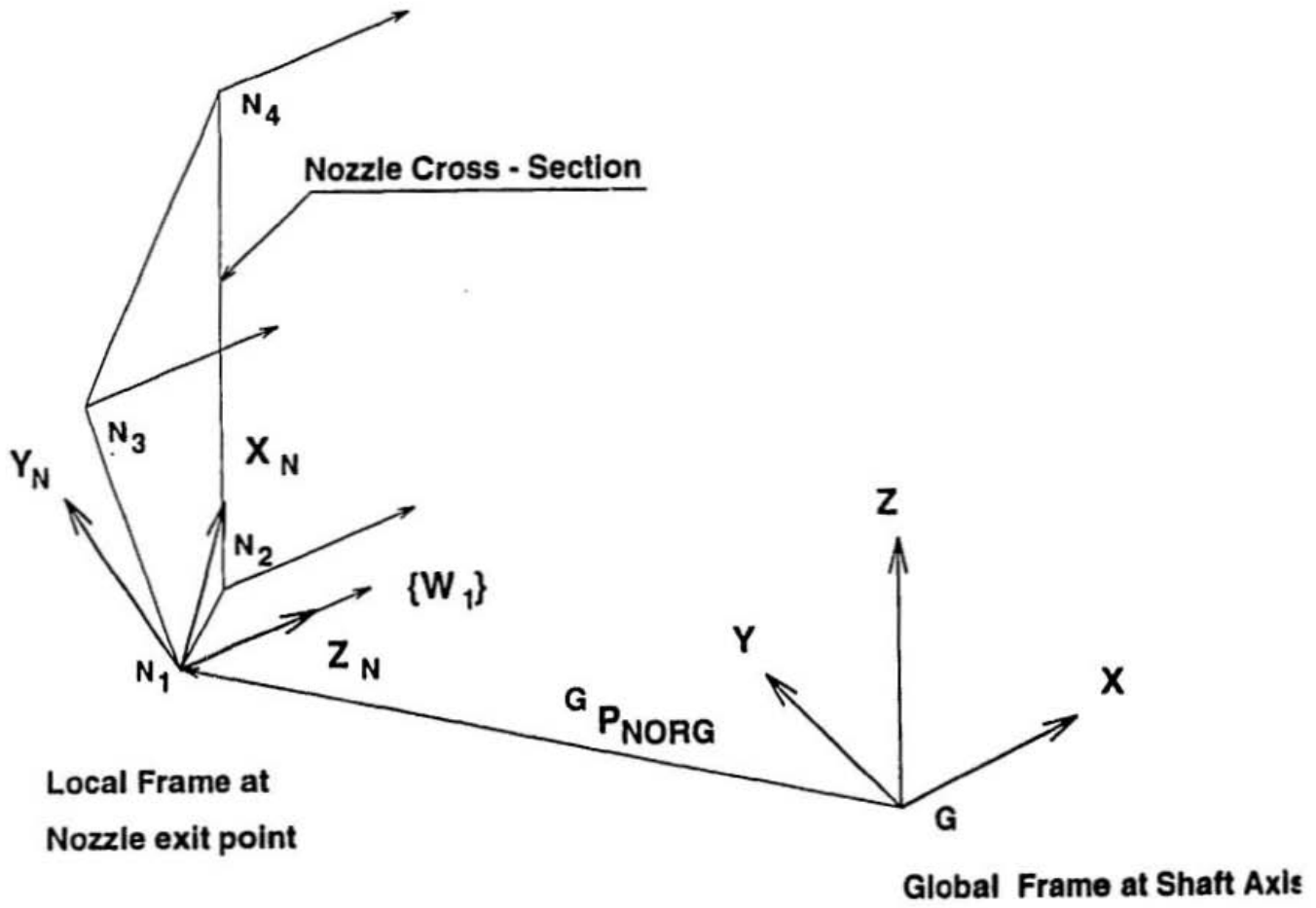

Fig. 2.13 SCHEMATIC OF NOZZLE CROSS-SECTION IN GLOBAL FRAME

N_2, N_3, and N_4 are the four corner points of the nozzle cross-section at the flow exit. The coordinates of these four corner points, N_1, N_2, N_3, and N_4 of the nozzle are known in the global frame. Having known the relative velocity and the origin of the triad in global frame, we have to define the triad in such a way the Z_N - axis of the triad is parallel to the flow direction and the X_N - Y_N plane defines a flow front normal to the incident relative velocity. The computational scheme involved in establishing the N - frame consists of the following steps:

Step 1. Compute the unit vector ${}^G\{\hat{Z}_N\} = {}^G\{\hat{W}_1\}$

Step 2. Define a plane which is normal to the incident relative velocity vector ${}^G\{\hat{W}_1\}$, containing the point N as shown in the Fig. 2.14. The equation of this plane is given by:

$$G\begin{Bmatrix} x_N - x_M \\ y_N - y_M \\ z_N - z_M \end{Bmatrix} \cdot G\begin{Bmatrix} \\ \hat{W}_1 \\ \\ \end{Bmatrix} = 0 \qquad (2.23)$$

where (x_N, y_N, z_N) represent the coordinates of the point N which defines the origin of the local frame. The coordinate of the point N is known in the global frame. Similarly (x_M, y_M, z_M) represent the point M, which is any arbitrary point on the X_N - Y_N plane.

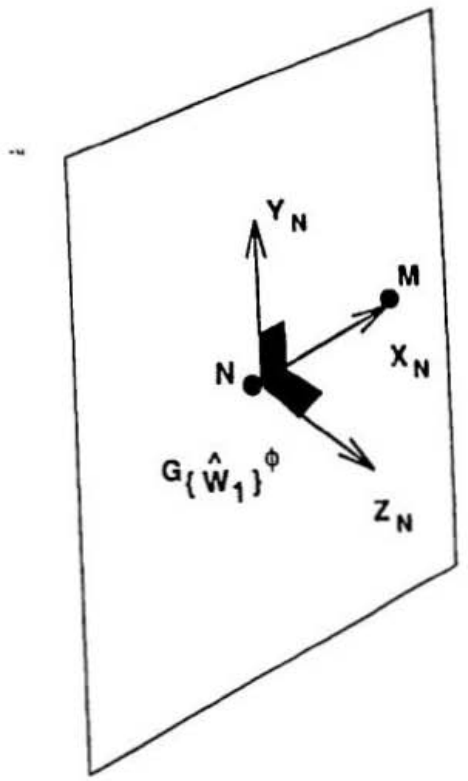

Fig. 2.14 SCHEMATIC OF A PLANE NORMAL TO THE INCIDENT RELATIVE VELOCITY, AT ONE OF THE CORNER POINTS OF THE NOZZLE CROSS-SECTION

Step 3. Select arbitrarily the y, z co-ordinates of the point M on this plane, and obtain its x coordinate by substituting them in Eq. (2.23)

Step 4. Obtain a unit vector along the line NM which is given by ${}^{G}\{\hat{X}_N\}$

Step 5. Obtain ${}^{G}\{\hat{Y}_N\}$ using

$$ {}^{G}\{\hat{Y}_N\} = {}^{G}\{\hat{Z}_N\} \times {}^{G}\{\hat{X}_N\} \tag{2.24} $$

Step 6. Obtain the following transformation matrix

$$ {}^{G}_{N}[T] = \left[\begin{array}{ccc|c} {}^{G}\{\hat{X}_N\} & {}^{G}\{\hat{Y}_N\} & {}^{G}\{\hat{Z}_N\} & {}^{G}P_{NORG} \\ \hline 0 & 0 & 0 & 1 \end{array}\right] \tag{2.25} $$

where ${}^{G}P_{NORG}$ is the position vector of the origin of the frame N relative to the global frame (refer to Section 2.2.2.1). Now, in order to represent the global frame in terms of the local frame at nozzle exit one has to use the inverse transformation of the above as given by:

$$ {}^{N}_{G}[T] = \left[{}^{G}_{N}[T] \right]^{-1} \tag{2.26} $$

The cross-section of the nozzle at flow exit and the finite blade surfaces can be projected over the (X_N - Y_N) plane at this local triad by premultiplying the transformation matrix. A surface (blade elemental surface or nozzle cross section), represented by a quadrilateral with all four corner points defined in global frame, can be projected onto the (X_N - Y_N) plane by defining the position vector of each of the corners of the quadrilateral in (X_N - Y_N - Z_N) system using the following transformation

$$ {}^{N}\begin{Bmatrix} x \\ y \\ z \\ 1 \end{Bmatrix} = {}^{N}_{G}[\,T\,] \; {}^{G}\begin{Bmatrix} x \\ y \\ z \\ 1 \end{Bmatrix} \qquad \textbf{(2.27)} $$

and the equating the z component of this transformed vector to zero. In other words, once the co-ordinates of the nozzle and blade finite surfaces are mapped in the local frame, the x, y co-ordinates of the individual corner points define the projection onto the X_N - Y_N plane which is a plane perpendicular to the incident relative velocity, ${}^{G}\{W_1\}$.

An important point to note is that X_N-Y_N plane is perpendicular to $\{W_1\}$. The vector, $\{W_1\}$, is a function of the tangential velocity of the blade surface, which varies along the blade height. Thus the X_N - Y_N plane is a dynamic plane whose orientation depends on the surface of the blade in consideration. Again, one should also note that the X_N - Y_N plane is different from the plane defined by the nozzle cross - section (defined by four corner points N_1, N_2, N_3, and N_4).

Fig. 2.15(a) shows schematic of the projection of the nozzle cross - section on the X_N - Y_N plane. N_1', N_2', N_3', and N_4' are the projection of four corner points (N_1, N_2, N_3, and N_4) of the nozzle cross section on the plane. Fig. 2.15(b) shows the projection of one of the blade surfaces onto this plane. This is shown by a shaded quadrilateral. Fig. 2.15(c) shows both the projections superimposed on each other. In this figure, one can notice that the area enclosed within the dotted lines represents the maximum of the upper limit of the forces on the blade. Although the momentum will be experienced by all the areas falling within the region which is actual projection of the nozzle, yet the approximation within the dotted line region would be reasonable otherwise the computation becomes enormous. In this way the element surfaces which experience the impact due to nozzle excitation can be selected.

Next, to determine the momentum on an elemental surface of the blade, we have to project each finite element surface areas normal to the incoming relative velocity, ${}^{a}\{W_i\}$. The projected surface area normal to the incident flow can be given by:

$$(\Delta A_n)^{\phi} = (\Delta A)^{\phi} \cdot \cos(\gamma_i)^{\phi} \qquad \textbf{(2.28)}$$

where $(\Delta A)^{\phi}$ represents the finite surface area, and $(\Delta A_n)^{\phi}$ refers the finite area normal to the impinging flow, and $(\gamma_i)^{\phi}$ has already been mentioned earlier in Eq. (2.9).

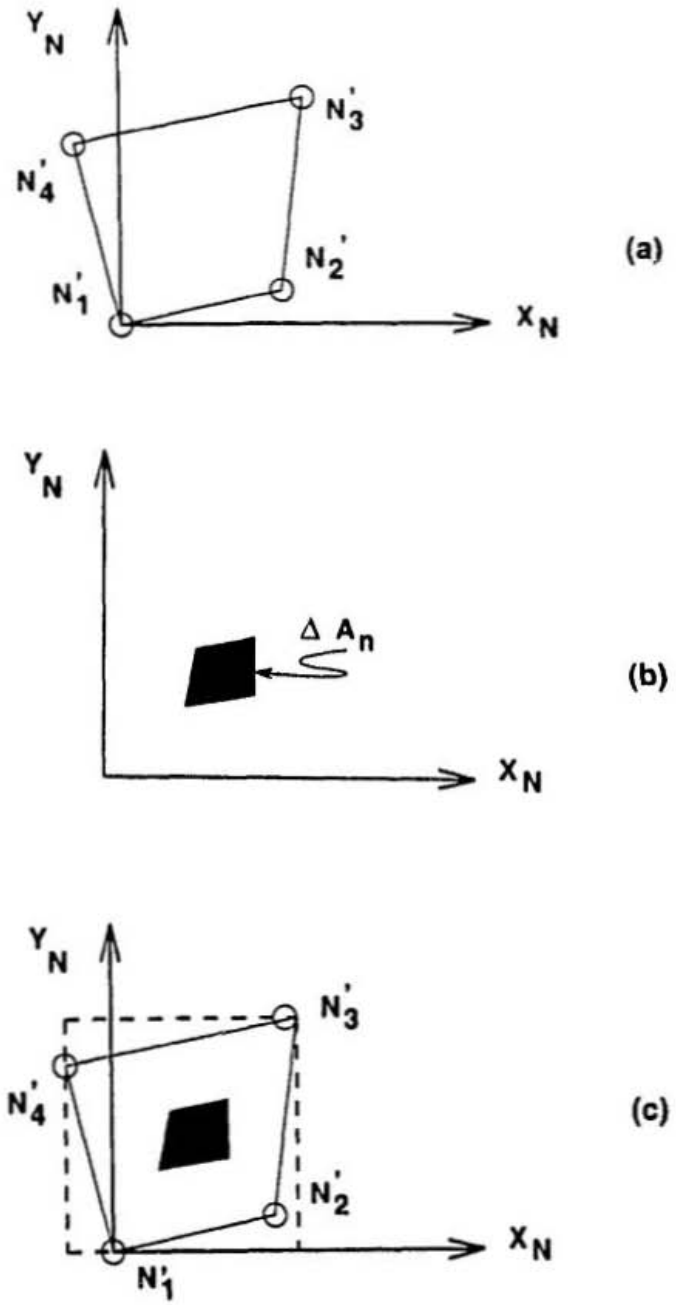

Fig. 2.15 PROJECTION OF (a) NOZZLE CROSS-SECTION; (b) A BLADE FINITE ELEMENT SURFACE; (c) BOTH (a), AND (b) SUPERIMPOSED OVER X_N- Y_N PLANE

Once the projected areas have been calculated, the mass flow of the gas hitting the blade surfaces can be given as:

$$(\Delta \dot{m}_n)^{\phi} = \rho \left| \{W_1\} \right|^{\phi} (\Delta A_n)^{\phi} \qquad (2.29)$$

where ρ is the density of the fluid.

2.2.4 CALCULATION OF IMPULSE FORCE AND DRIVING TORQUE

The impulse force on a finite surface for an elemental layer of the blade can be given by:

$$^{G}\{\Delta F\}^{\phi} = (\Delta \dot{m}_n)^{\phi} \, . \, ^{G}\{\Delta W\}^{\phi} \qquad (2.30)$$

The point of application of the impulse force on each finite surface is assumed to be at geometric centroid of the finite surface.

Once the surface force for all elements in a layer is calculated, the same procedure is repeated for the elements in other layers, and finally all surface forces are summed up. The resultant impulse over the entire blade profile can be given by:

$$^{G}\{F\} = \sum_{\phi} {}^{G}\{\Delta F\}^{\phi} \qquad (2.31)$$

The y-component of the resultant impulse force, {F}, represents the resultant tangential force. This defines the driving force due to gas forces on an isolated rotor blade. The x, and z components of the resultant force will be in axial and radial directions respectively.

Considering the three components of each of the elemental forces {ΔF} as {ΔF_x}, {ΔF_y}, and {ΔF_z} respectively, one can write the corresponding point of application of the resultant impulse force as:

$$\begin{Bmatrix} X_c \\ Y_c \\ Z_c \end{Bmatrix} = \frac{1}{|\{F\}|} \sum_{\phi} \begin{Bmatrix} x_c \\ y_c \\ z_c \end{Bmatrix}^{\phi} \times \begin{Bmatrix} \Delta F_x \\ \Delta F_y \\ \Delta F_z \end{Bmatrix}^{\phi} \qquad \textbf{(2.32)}$$

In the above equation x_c, y_c, and z_c are the coordinate of the geometric centroid of an elemental surface.

The position vector of the point of application in global frame can be given by:

$$\{R_d\} = \begin{Bmatrix} X_c \\ Y_c \\ Z_c \end{Bmatrix} \qquad \textbf{(2.33)}$$

The corresponding moment of the resultant force {F} acting on a single blade about the origin of the global frame at rotor axis is given by:

$$\{T\} = \{R_d\} \times \{F\} \qquad (2.34)$$

In the above equation the moment {T} has three components. The x - component of the moment represents the driving torque on the wheel, the y - component of the moments represents the bending moment on the blade about the rotor centre, while the z - component represents the twisting moment on the blade.

One should note that in the above formulation, the forces and the torques are calculated for a single three-dimensional blade excited by a single nozzle at any instant of angular position about the global X - axis during the course of its angular motion.

2.2.5. CALCULATION OF ANGULAR ACCELERATION

As the gases impinge on to the blades, they result in a driving torque as mentioned above, which causes the rotor-blade assembly to accelerate. The angular acceleration of the rotor - blade assembly can be expressed as follows:

$$\alpha = \frac{T_x}{I_{xx}} \qquad (2.35)$$

where T_x is the driving torque denoted by the x - component of the moment {T} as mentioned in the Eq. (2.34). In the above equation I_{xx} denotes the combined mass moment of inertia of the rotor disc and the blade assembly about the global X - axis, which is nothing but the rotor axis about which the entire assembly rotates. However, the combined mass moment of inertia, I_{xx}, in this equation accounts for a single blade, and the rotor disc. This will be discussed in the next section.

2.2.6. DERIVATION OF THE MASS MOMENT OF INERTIA OF THE COMBINED DISC-BLADE ASSEMBLY

Fig. 2.16 shows a schematic diagram of the rotor disc, and the blade mounted on it. The moment of the inertia of the blade is known at the root (refer to Section 2.2.2.1). By using parallel axis theorem, one can calculate the corresponding moment of Inertia of the blade, ${}^{G}(I_{xx})_b$, about the rotor axis as follows:

$$ {}^{G}\left(I_{xx} \right)_b = {}^{B}\left(I_{xx} \right)_b + M_b \left(\frac{d}{2} \right)^2 \qquad (2.36) $$

where ${}^{B}(I_{xx})_b$ represents the mass moment of inertia of the blade about root of the blade. This is represented in the blade frame about the origin, B. M_b represents the mass of an individual blade, and d represent the diameter of the rotor disc.

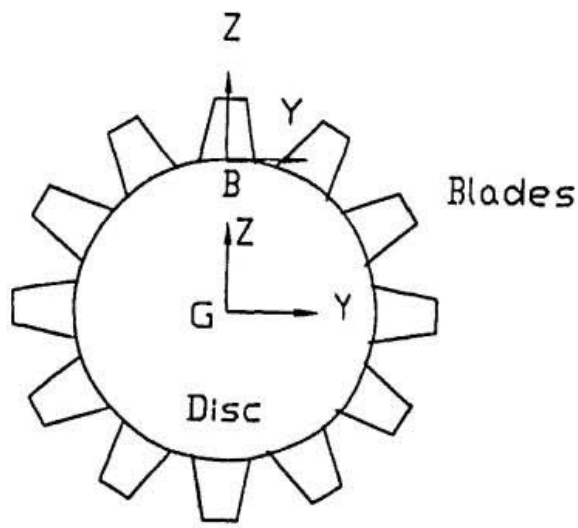

Fig. 2.16 SCHEMATIC OF ROTOR DISC AND THE TURBINE BLADES

Now the combined mass moment of inertia of the disc and the blades about the rotor X - axis can be expressed as follows:

$$I_{xx} = {}^{G}(I_{xx}) = {}^{G}(I_{xx})_{d} + {}^{G}(I_{xx})_{b} \qquad (2.37)$$

where ${}^{G}(I_{xx})_{d}$ denotes the mass moment of inertia of the rotor disc about the global X - axis. One can notice that the combined moment of inertia is obtained by the summation of the former with the mass moment of inertia of the blade about the global X - axis. However, the above equation is valid for a single blade and the rotor disc assembly.

CHAPTER 3

VERIFICATION AND ANALYSES OF THE MODEL

3.1 INTRODUCTION

In the previous chapter we discussed the mathematical modelling of a gas turbine stage to determine impulse forces acting on the entire blade at any instant of time or any angular position of the rotor. As a follow-up, this chapter presents the results of impulse forces calculated by the method described in the previous chapter. The results are compared with a conventional impulse model to validate the model developed in the Chapter 2.

Results for two different blade geometries viz. a straight blade, and a tapered blade have been presented. The effect of partial-admission due to nozzle boundary on the incoming flow over the blade is shown in conjunction with the blade dynamics. The effect of blade geometry on impulse and the driving torque has been brought into light.

Angular acceleration has been calculated by considering the inertia of the whole rotor system. Total forces and torque equations have been formulated for equal number of nozzle and blade pairs and the results have been presented.

3.2 MODEL VERIFICATION

3.2.1 BLADE NOMENCLATURE AND THE CONVENTIONAL IMPULSE EQUATION

The common nomenclature of a gas turbine blade can be seen in Fig. 3.1 which shows a section taken through the blading at any chosen diameter.

α_1 and α_2 represent the flow angles at entry and the exit points in the blade passage respectively. β_1, and β_2 are the blade angles at the leading and trailing edge of the blade airfoil. The chord is represented by c.

$\{W_1\}$, and $\{W_2\}$ represent the relative flow velocities at entrance and the exit of the blade passage and their directions are determined by the flow angles at inlet and exit. The blade geometry and the flow angles are, however, quite important parameters to determine the turbomachinery performance.

It is well known that the change in the momentum of the fluid flow causes the exertion of the impulse force on the blade which can be given by conventional equation [Harman, 1981] as follows:

$$\left|\{F\}\right| = \frac{\dot{m}_n}{n} \frac{\left(\left|\{W_1\}\right| + \left|\{W_2\}\right|\right)}{2} (\alpha_1 - \alpha_2) \qquad (3.1)$$

where n is the number of rotor blades being simultaneously activated by a single nozzle. The flow angles, α_1, and α_2 are expressed in radians. The force, {F}, exerted by the gas flow acts against the concave side of the blade, and is the resultant effect of the impulse forces exerted on the overall blade surface. The impulse force, {F} is approximately normal to the blade chord [Harman, 1981].

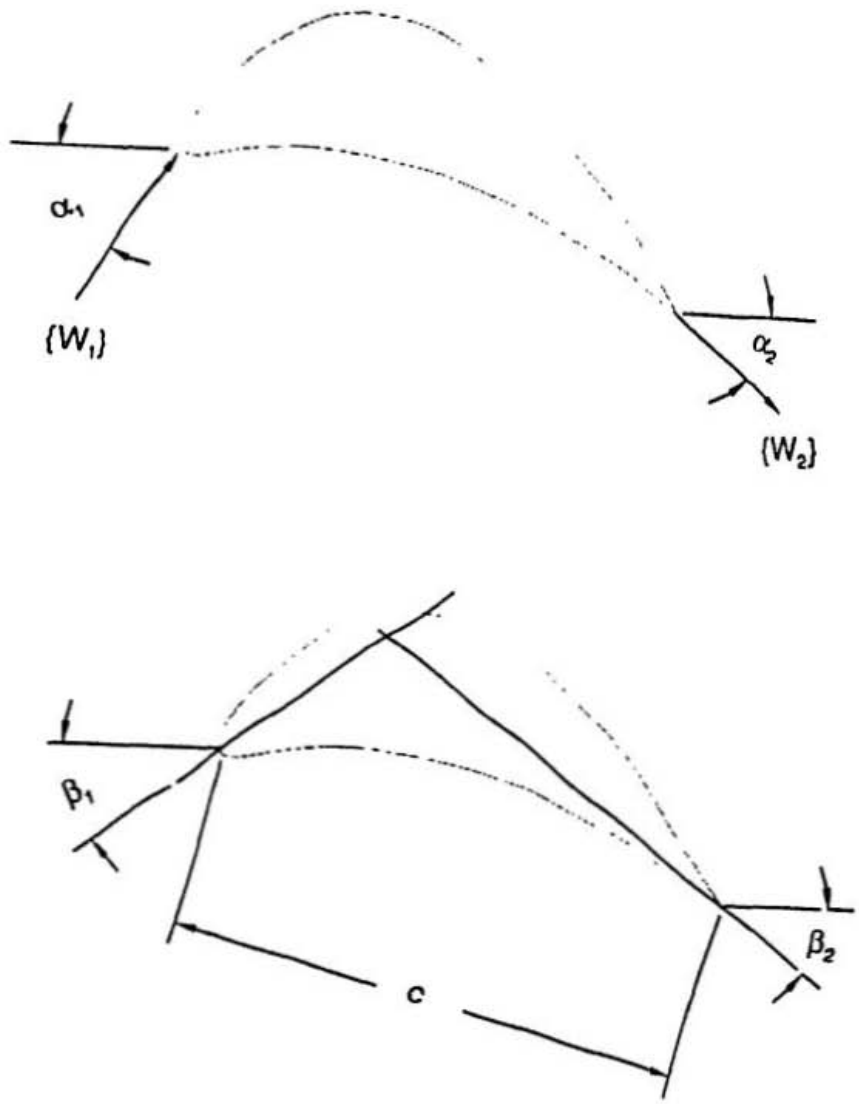

Fig. 3.1 THE TURBINE BLADE NOMENCLATURE

3.2.2 REPRESENTATIVE MODEL - A STRAIGHT BLADE

The conventional planar model, however, can be extended to a three-dimensional model, if the same blade profile were used along the height. In this case, the mass flow will be accounted for the entire three-dimensional blade. Thus, the theory developed for a general three-dimensional model in the previous chapter can be compared with the conventional model by taking an example of a blade with constant profile along the height.

3.2.2.1 DETAILS OF THE BLADE

The Fig. 3.2 shows a three-dimensional finite element model of a straight blade used as a representative model. The finite element discretization of the blade is done using 20-noded, C^0-continuity, serendipity elements as discussed in the Section 2.2.2.1. The elements are shown staggered for the sake of clarity.

The profile data of the blade is detailed in the Appendix C, whereas other geometric details viz. the blade volume, the centroid of the elemental layer, the mass moment of inertia, etc. have been described in the Table 3.1

The aerodynamic details (to the actual scale) are shown in the Fig. 3.3. As evident from the figure, the values of the blade angle β_1, and β_2 were approximated by the geometry of the suction surface of the first element at the leading edge and the pressure surface of the element at the trailing edge of the blade respectively. The blade chord subtends an angle (ψ = - 13.6°) with the axial direction.

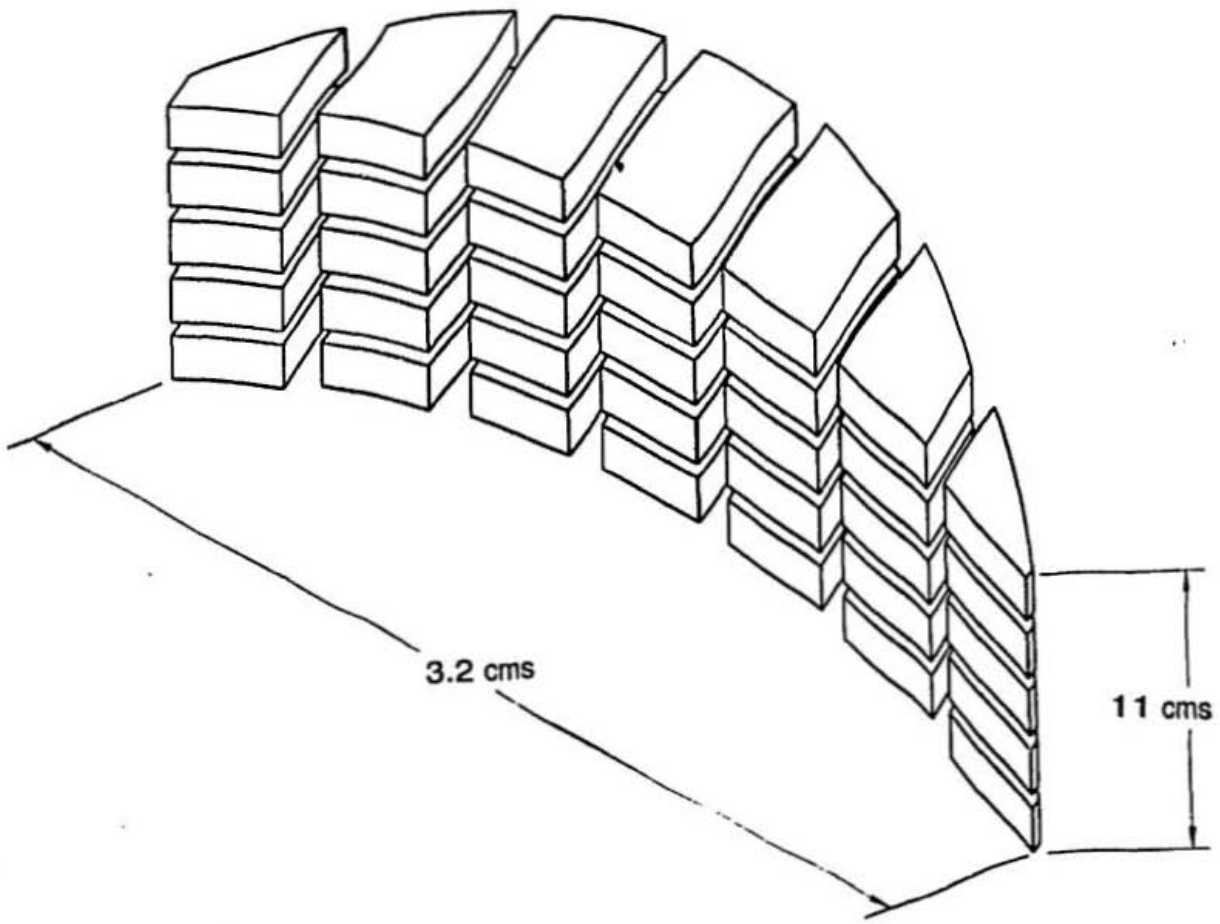

Fig. 3.2 THREE-DIMENSIONAL FINITE ELEMENT MODEL OF A STRAIGHT BLADE

TABLE 3.1 GEOMETRIC PROPERTIES OF THE STRAIGHT BLADE

Density of the blade material = 8256 kg/ m^3

Total volume of the blade = 0.2347×10^{-4} m^3

Height of the centroid of the blade from the blade root = 0.055 m

Mass moment of inertia of the blade about the origin of the blade frame,

${}^{B}(I_{xx})_b = 7.84 \times 10^{-4}$ kg-m^2.

Height of the centroid of the elemental layers from the blade root:

Elemental Layer from the root	ε_h x 10^{2} m
1	1.1
2	3.3
3	5.5
4	7.7
5	9.9

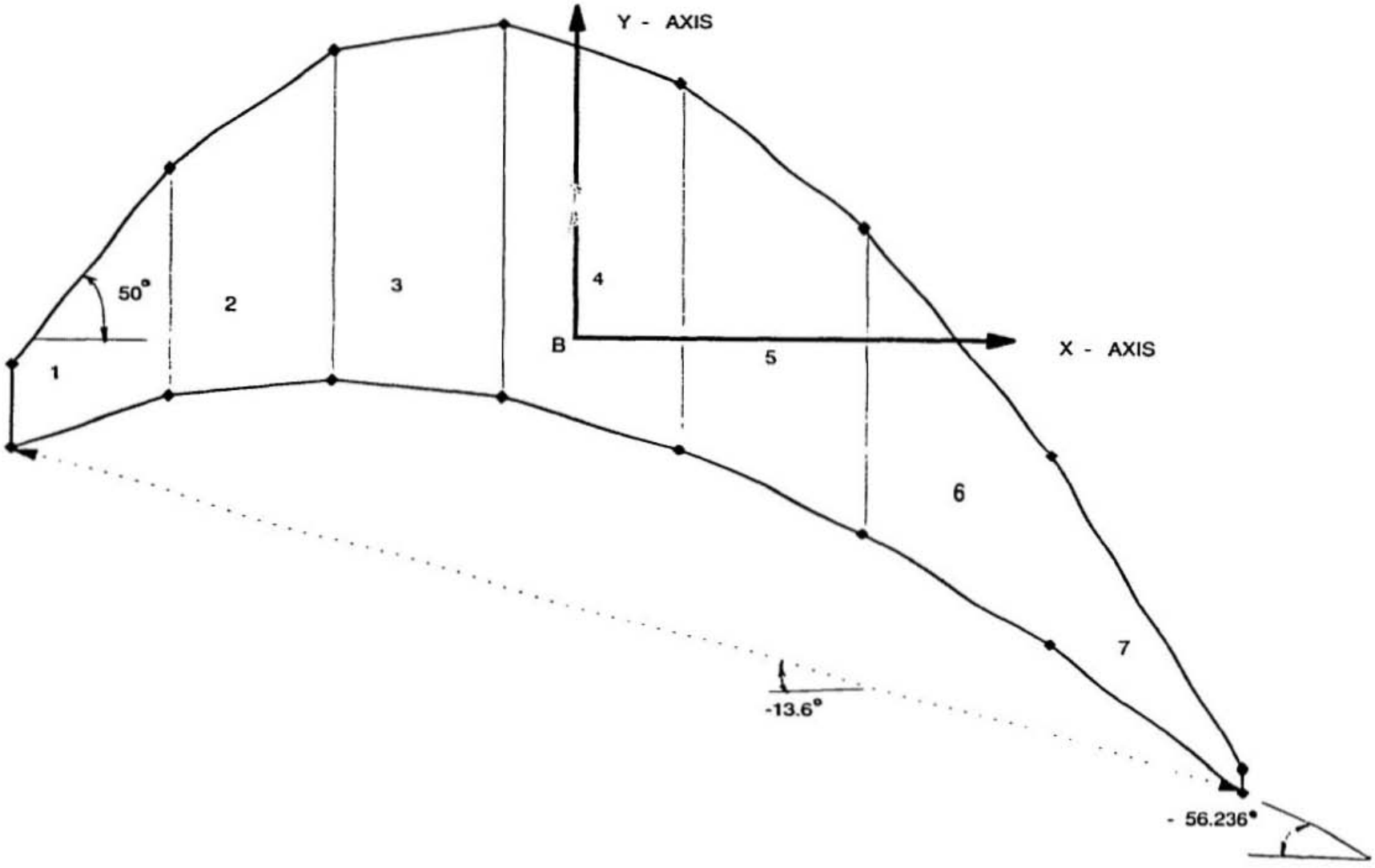

Fig. 3.3 AERODYNAMIC DETAILS OF THE REPRESENTATIVE BLADE MODEL

3.2.3 ASSUMPTIONS FOR VERIFICATION

The conventional model, however, does not provide detailed or sufficient information about the partial flow-admission, and the three-dimensional effect of the relative flow velocity and the flow attack due to blade rotation. In order to compare the results with present modelling, these issues can be easily handled by assuming the rotor at rest and the full-flow admission to the blade.

Now, for a stationary blade:

$$|\{U\}| = 0 \; ; \; \alpha_1 = \alpha_0 \; ;$$

$$\alpha_2 = \beta_2$$

where $|\{U\}|$ is the magnitude of blade velocity, and α_0 is the angle subtended by absolute flow at nozzle exit as explained in the Fig. 2.7(b). One can also simulate the design condition by considering the orientation of flow vector identical to the blade angle β_1 which means $\alpha_1 = \alpha_0 = \beta_1$. Thus, in the present case the value of α_1 is 50°, while value of α_2 is equal to - 56.236°.

3.2.4 COMPARISON OF IMPULSE FORCE

The calculation for impulse force was carried out with the formulation described in the previous chapter by considering the following parameters:

The absolute flow velocity, $V_1 = 500.00$ m/s.

The density of the flow, $\rho = 2.89$ kg/m^3.

The dissipative velocity loss factor in the blade passage, $K = 0.9$

The blade speed, $|\{U\}| = 0$

Thus, $|\{W_1\}| = |\{V_1\}| = 500.00$ m/s.; and

$|\{W_2\}| = 0.9 \times 718.05$ m/s $= 450.00$ m/s.

The mass flow over the entire blade profile was calculated by summing up the flow over individual active surfaces as discussed in the Eq. (2.28). The mass flow rate thus obtained over the entire blade, $\dot{m}_n = 4.936$ kg/s

The forces over the entire blade profile were computed along the global frame using Eq. (2.31) were:

The total force obtained , $|\{F\}| = 3937.44$ N

The axial component of the force $F_x = 1523.31$ N

The tangential component of the force $F_y = 3630.84$ N, and

the radial component of the force $F_z = 0.0$ N

The angle subtended by the force with the axial direction $= \tan^{-1}(F_y/F_x) = 67.24°$ i.e. it subtends an angle of $(67.24 + 13.6) = 80.84°$ with the blade chord, which is approximately 9° off from the normal to the chord against the concave side of the blade.

For a single blade per nozzle we consider $n = 1$, and on substituting the values of the above parameters in Eq.(3.1), we obtain the conventional impulse force as:

$|\{F\}| = 4347.5$ N

Thus, the value of the impulse force obtained by following the theory developed is found to be fairly close to the conventional one (The difference is about 9%). Moreover, the impulse force is found to be almost perpendicular to the blade chord. This verifies the modelling concept employed in the previous chapter.

3.3 A STUDY OF THE EFFECT OF THE STAGE GEOMETRY

The impulse force acting on the turbine blade at any given angular position depends upon several geometrical parameters. These geometrical parameters include the nozzle geometry, the location of the nozzle corresponding to the blades, and the geometry of the blade itself. In the present work, a study was carried out to present the effect of these geometrical parameters which are quite important from the design point of view.

3.3.1 THE EFFECT OF THE NOZZLE GEOMETRY

Fig. 3.4 shows the schematic of the radial arrangement of the discrete nozzles along the annular periphery of a circular disc. It can be seen from the figure that each finite nozzle serves the purpose of partial admission of flow to the blades in motion. It is obvious that the magnitude of impulse forces acting on the blade will be directly proportional to the amount of mass actually hitting the blade surfaces (refer to the Eq. (2.30)). The quantity of flow admission can be controlled by the angular opening, θ_N, of the nozzle. Fig. 3.5 shows the variation of the resultant tangential and the axial forces acting on a stationary straight blade described previously. One can observe from the figure that with increase in the nozzle opening, the forces increase almost linearly. This is because of the proportional increase in the gas flow hitting the blade surfaces. However, one can also note that this behaviour is observed up to a certain degree of the nozzle opening (4° in this case), and beyond that there is no further increment in the forces due to further opening of the nozzle. This is because at this particular opening the

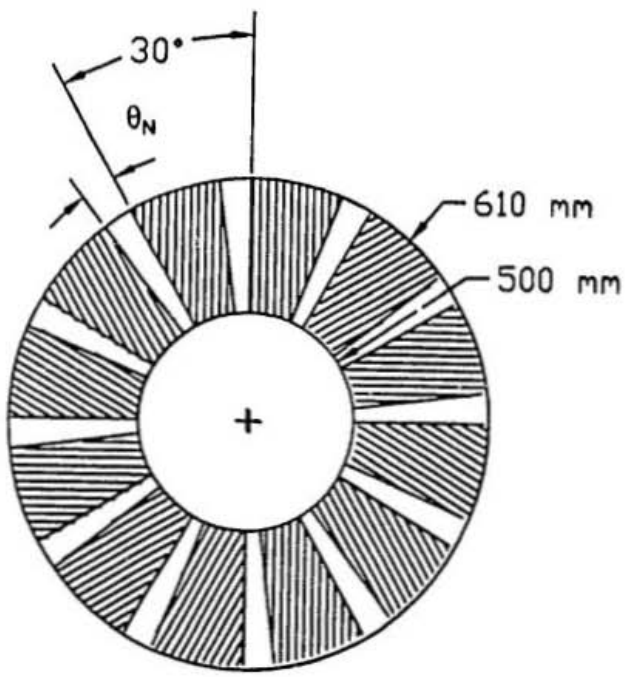

Fig. 3.4 SCHEMATIC DIAGRAM OF THE NOZZLE ARRANGEMENT

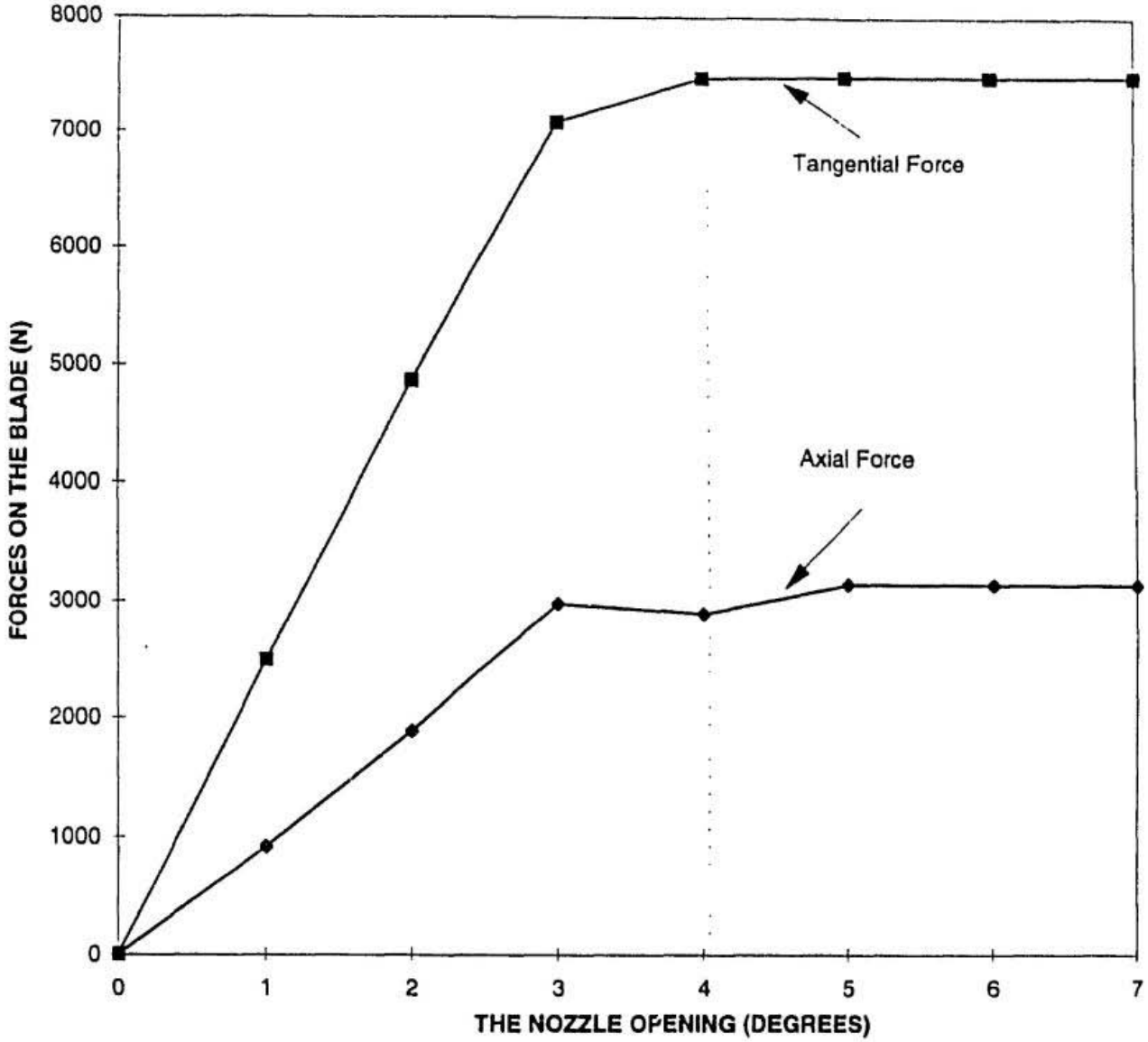

Fig. 3.5 VARIATION OF FORCES IN A STRAIGHT BLADE WITH NOZZLE OPENING

mass flow hitting the blades cover the entire blade geometry and further increment of the flow goes beyond the blades, and the effective mass of the gases hitting the blade remains invariant. In this figure, the undulation in the curve is due to lack of smoothness in the blade profile.

3.3.2 THE EFFECT OF THE BLADE GEOMETRY

The forces on the blade were obtained by calculating the flow distribution on each element in a given blade layer. One can note that the force distribution on each blade finite element surface depends upon its orientation with respect to the relative flow vector. Fig. 3.6 shows the variation of the axial and the tangential force distribution along the pressure surfaces in one of the elemental layer at the root of the blade from leading edge to the trailing edge. One can easily notice that the effect of the blade geometry (i.e., the orientation of surfaces) is quite pronounced on the force distribution from the leading edge to the trailing edge of the blade. There is a negative gradient in the axial force at the second surface of the blade (the axial force on element 2 is less than that on element 1) which is due to the lack of smoothness in the blade. The distributions of the forces were found to be the same in other elemental layers of the straight blade.

3.3.2.1 THE EFFECT OF TAPER

The straight blade discussed in earlier sections was modified to a tapered blade. The coordinates of the cross-section at the tip of the blade were multiplied by a factor of 0.59 while the profile at the root was kept the same as that of the straight

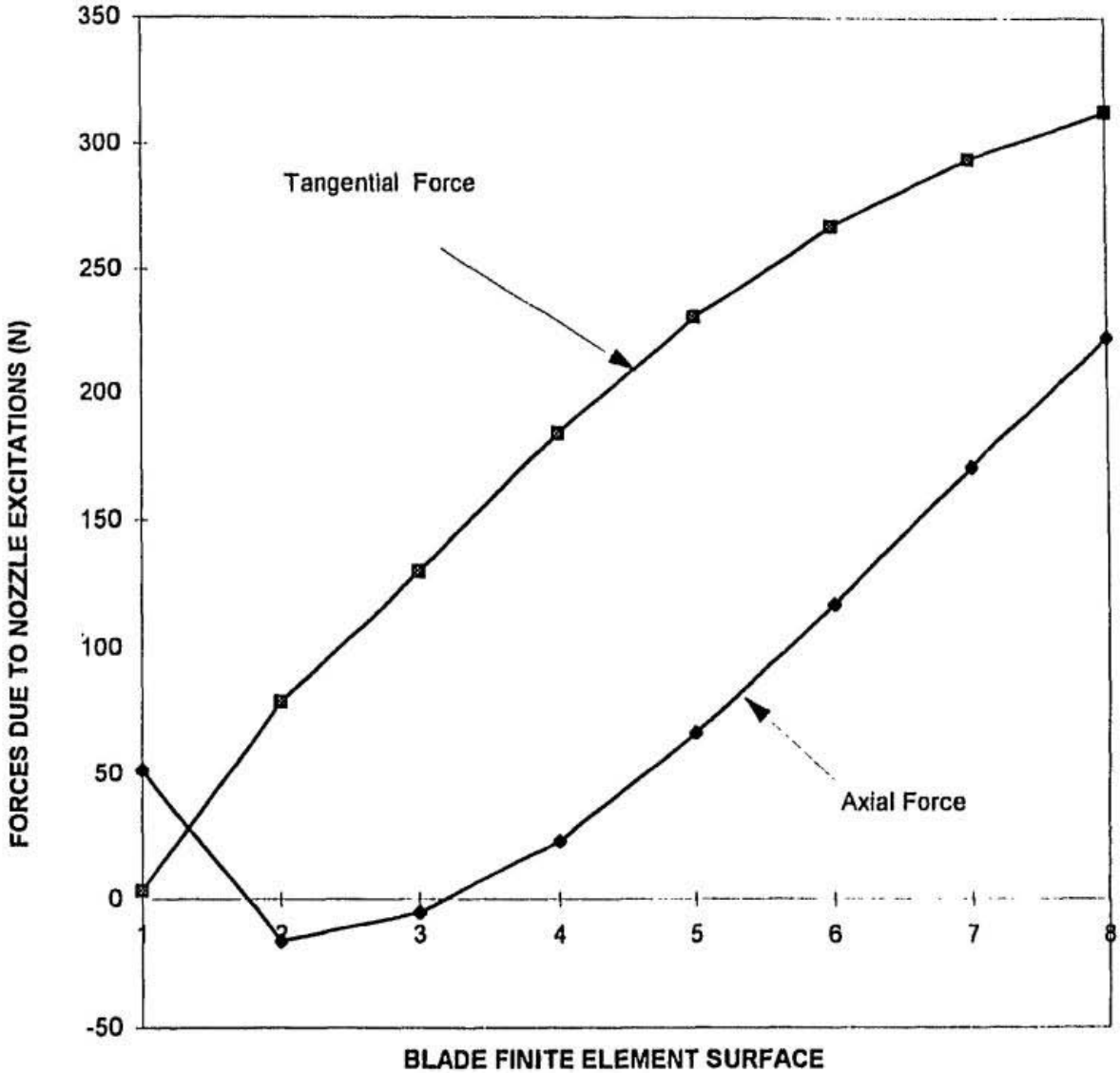

Fig. 3.6 DISTRIBUTION OF FORCES ALONG THE PRESSURE SURFACE OF FIRST ELEMENTAL LAYER FROM ROOT OF THE STRAIGHT BLADE

blade. The geometric properties of the tapered blade are detailed in the Table 3.2. Figs. 3.7 and 3.8 show the distribution of the forces along the elemental surfaces and their corresponding variation in elemental layers from the root to the tip of the blade. It can be seen from the figure that the distributions of both axial and tangential forces show the similar characteristics as exhibited by the straight blade. This is because the nature of the blade profile along the cross section does not vary. However, a significant reduction in the forces is observed in the elemental layers along the height of the tapered blade. The reduction in the magnitude of the forces is due to the reduction in the effective surface area of the blade elements and correspondingly, the amount of the flow impinging on the surfaces also get reduced. Fig. 3.9 shows the variation of the total axial and tangential forces along each elemental layer along the blade height.

3.4 THE EFFECT OF THE VELOCITY VARIATION

3.4.1. THE EFFECT OF THE ABSOLUTE GAS VELOCITY VARIATION

The effect of variation of the absolute flow velocity, $\{V_1\}$ at nozzle exit on the impulse forces over a straight blade can be observed in Fig. 3.10. The blade is kept stationary against the flow to observe the effect of the variation of the flow. The results show that the forces increase with the increment of the flow velocity, and the nature of the increment is parabolic. This can be understood by referring to Eqs. (2.29) and (2.30). If we substitute $\Delta\dot{m}_n$ from Eq. (2.29) into Eq. (2.30), we get:

TABLE 3.2 GEOMETRIC DETAILS OF A TAPERED BLADE

Density of the blade material = 8256 kg/ m^3

Total volume of the blade = 0.15162 x 10^{-4} m^3

Height of the centroid of the blade from the blade root = 0.04575 m

Mass moment of inertia of the blade about the origin of the blade frame,

${}^{B}(I_{xx})_b$ = 3.80 x 10^{-4} kg-m^2.

Height of the centroid of the elemental layers from the blade root:

Elemental Layer from the root	ε_h x 10^2 m
1	1.0687
2	3.2657
3	5.4622
4	7.6597
5	9.8524

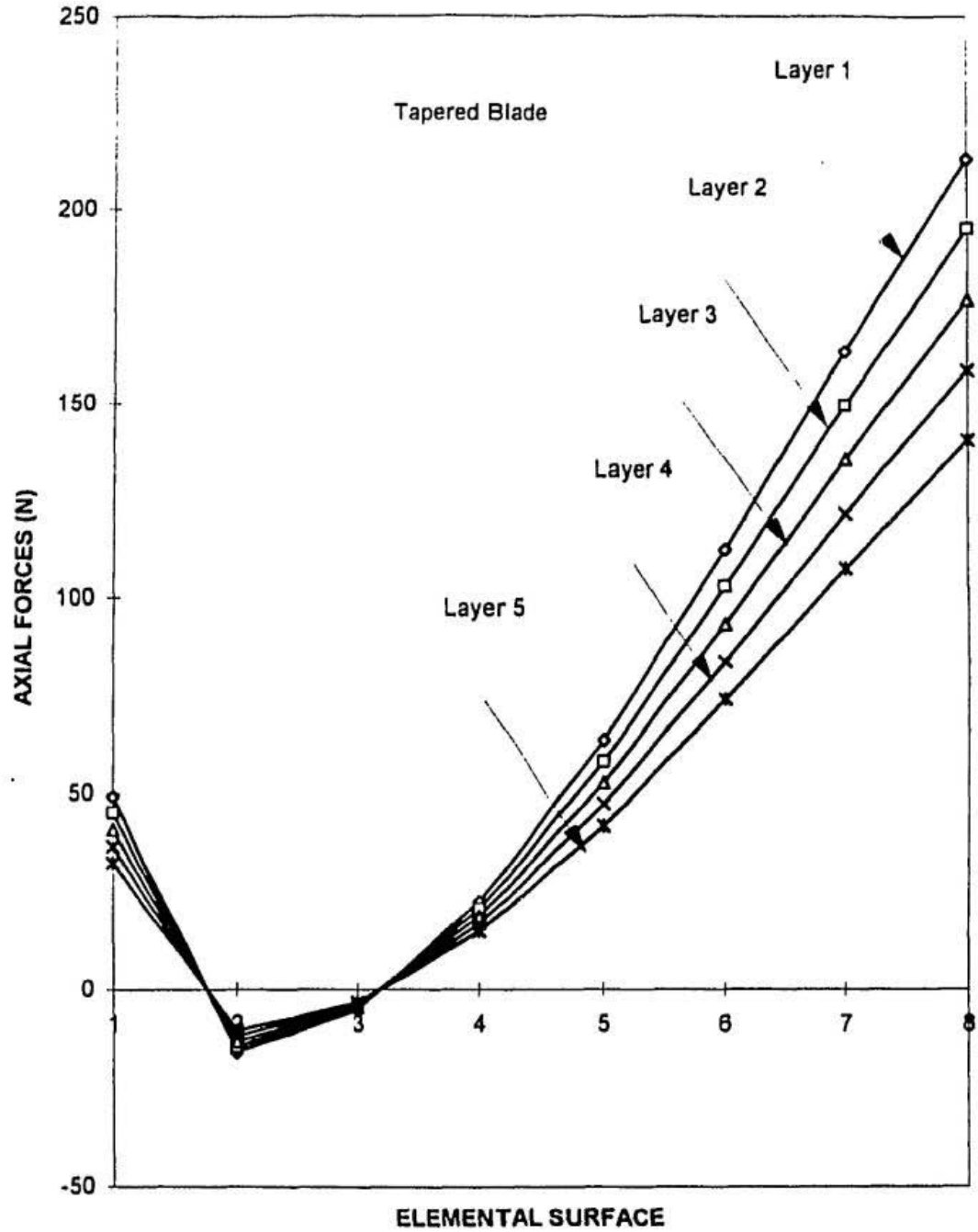

Fig. 3.7 DISTRIBUTION OF AXIAL FORCES ON THE ELEMENTAL SURFACES AND THEIR VARIATION IN ELEMENTAL LAYERS ALONG THE BLADE HEIGHT

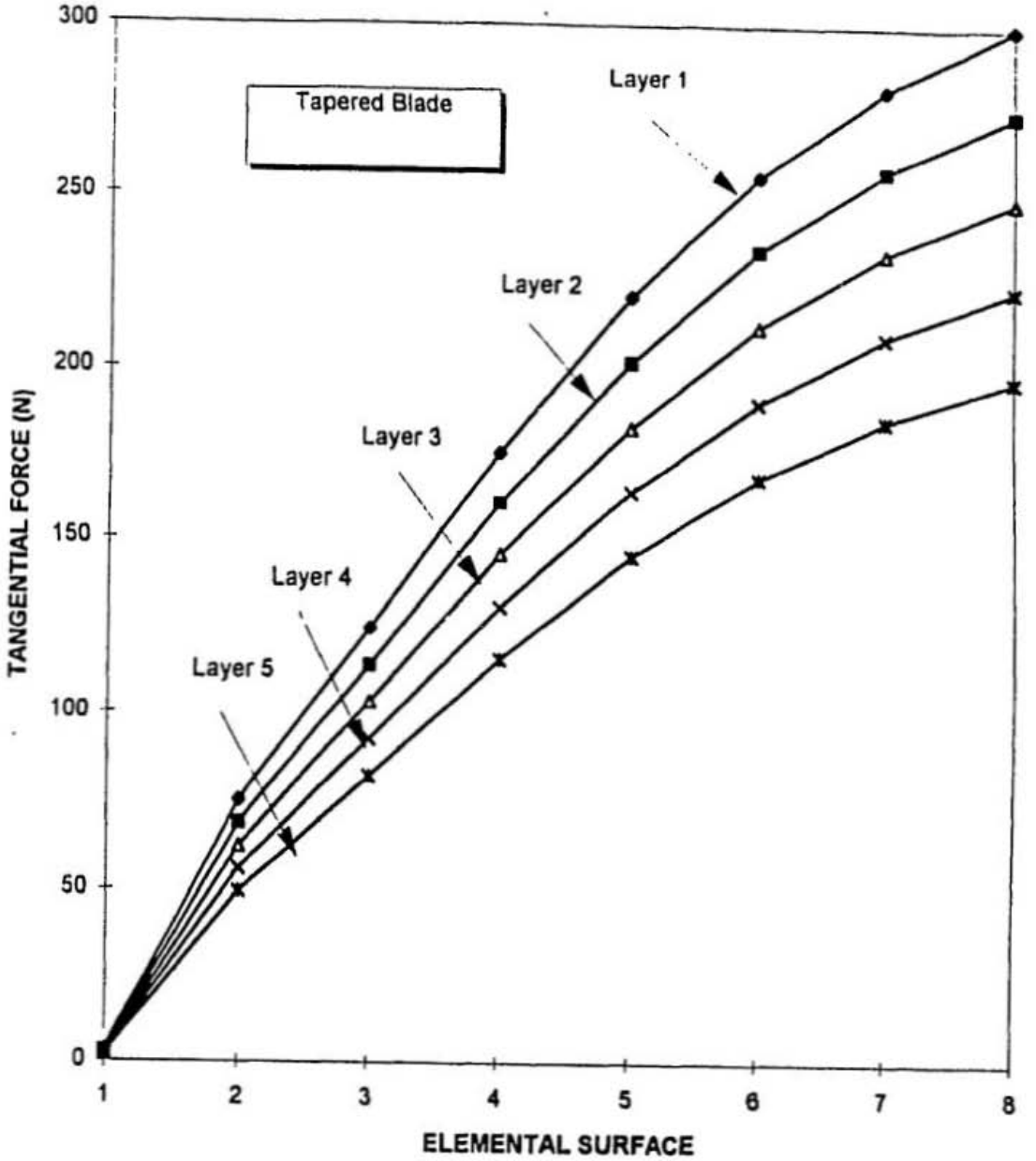

Fig. 3.8 DISTRIBUTION OF TANGENTIAL FORCES ON THE ELEMENTAL SURFACES AND THEIR VARIATION IN ELEMENTAL LAYERS ALONG THE BLADE HEIGHT

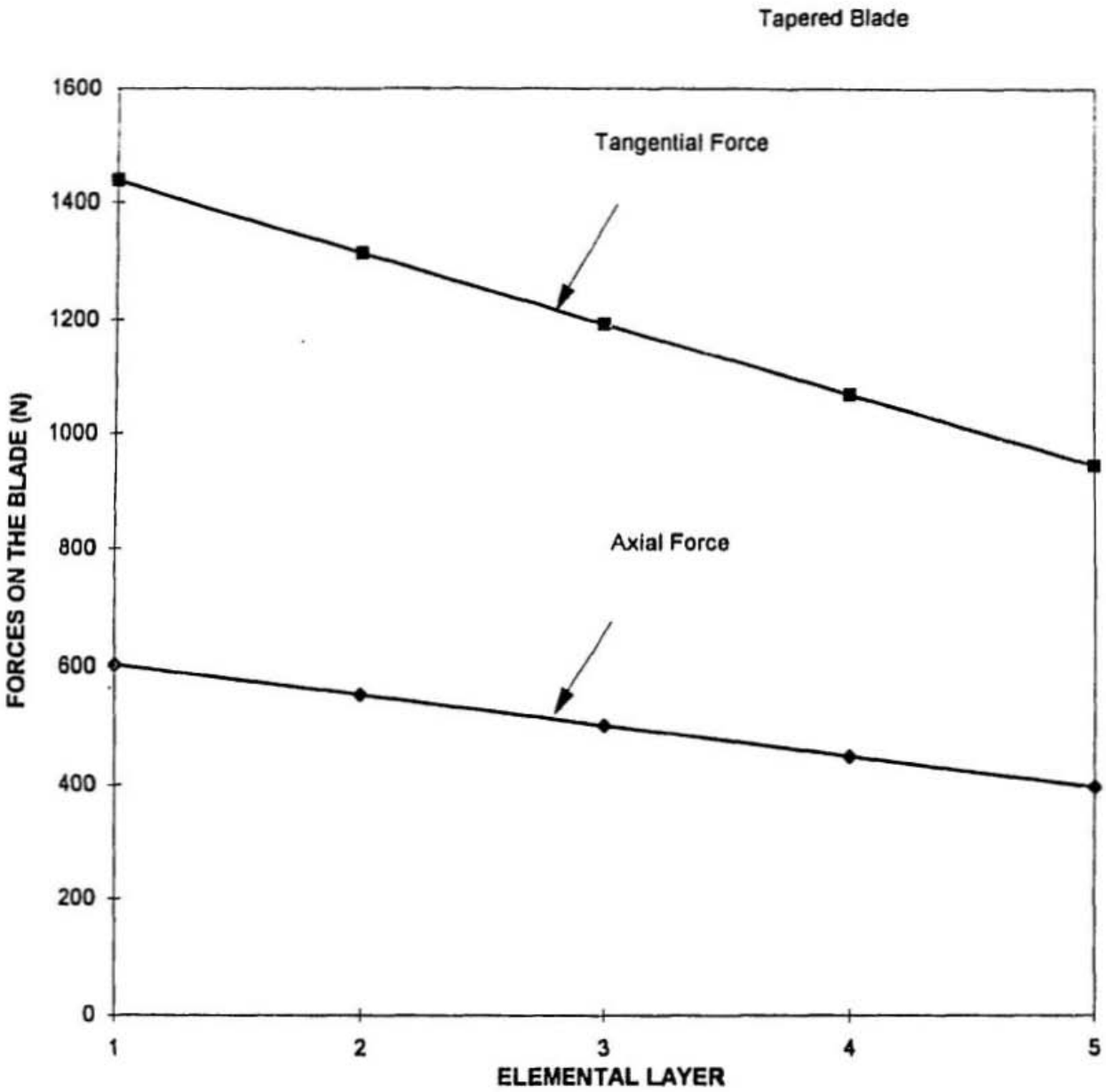

Fig. 3.9 VARIATION OF TOTAL TANGENTIAL AND AXIAL FORCES IN THE ELEMENTAL LAYERS ALONG THE BLADE HEIGHT

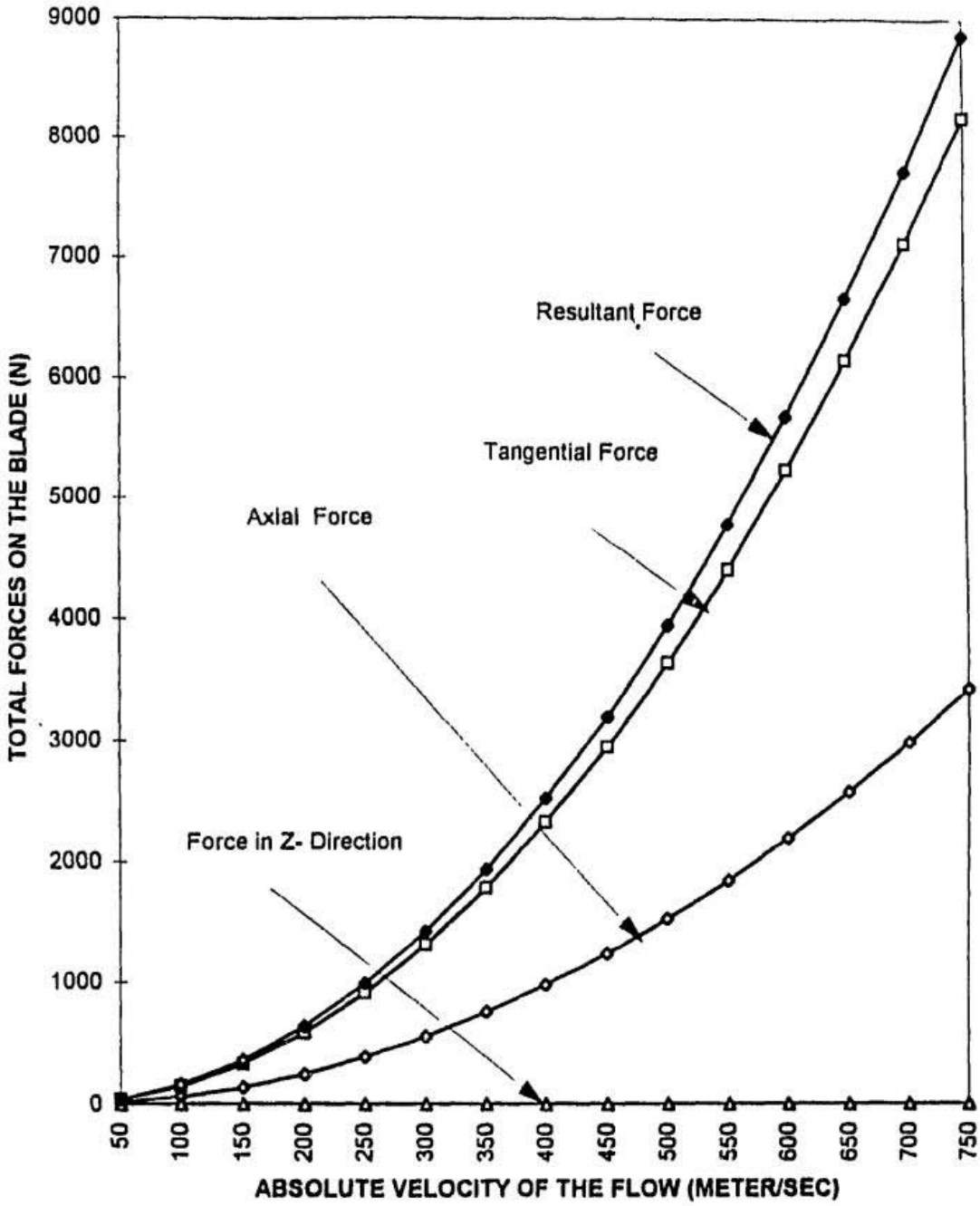

Fig. 3.10 VARIATION OF GAS FORCES DUE TO VARIATION IN ABSOLUTE VELOCITY

$$
\begin{aligned}
{}^{G}\{\Delta F\}^{\phi} &= \rho\, {}^{G}|\{W_1\}|\, (\Delta A_n)^{\phi} \,.\, {}^{G}\{\Delta W\}^{\phi} \\
&\sim f(W_1)^2 \\
&\sim f(V_1)^2 \quad \text{at } \omega = 0 \ ;
\end{aligned}
\tag{3.2}
$$

Thus the force is a second order function of the absolute velocity, which explains the parabolic nature of the variation of forces. The parabolic nature of the curves hold good for both axial, and tangential components of the forces. Similar results are also obtained for the driving torque as shown in the Fig. 3.11. This is because the torque is nothing but the moment of the tangential forces about the global X - axis.

3.4.2 THE EFFECT OF THE ROTOR SPEED VARIATION

Fig. 3.12 shows that the forces acting on the blade decrease with increase in the rotor speed. This decrease shows a linear behaviour. This is primarily due to the decrease in the relative velocity, $\{W_1\}$ of the flow entering the blade passage (refer to Fig. 2.7), and the decrease in the flow entry angle α_1. Similar results were also obtained by other researchers [Rieger et al., 1978].

3.5 A STUDY OF FORCES, TORQUES, AND ANGULAR ACCELERATIONS AT DIFFERENT ANGULAR POSITIONS OF A SINGLE BLADE

The dynamics of the blade under instantaneous nozzle excitations completely depends upon the nozzle geometry, the blade geometry, and the gas flow. A simulation study was carried out at several discrete steps of the angular positions of the blade from

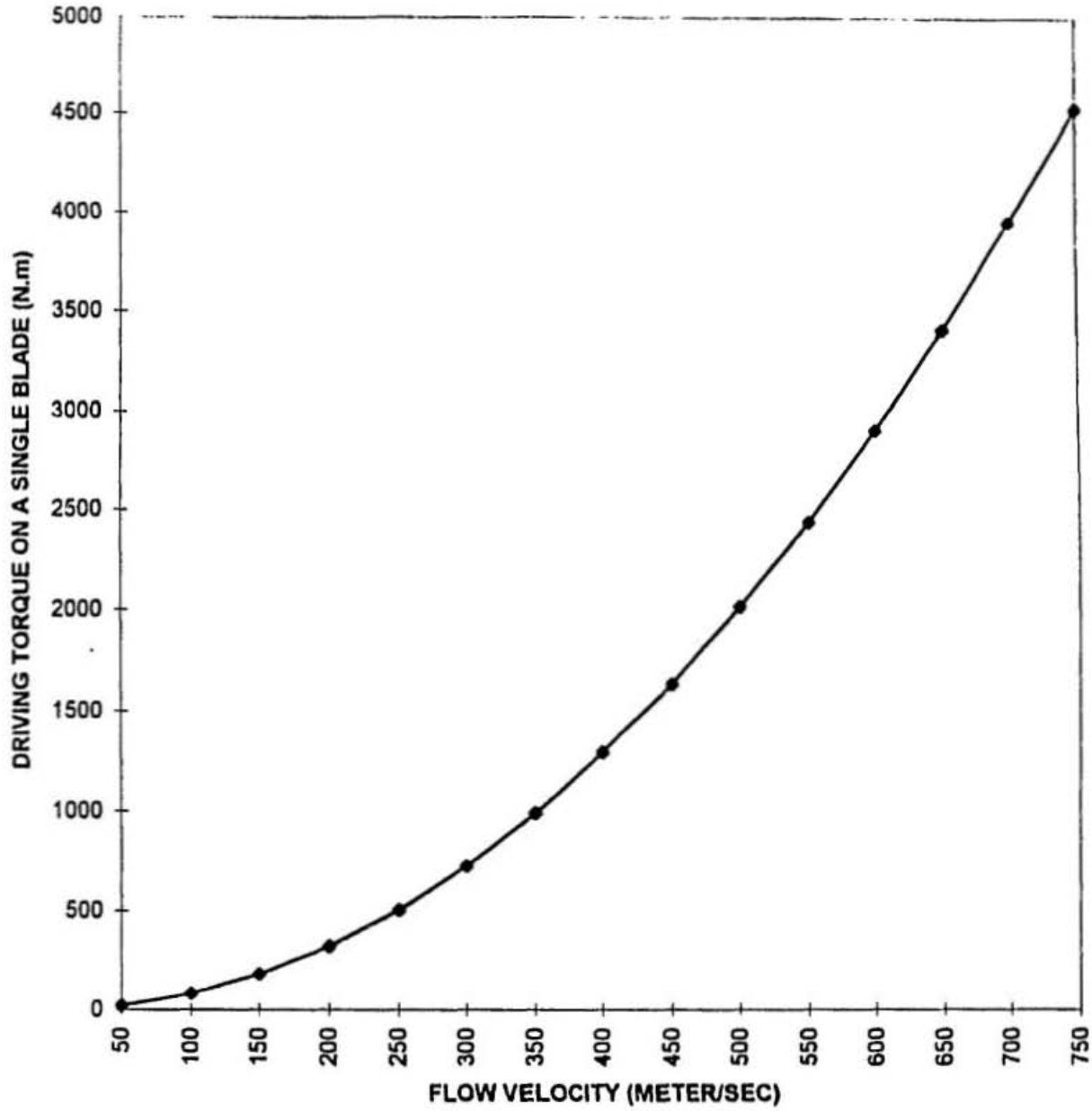

Fig. 3.11 VARIATION OF TORQUE DUE TO VARIATION IN ABSOLUTE VELOCITY

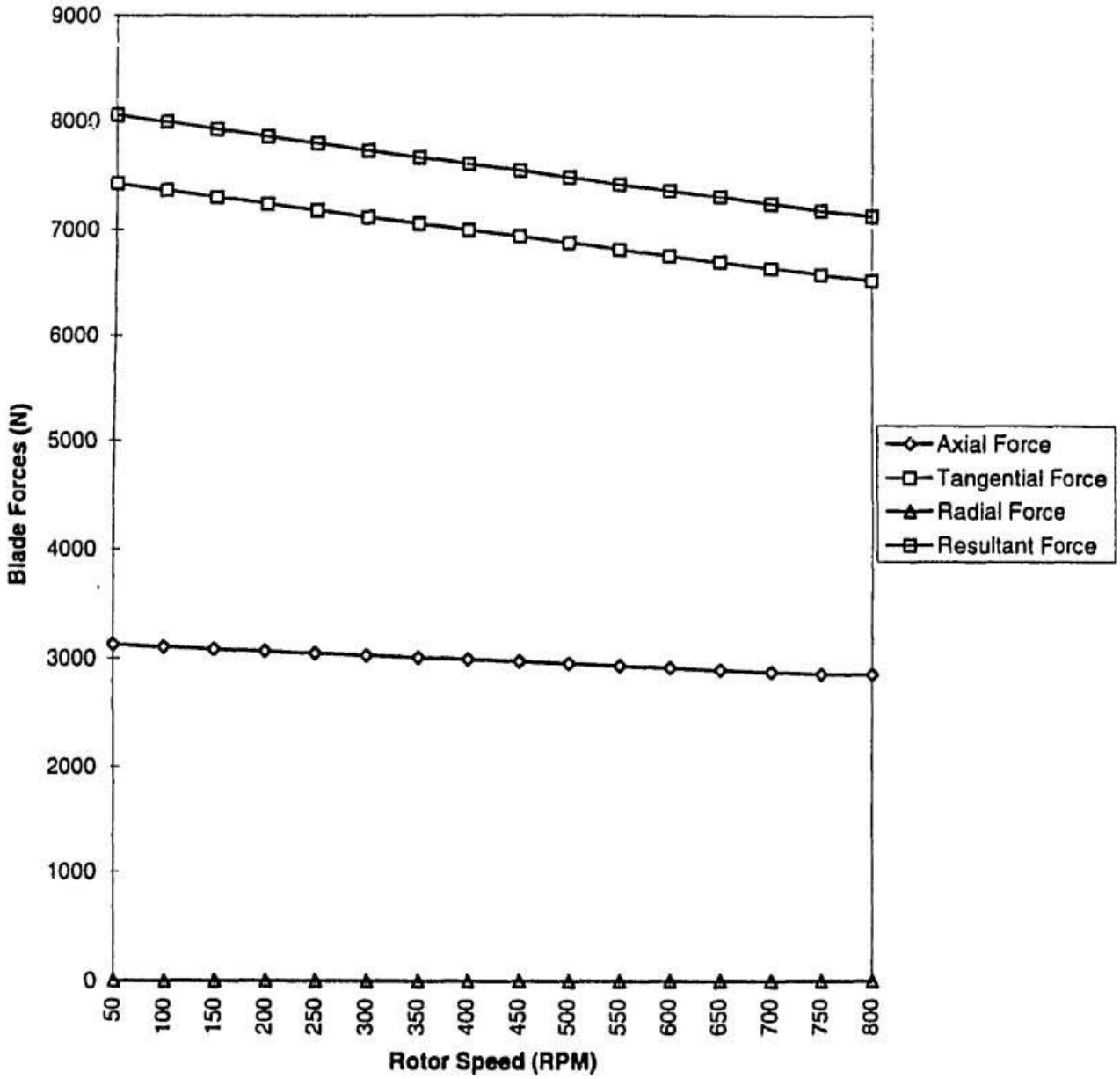

Fig. 3.12 VARIATION OF FORCES DUE TO VARIATION IN ROTOR SPEED

-15° through 15° which covers the rotation of the blade by one circular pitch. The axial spacing between the two (the stator and the rotor) was taken to be 50 % of the chord length. The absolute velocity of the flow has been taken to be 718.05 m/s [Dhar, 1994].

In the previous chapter we developed formulation for a single nozzle causing excitations on a single blade mounted on a rotor disc. For the sake of simplicity, we considered a solid circular disc with its thickness identical to the axial blade width. Table 3.3 shows the calculation of mass moment of inertia of the rotor - disc assembly about the global X - axis.

Figs. 3.13 through 3.17 show the results of the simulation study carried out on a single blade-rotor system excited by a single nozzle. As can be seen from the figure that the gas from the finite nozzle hits the blade only between a range of rotor angular positions. As soon as the gases hit the rotor blade, it starts gaining the momentum and reaches to a peak at certain angular position of the blade where it is completely exposed to the flow from the nozzle. On further movement of the rotor, the mass flow hitting the blade reduces, which explains the reduction in the forces, torque, and the angular acceleration. The position of the peak, however, depends on the flow angle and the axial spacing between the stator, and rotor stage. Also, it can be observed from the Fig. 3.17 that the angular speed of the rotor builds up till the blade remains in the zone of nozzle excitation. The angular speed becomes again constant once the blade loses the flow contact. The angular acceleration at each instant of the angular position of the rotor was

TABLE 3.3

CALCULATION FOR MASS MOMENT OF INERTIA OF A SINGLE BLADE - DISC ASSEMBLY

d, the diameter of the disc = 0.1 m

h, the thickness of the disc = 0.032 m

ρ_d, the density of the material (steel) of the disc = 7860 kg/m^3

M_d, The mass of the rotor disc = $\pi d^2 h \rho_d$ = 197.54 kg.

$^G(I_{xx})_d$, the mass moment of inertia about X - axis = ½ M_d $(d/2)^2$ = 24.6925 Kg-m^2.

$^G(I_{xx})_d$ kg-m^2	$^B(I_{xx})_b$ kg-m^2		$^G(I_{xx})_b$ kg-m^2		$^G(I_{xx})$ kg-m^2	
	Straight Blade	Tapered Blade	Straight Blade	Tapered Blade	Straight Blade	Tapered Blade
24.6925	7.84 x 10^{-4}	3.80 x 10^{-4}	0.04926	0.03167	24.741	24.724

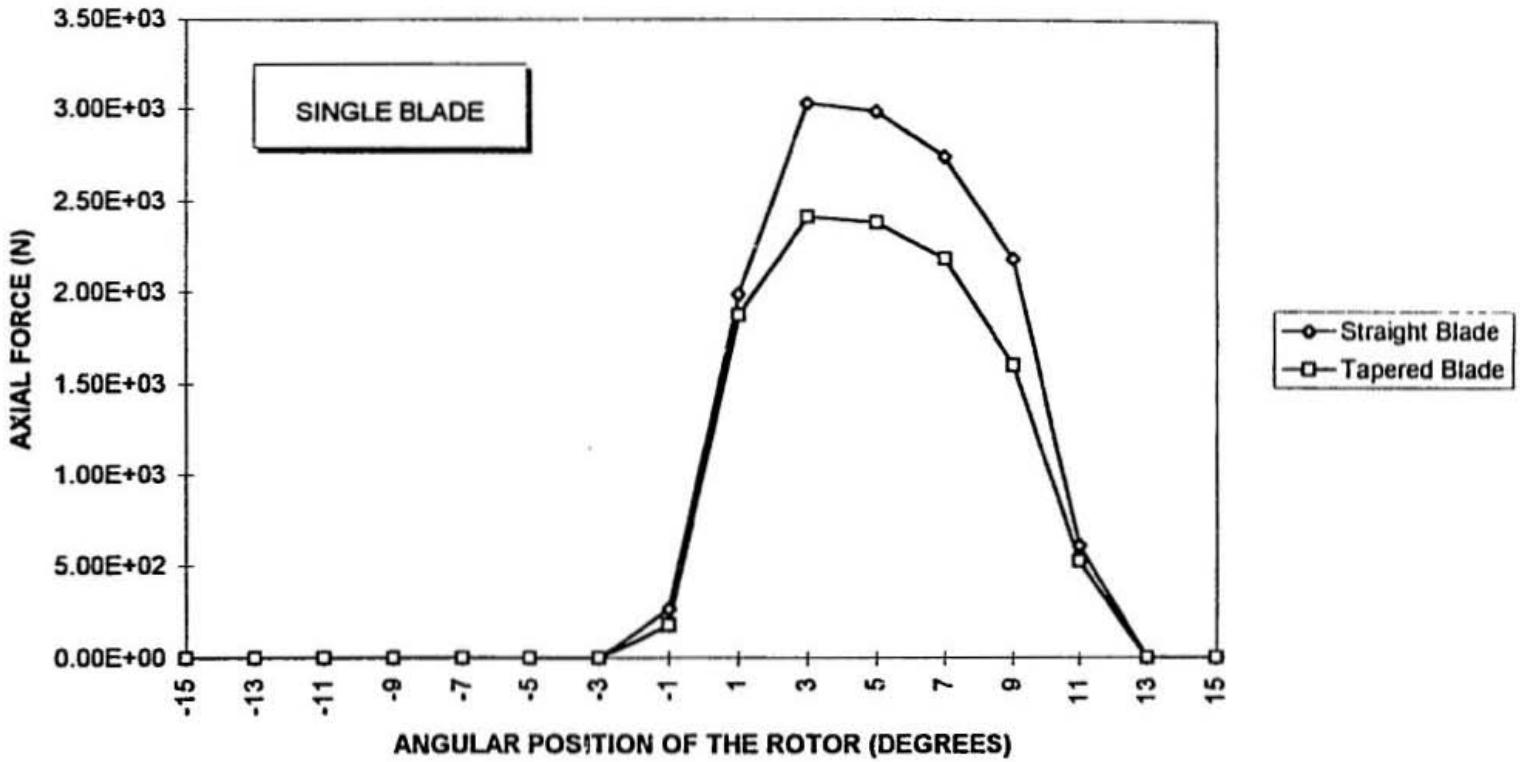

Fig. 3.13 VARIATION OF AXIAL FORCE ON A SINGLE BLADE AT VARIOUS ANGULAR POSITION OF THE ROTOR

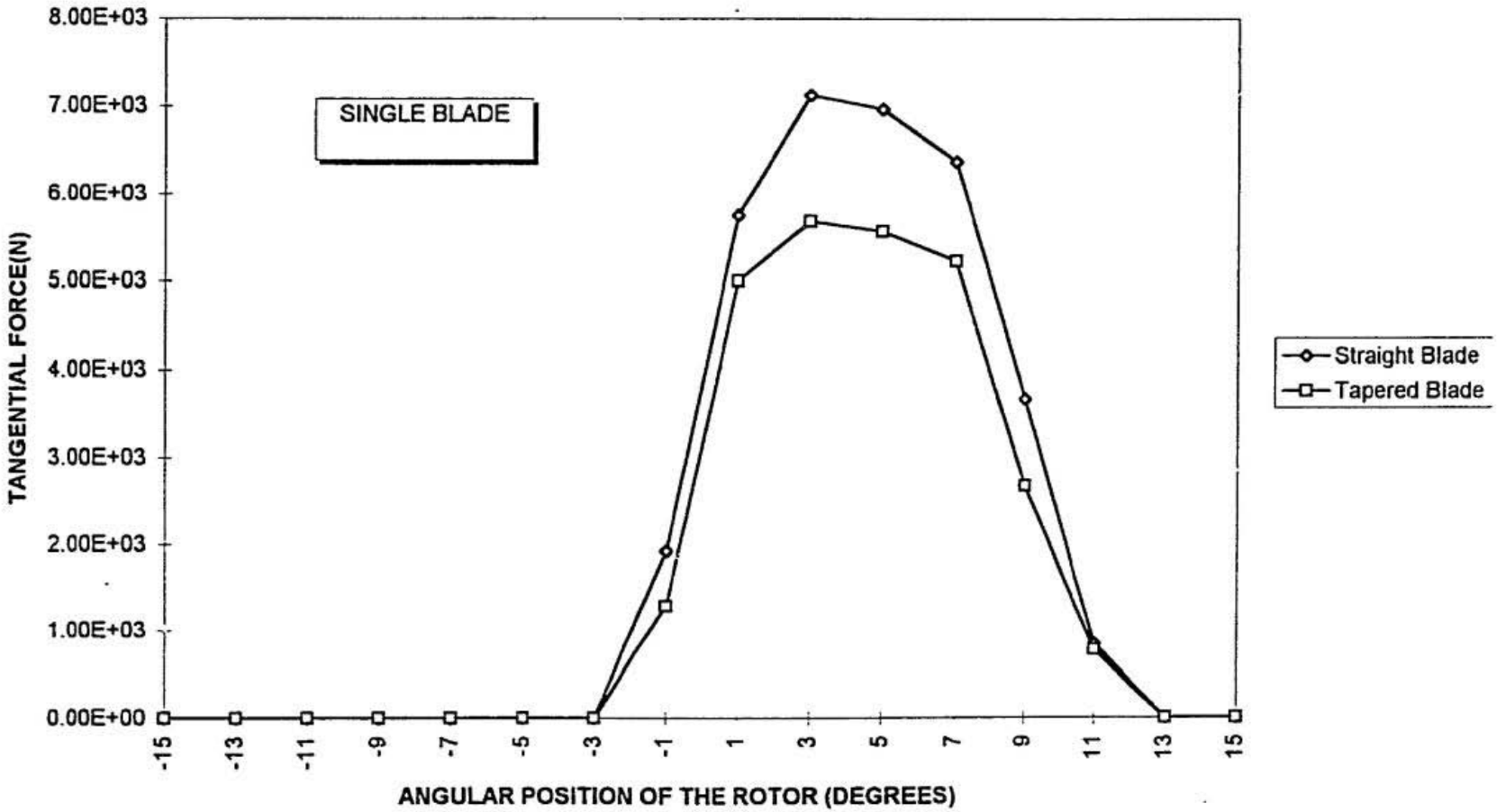

Fig. 3.14 VARIATION OF TANGENTIAL FORCE ON A SINGLE BLADE AT VARIOUS ANGULAR POSITION OF THE ROTOR

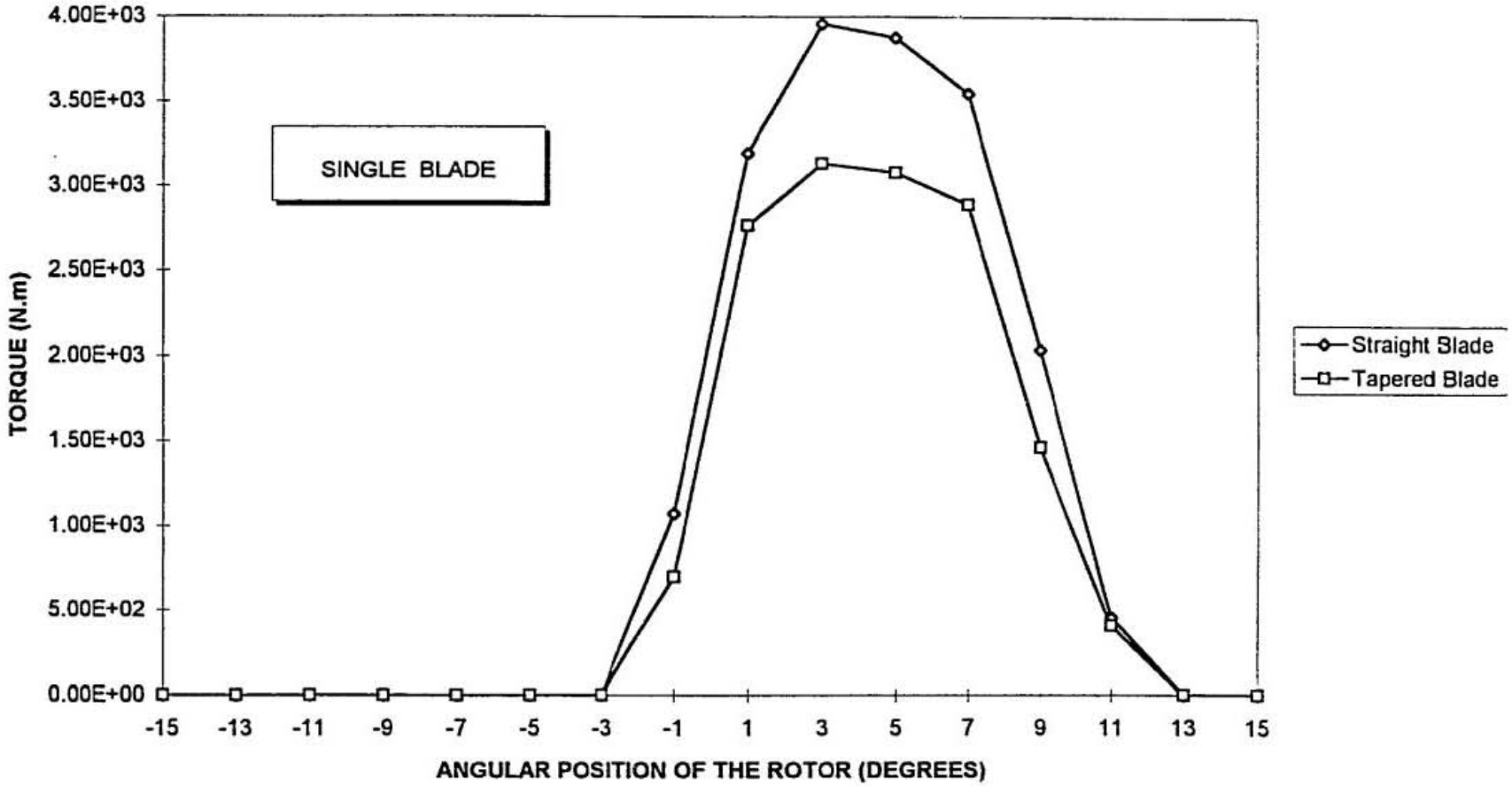

Fig. 3.15 VARIATION OF TORQUE ON A SINGLE BLADE AT VARIOUS ANGULAR POSITION OF THE ROTOR

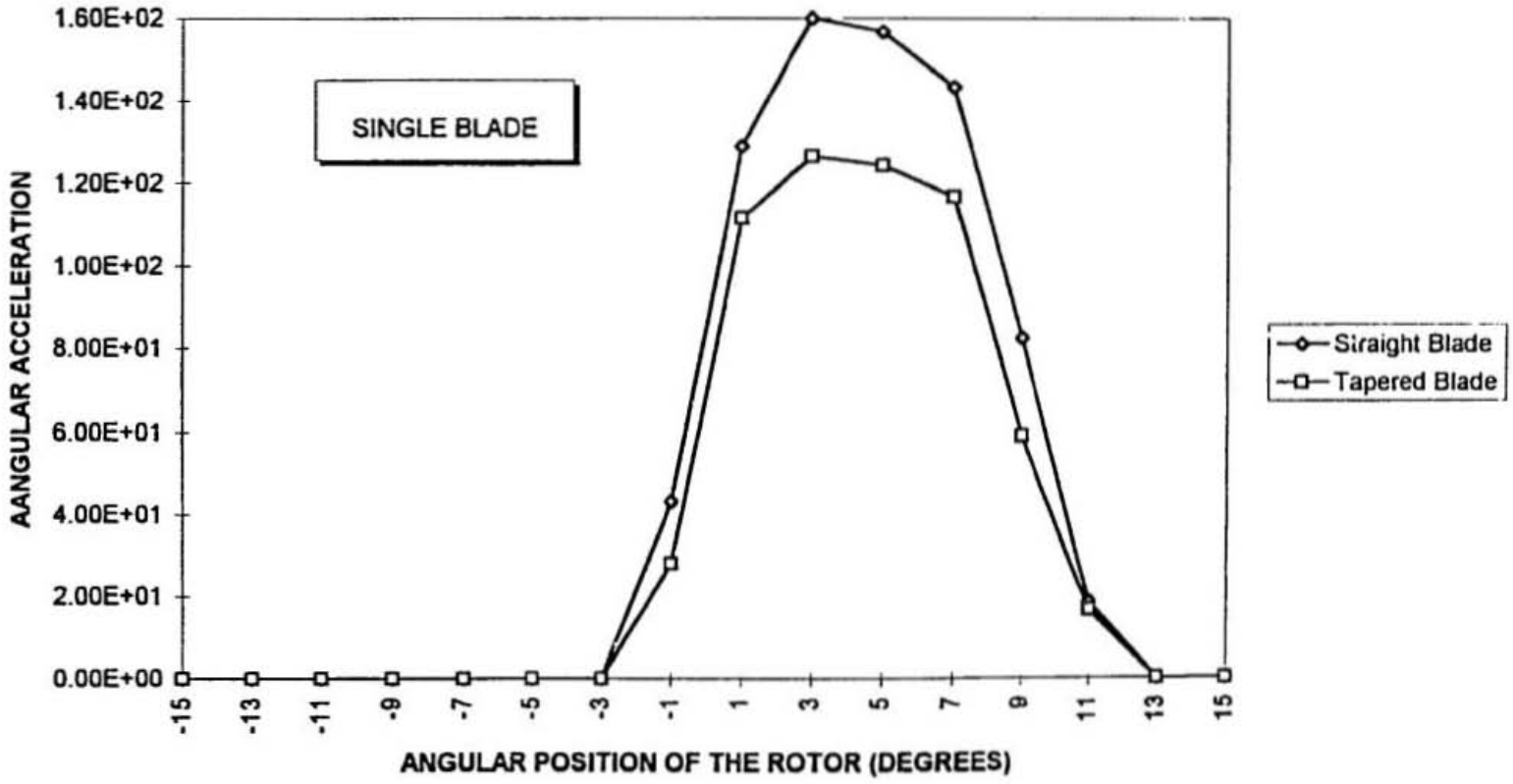

Fig. 3.16 VARIATION OF ANGULAR ACCELERATION OF A SINGLE BLADE AT VARIOUS ANGULAR POSITION OF THE ROTOR

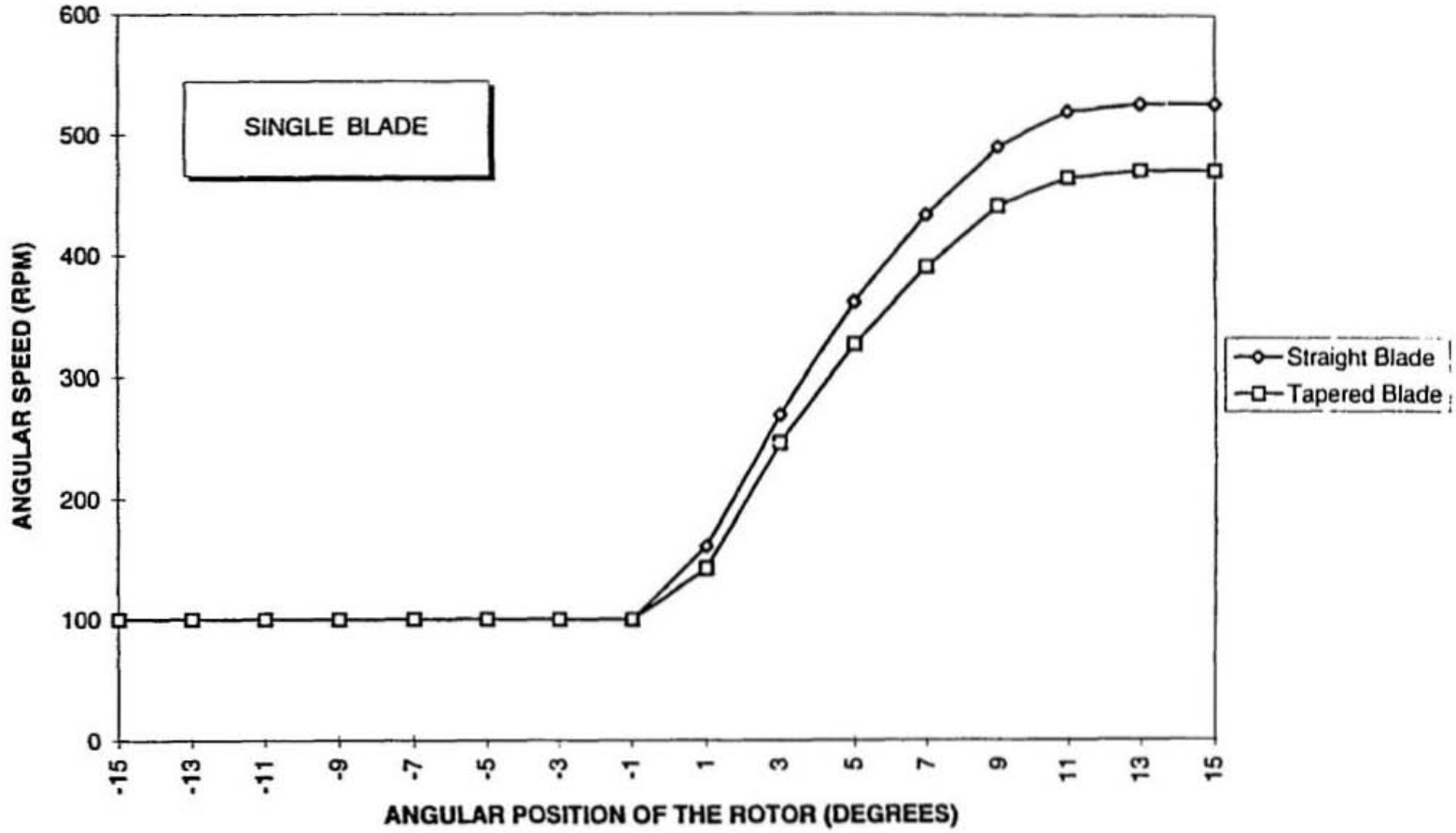

Fig. 3.17 VARIATION OF ANGULAR SPEED OF A SINGLE BLADE AT VARIOUS ANGULAR POSITION OF THE ROTOR

calculated using Eq. (2.35), and was used to obtain the angular speed at that instant. The angular speed over a short interval was calculated using the equation:

$$\omega_f^2 = \omega_i^2 + 2\alpha\Delta\theta \qquad (3.3)$$

It should be noted that the angular acceleration, α, is a variable and varies with the torque. Therefore, it was necessary to discretize the interval -15° to 15° into equal angular steps. The value of α was assumed to be the constant between these steps. The final ω values (i.e. ω_f) shown in Fig. 3.17 would increase further when the blade goes through another nozzle excitation.

The simulation results in Figs. 3.13 to 3.17 also show the comparative study of the straight, and the tapered blades. It can be seen from figures that the forces, and other dynamic parameters in the case of a tapered blade are comparatively quite as compared to the straight blade.

3.6 COMBINED FORCES ON THE ROTOR-BLADE ASSEMBLY SYSTEM

In the previous chapter formulations were developed for a single blade in association with the rotor. However, In order to design an actual system one must consider total forces i.e. the forces on each of the blades being simultaneously excited by each of the nozzles. In the present work, we have assumed the number of nozzles to be equal to the number of blades.

For an identical set of nozzles and blades, the impulse excitation on each blade will be identical. The total forces acting on the complete disc and blade assembly due to nozzle excitations can be given by:

$$\Sigma \{F\} = \sum_{\lambda=1}^{n_b} [R_x(\theta_\lambda)] \{F\}_1 \qquad (3.4)$$

where n_b is the number synchronous sets of blades or nozzles arranged radially. $\{F_1\}$ is the force obtained on a single blade. Here, $[R_x(\theta_\lambda)]$ is the rotation matrix (rotational operator) about the global X - axis passing through the centre of the rotor-disc assembly. It is used to obtain the simultaneous forces on the other blades spaced at angle θ_λ form the first blade. It can mathematically be expressed as:

$$\theta_\lambda = \theta_1 + (\lambda - 1) \times \frac{2\pi}{n_b} \qquad (3.5)$$

where θ_1 is the angular position of the first blade in Y - Z plane of the global frame.

In the force equation, one should note that the overall force, $\Sigma\{F\}$ has three components where:

ΣF_x = Net force in X - direction. This is the total reaction force on the bearings.

ΣF_y = Net force in tangential direction. For blades at equal angular spacing, this force accrues to nil.

ΣF_z = Net force in radial direction. This force is responsible for the bending of the rotating wheel shaft. For blades at equal angular spacing, this force accrues to nil.

Similarly, the net driving torque on the rotor - blade system can be given by the cross product of the point of application, and the corresponding impulse force on the blade will be

$$\Sigma \{T\} = \sum_{\lambda=1}^{n_b} \left\{ [\, R_x(\theta_\lambda)\,]\, \{R_d\}_\lambda \right\} \times \left\{ [R_x(\theta_\lambda)]\, \{F\}_1 \right\} \qquad (3.6)$$

where $\{R_d\}$ is a 3 x 1 column matrix representing the position vector of the point of application of the impulse force on an individual blade. Now, the total driving torque on the turbine rotor stage is given by the x - component of overall moment about the origin of the global frame.

The angular acceleration in this case would be:

$$\alpha = \frac{\Sigma T_x}{\Sigma I_{xx}} \qquad (3.7)$$

where ΣI_{xx} is the combined mass moment of inertia of the rotor disc and the total number of blades. Referring to Eqs. (2.38) and (2.39), one can write

$$\Sigma I_{xx} = {}^{G}(I_{xx}) + (n_b - 1)\, {}^{G}(I_{xx})_b \qquad (3.8)$$

where ${}^{G}(I_{xx})$ is the combined mass moment of inertia of the rotor disc and a single blade whereas ${}^{G}(I_{xx})_b$ is the mass moment of inertia of an individual blade about the global X - axis.

Fig. 3.18 shows the total resultant force characteristics of the entire stage consisting a set of twelve nozzles, and identical number of blades arranged radially at equal angular interval. From the figure, one can observe that both the tangential, and the radial forces get cancelled due to synchronous effect on the radially opposite blades. However, the axial forces on all individual blades get combined to give the net bearing force on the rotor. From this figure, it can also be seen that the total bearing force varies with the blade rotation. Fig. 3.19 shows the similar combined effects on the total driving torque on the rotor.

Table 3.4 shows the distribution of the forces on a set of twelve tapered blades simultaneously excited upon by the identical number of nozzles at a given angular position. The last row shows the summation of all the blade forces along the global direction. One can see that the sum of all the forces in radial and tangential direction becomes nil. These results clearly depict a balanced system in the global Y - Z plane. All axial forces acting in the same direction get accrued, and thus suggests the need of suitable bearing to take up the loads in axial direction.

Fig. 3.20 shows the comparative variation of angular acceleration due to simultaneous excitations on all twelve blades with that of a single blade. The angular acceleration in the case of twelve blades is approximately equal to twelve times the value for a single blade. It would not be strictly equal to 12 times since the inertia of the other 11 blades is also included in results for a single blade.

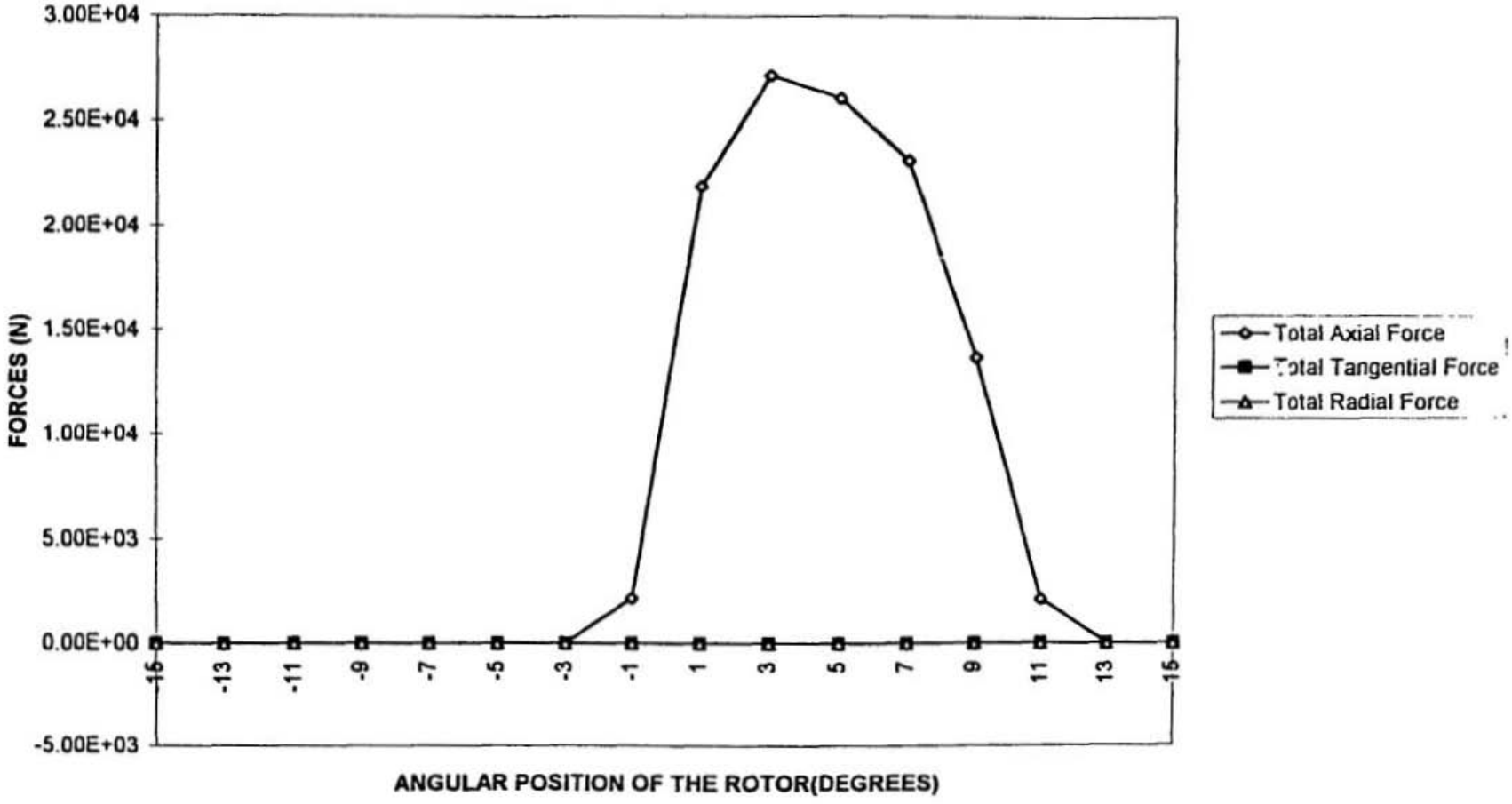

Fig. 3.18 VARIATION OF TOTAL FORCES DUE TO SIMULTANEOUS EXCITATIONS ON ALL BLADES

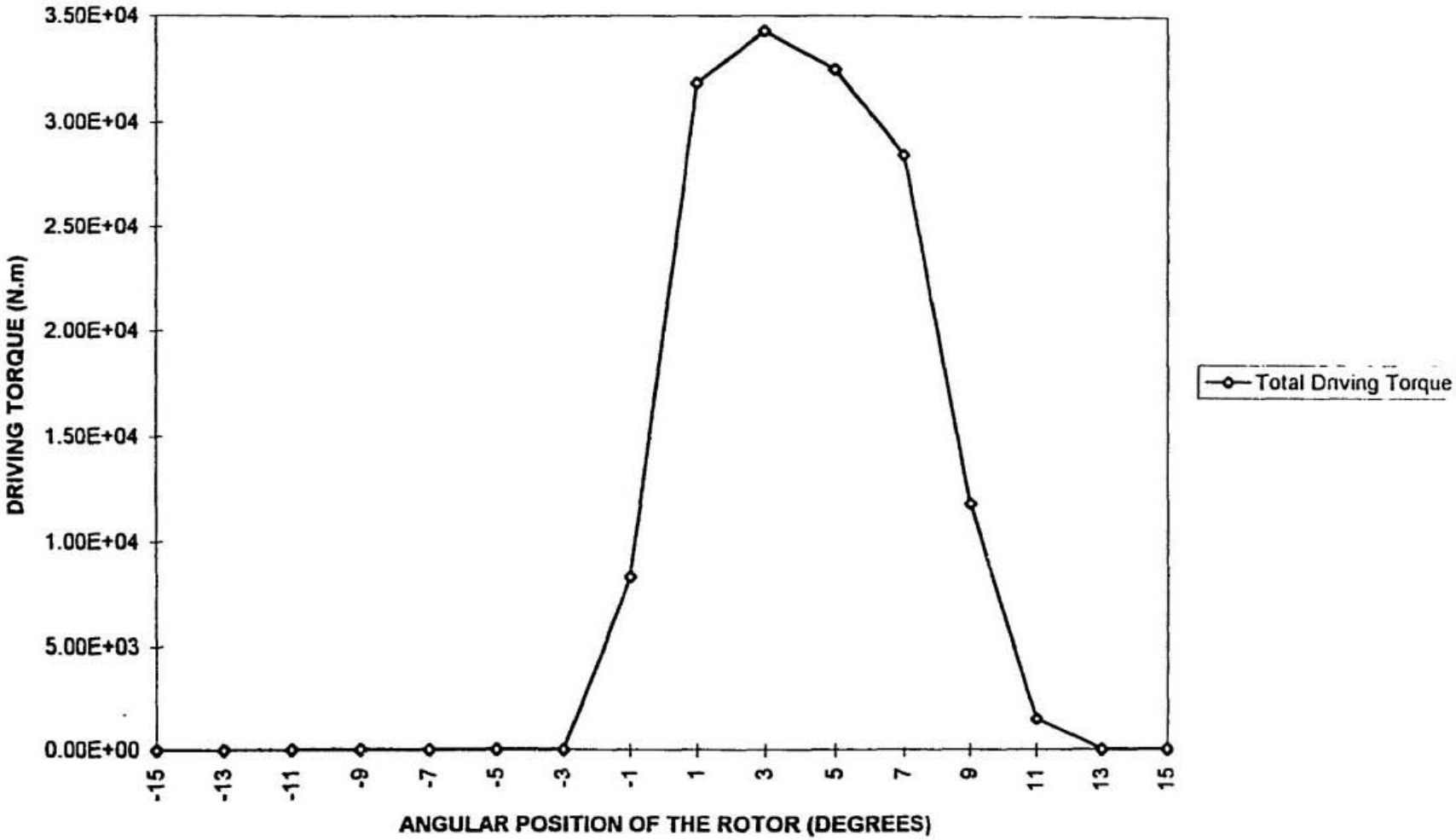

Fig. 3.19 TOTAL DRIVING TORQUE DUE TO SIMULTANEOUS EXCITATIONS ON ALL BLADES

TABLE 3.4

DISTRIBUTION OF SIMULTANEOUS NOZZLE EXCITATIONS ON ALL BLADES AT $\theta_1 = 3°$

Blade Number	Angular Position θ_λ	Axial Force (N)	Tangential Force (N)	Radial Force (N)
1	3°	2260.316	5187.046	-279.4247
2	33°	2260.316	4631.827	2351.532
3	63°	2260.316	2835.515	4352.399
4	93°	2260.316	279.4313	5187.045
5	123°	2260.316	-2351.526	4631.83
6	153°	2260.316	-4352.396	2835.52
7	183°	2260.316	-5187.045	279.4366
8	213°	2260.316	-4631.832	-2351.522
9	243°	2260.316	-2835.526	-4352.392
10	273°	2260.316	-279.444	-5187.045
11	303°	2260.316	2351.514	-4631.836
12	333°	2260.316	4352.387	-2835.533
$\Sigma\{F\}$		27123.792	0.00	0.00

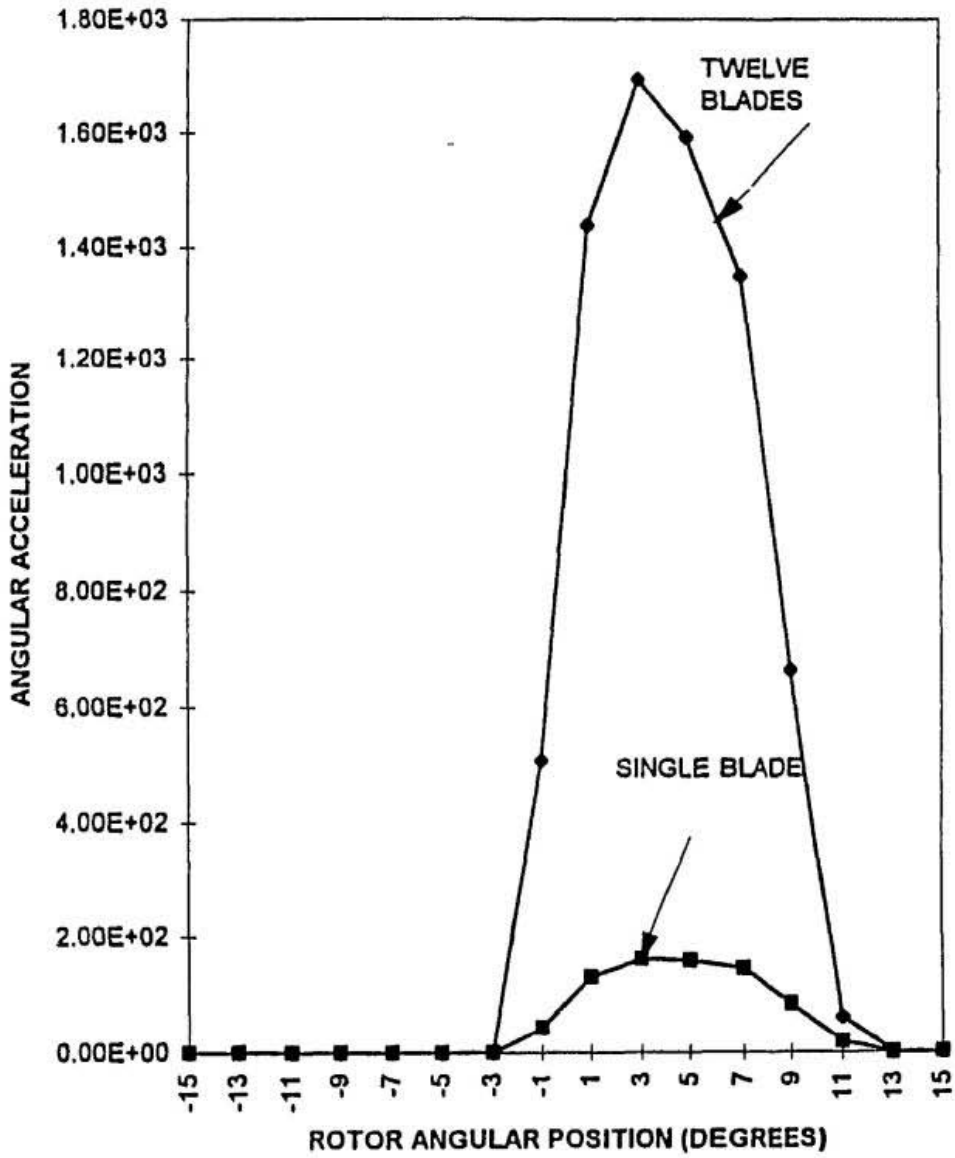

Fig. 3.20 VARIATION OF ANGULAR ACCELERATION - SINGLE BLADE VS. TWELVE BLADES

Fig. 3.21 shows the comparative results due to variation in the angular speed of the rotor. One can notice that the angular speed of the twelve blade-rotor system was not twelve times the angular speed of the single blade-rotor system. This is because the square of angular speed varies linearly with the acceleration which is quite evident from Eq. (3.3).

In summary, we can say as mentioned in the Section 3.1, the forces on the rotor blades at any position were calculated by dividing the blade surface into several finite surfaces. The effect of the nozzles geometry and the gas velocity were considered. Finally, the angular speed of the rotor-blade and the shaft system was also calculated based on the forces on all the blades.

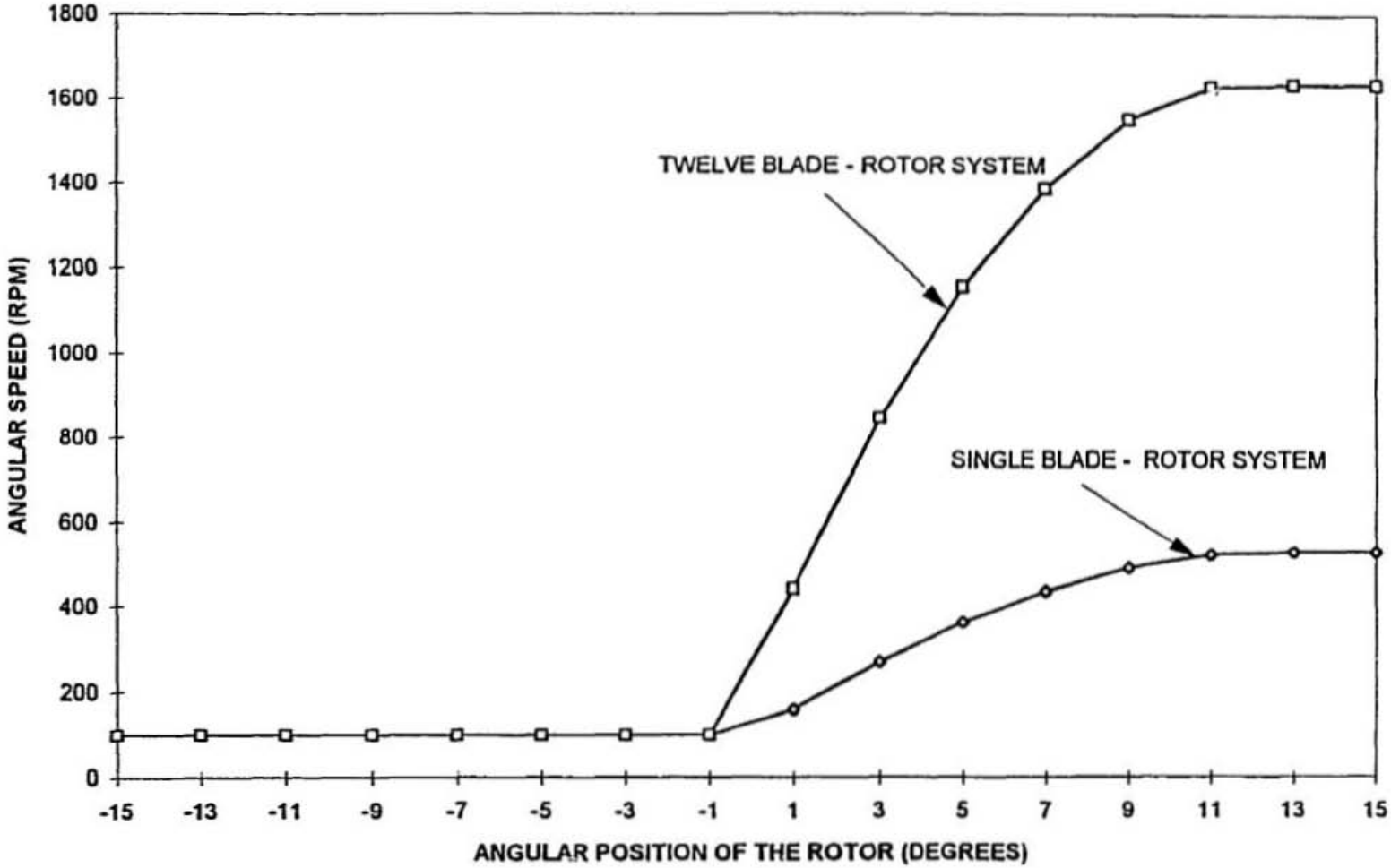

Fig. 3.21 VARIATION OF ANGULAR SPEED - SINGLE BLADE VS. TWELVE BLADES

CHAPTER 4

CONCLUSIONS AND RECOMMENDATIONS

4.1 DISCUSSION AND CONCLUSIONS

The objective of the present work was to develop an analytical model, and to study the impulse forces acting on the rotating blade by considering the flow interaction with the entire blade in three-dimensional frame work. The theoretical formulations were developed in Chapter 2 where this was achieved by suitably defining the coordinate systems on the blade, the rotor shaft, and the nozzle at its one of the exit points. The blade was discretized using C°-continuity, 20-noded serendipity elements in order to map the complicated geometry. Each surface of the blade finite element was defined by two sets of vectors, one along the cross-section facing the nozzle, and the other along the blade height. The nozzles and blades were spaced at approximately 50% of blade chord length. The velocity of the fluid flow from the finite nozzle was modelled as a vector, and its corresponding interaction with the rotating blade surface was obtained. Such a modelling tends to be quite complicated because (a) the geometries are quite complicated, and (b) there is always a relative motion between the blade and the nozzle. The major difficulty in modelling is the orientation of the vectors in three dimensions. The flow interaction with the blade surface was modelled as a reflection process in three dimension. This was done by defining the local frame of references at each of the dynamic blade

surfaces, and the incident flow vector was rotated in a plane normal to the blade surface to obtain the reflected flow vector, and then the corresponding change in the momentum was calculated by their difference in the global frame. The mass flow was estimated for each finite surface by considering projection of the surface over a plane normal to the incident relative velocity vector. The impulse force was calculated by the change of momentum over each finite element, and then were summed up to obtain the total force over the blade surface. In Chapter 2, The torque, and angular acceleration were calculated for a single blade rotor system, and the blade dynamics were presented.

In Chapter 3, the model was compared with the conventional model. The variations of various parameters viz. the geometry of the nozzle, and the blade, the absolute flow velocity etc. were carried out on a single blade at a typical position. Finally, the equations were formulated for a multi-blade rotor system to calculate the combined forces, torques, and angular accelerations using the inertia of the combined system, and results were presented for a set of 12 nozzle-blade system.

The studies carried out in this investigation helps one to draw the following conclusions:

1. The present analytical model can be successfully used to present the state of the forces, the torques, angular acceleration, etc. on a gas turbine blade under nozzle excitations. On a comparative study of forces computed based on this investigation and those obtianed by the conventional model, a close agreement was obtained.
2. The forces on the blade increase with the increase in the nozzle opening angle, θ_N, to a limiting value. Beyond that, the forces become constant, i.e. a saturation is reached.

3. The forces acting on the blade are highly dependent on the blade geometry in terms of the orientation of the blade surfaces with respect to the incident relative velocity.

4. The forces and torques on the tapered blade were found to be significantly less compared to that on the straight blade.

5. A parabolic nature of the forces and torques were obtained due to increase in the absolute velocity of the gases.

6. With increase in the rotor speed the magnitude of the forces and torques decrease.

7. The forces, and the torques acting on the blade are a function of the blade position with respect to the nozzle. These forces and torques increase to a maximum value, and then decrease with the rotation of the blade.

4.2 LIMITATIONS OF THE PRESENT WORK AND RECOMMENDATIONS FOR FUTURE WORK

1. There is a possibility that the flow, after getting reflected from the blade surface might hit some other element(s) of the same blade and, or the adjacent blade. The reflected flow velocity can be traced forward and its further interaction with the blade surfaces can be investigated. Moreover, one can also trace the velocities at exit from one stage as the inlet velocity for the next stage.

2. In Section 2.2.3.3, the formulation for mass flow calculation was developed by using an approximate method by considering the maximum X-Y bound of the

nozzle projection. This is supposed to give a conservative estimate of the force over the blade. However, the method should be revised to calculate the exact value of the exposed area.

3. An experimental verification is required to investigate the accuracy of the results.

4. The excitations give rise to fluctuating loads on the blade, and are well known to cause vibration in the turbines. The forces obtained from the present work can be used to study the vibratory effects on the blades and rotor disc systems.

REFERENCES

Adamczyk, J. J., Mulac, R. A., and Celestina, M. L., 1986, " A Model for Closing the Inviscid Form of the Average Passage Equation System, " ASME paper No. 86-GT-227; NASA TM-87199.

Adamczyk, J. J., 1984, "Model Equation for Simulating Flows in Multistage Turbomachinery," ASME paper No. 85-GT-226; NASA TM-86896.

Bahree, R., 1987. "Analysis and Design of Rotor Blades Due to the Transient Thermal and Vibratory Loads", M. Eng. thesis, Memorial University of Newfoundland, Canada.

Boyce, P. Maherwan, 1982. "Gas Turbine Engineering Handbook", Gulf Publishing Company.

Craig, J., 1989. "Introduction to Robotics - Mechanics and Control", Addison-Wesley Publishing company, Inc.

Csanady, G.T., 1964. "Theory of Turbomachines", McGraw-Hill Book Company.

Denton, J. D., and Singh, U. K., 1979, "Time Marching Methods for Turbomachinery Flow Calculations," Applications of Numerical Methods to Flow Calculation in Turbomachines, VKI-LEC-SER, 1979-7, Von Karman Institute for Fluid Dynamics, Rhode-Saint-Genese, Belgium.

Dhar, D., 1994, "Fatigue Life Estimation Of Turbine Blades doe to Transient Thermal, Vibratory, and Centrifugal Stresses", M. Eng. Thesis, Memorial University of Newfoundland, Canada.

Dzung, L.S., 1970. " Flow Research On Blading", Proceeding Of the symposiums\ on flow research on Blading, Brown, Boveri & Company Limited, Baden, Switzerland, Elsevier Publishing Company.

Gundy-Burlet, K.L., Rai, M. M., Stauter, R. C. and Dring R. P., 1990, "Temporally and Spatially Resolved Flow in a Two Stage Axial Compressor. Part 2 - Computational Assessment", ASME, 90-GT-299.

Hoyt, J. W., 1962, " The Hydraulic Analogy for Compressible Gas Flow," *Applied Mechanics Review,* Vol. 15, No. 6, p. 419-425.

Huebner H.B. and Thornton, E.A., 1982. "The Finite Element Method for Engineers", John Wiley & Sons.

Jennings, B. H. and Rogers, W. L., 1953, "Gas Turbine Analysis and Practice", McGraw-Hill Book Company, Inc.

Karman, T. and Sears, W. R., 1938, "Airfoil Theory for Non-Uniform Motion", J. Aero Sci., 5, p. 371

Kemp, N. H. and Sears, W. R., 1953, "Aerodynamic Interference Between Moving Blade Rows", J. Aero Sci., 20, p. 585

Kerrebrock, J. L., 1977, "Aircraft Engines and Gas Turbines", The MIT Press.

Loh, W. H. T., 1959, "Hydraulic Analogy for Two-Dimensional and One Dimensional Flows," Journal of the Aero/Space Sciences, Vol. 26, No. 6, p. 289-291.

McFarland, E. R., 1982, "Solution of Plane Cascade Flow Using Improved Surface Singularity Methods", J. of Engineering for Power, Vol. 104, p. 668-674.

Ni, R. H., 1987, "Flow Simulation in Multistage Turbine," presented at the NASA Marshall Space Flight Center Computational Fluid Dynamics Workshop, Apr.

Osborne, C., 1971, " Compressibility Effects in the Unsteady Interaction Between Blade Rows", Ph. D. Thesis, Cornell University, 1971.

Rai, M. M., 1985, "Navier-Stokes Simulations of Rotor-Stator Interaction using Patched and Overlaid Grids", AIAA-85-1519.

Rao, V. V. R., and Rao, J. S., 1987," Effect of Downwash on the Non-steady Forces in a Turbomachine Stage", *Bladed Disk Assemblies*, ASME DE-vol 6, p. 21.

Rao, J. S. et al., 1985, "Nonsteady Force Measurement in Orpheus Gas Turbine Engine Using Hydraulic Analgoy", Def. Sci., Journal, 35, p. 391.

Rao, J. S. et al., 1991, "Turbomachine Blade Vibration", Wiley Eastern Limited.

Rao, J. S., 1980-81, "Hydraulic Analogy for Compressible Gas Flow in Converging Nozzles" 80-ID002-1;, "Simulations of Compressible Gas Flow in Converging-Diverging Nozzles by the use of Hydraulic Analogy ", 80-ID002-2;,"An Examination of Errors in Hydraulic Analogy for Nozzle Flows with Compressible Normal Shock", 80-ID002-3; "The Effect of Straight Oblique Shock Waves on Hydraulic Analogy", 80-ID002-4; " A study of Nozzle Exit Flows by Hydraulic Analogy", 80-ID002-5; Stress Technology Inc., Rochester, NY.

Rieger, N. F., 1975," Theory of Hydraulic analogy in Cylindrical Coordinates for Non-Steady Potential Flow," Wehle Research Laboratory Report, 75 WRL-M3, Rochester Institute of Technology, Rochester, New York.

Sharan, A. M. and Agarwal, S., 1996, "Determination of Three-Dimensional Forces and Troques in an Impulse Turbine", accepted for presentation in the 6th International Symposium on Transport Phenomena and Dynamics of Rotating Machinery to be held at Hawaii in Feb. 1996.

Smith, L. H., Tr., 1966, " The Radial-Equilibrium Equation of Turbomachinery," ASME J. of Engineering for Power, Fol. 88, No, 1, p. 1-12

Treager, I.E., 1970. "Aircraft Gas Turbine Engine Technology", McGraw-Hill Book Company.

Vincent, E.T., 1950. "The Theory and Design of Gas Turbines and Jet Engines", McGraw-Hill Book Company Inc.

Wu, Chung-Hua, 1952," A General Theory of Three-Dimensional Flow in Subsonic and Supersonic Turbomachine of Axial-, Radial-, and Mixed-Flow Types," NACA TN 2604.

APPENDIX A

A.1 GENERAL MAPPING AND THE TRANSFORMATION OF THE FRAMES

Very often we know the description of a vector with respect to some frame B, and we would like to know its description with respect to another frame A. This can be done using a general mapping involving the translation and the orientation of the frame with respect to each other. As shown in the Fig. A.1, ${}^{A}P_{BORG}$ is a vector that locates the origin of the frame B with respect to frame A. Also the frame B is oriented with respect to A. Given a vector ${}^{B}P$ in the frame B, we wish to compute the vector ${}^{A}P$. This can be done as follows:

We can first change ${}^{B}P$ to its description relative to an intermediate frame which has the same orientation as frame A, but whose origin is coincident with the origin of the frame B. This is done by premultiplying by a 3X3 matrix called rotation matrix, ${}^{A}_{B}[R]$, which describes the orientation of frame B with respect to the frame A. This orientation matrix can be given by a set of three vectors as follows:

$$ {}^{A}_{B}[R] = \underset{3 \times 3}{\begin{bmatrix} {}^{A}\hat{X}_B & {}^{A}\hat{Y}_B & {}^{A}\hat{Z}_B \end{bmatrix}} = \underset{3 \times 3}{\begin{bmatrix} \hat{X}_B \cdot \hat{X}_A & \hat{Y}_B \cdot \hat{X}_A & \hat{Z}_B \cdot \hat{X}_A \\ \hat{X}_B \cdot \hat{Y}_A & \hat{Y}_B \cdot \hat{Y}_A & \hat{Z}_B \cdot \hat{Y}_A \\ \hat{X}_B \cdot \hat{Z}_A & \hat{Y}_B \cdot \hat{Z}_A & \hat{Z}_B \cdot \hat{Z}_A \end{bmatrix}} \qquad \textbf{(A.1)} $$

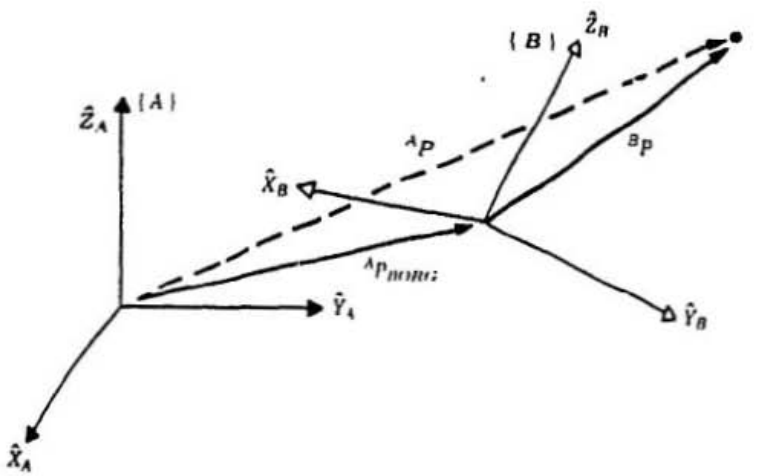

Fig. A.1 GENERAL MAPPING OF THREE DIMENSIONAL FRAMES [CRAIG, 1989]

Each component in the matrix represents the dot product of two unit vectors. This is nothing but the cosines of angle between them. The components of rotation matrix are often referred to as direction cosines.

We then account for the translation between origins by simple vector addition yielding

$$ {}^{A}P = {}^{A}_{B}[R]\ {}^{B}P + {}^{A}P_{BORG} \qquad \textbf{(A.2)} $$

Thus the above equation describes the general mapping of a vector from its description in one frame to a description in a second frame. The above equation can also be written as:

$$ {}^{A}P = {}^{A}_{B}T]{}^{B}P \qquad \textbf{(A.3)} $$

where ${}^{A}_{B}[T]$ is called transformation matrix. As it is evident form Eqs. (A.2), and (A.3) that this transformation matrix takes care of both the rotation, as well as the translation of the vector and is often called as transformation operator. In order that we can write the mathematics of Eq. (A.2) in the matrix operator form, we represent the transformation operator as a 4 x 4 matrix, and use a 4 x 1 position vector. If done so, the Eq. (A.2) takes the following structure

$$\begin{bmatrix} {}^{A}P \\ \hline 1 \end{bmatrix} = \begin{bmatrix} {}^{A}_{B}[R] & {}^{A}P_{BORG} \\ \hline 0 \quad 0 \quad 0 & 1 \end{bmatrix} \begin{bmatrix} {}^{B}P \\ \hline 1 \end{bmatrix} \qquad \textbf{(A.4)}$$

We adopt the convention that a position vector is 3 x 1 or 4 x 1, depending on whether it is multiplied by 3 x 3 rotation matrix or by a 4 x 4 transformation matrix. Thus, the above equation will take the following shape

$$\begin{matrix} {}^{A}P \\ 1 \end{matrix} = \begin{matrix} {}^{A}_{B}R\,{}^{B}P + {}^{A}P_{BORG} \\ 1 \end{matrix} \qquad \textbf{(A.5)}$$

The transformation operator is a homogeneous matrix , and is often called a **homogeneous transform**. It can be regarded purely as a construction matrix used to cast both rotation, as well as the transformation into a single matrix. Thus, one can use this transformation operator to describe a point or vector in any given frame relative to an another reference frame in three dimensional space.

A.2 ROTATION OF FRAMES ABOUT PRINCIPAL AXES

$$[R_x(\theta)] = \begin{bmatrix} 1 & 0 & 0 \\ 0 & \cos\theta & -\sin\theta \\ 0 & \sin\theta & \cos\theta \end{bmatrix} \tag{A.6}$$

$$[R_y(\theta)] = \begin{bmatrix} \cos\theta & 0 & \sin\theta \\ 0 & 1 & 0 \\ -\sin\theta & 0 & \cos\theta \end{bmatrix} \tag{A.7}$$

$$[R_z(\theta)] = \begin{bmatrix} \cos\theta & -\sin\theta & 0 \\ \sin\theta & \cos\theta & 0 \\ 0 & 0 & 1 \end{bmatrix} \tag{A.8}$$

APPENDIX B

ANSYS ALGORITHM FOR THREE-DIMENSIONAL FINITE ELEMENT DISCRETIZATION OF THE TURBINE BLADE, AND CALCULATION OF THE GEOMETRIC PROPERTIES

The three-dimensional model of the turbine blade was generated with the help of a general purpose finite element software, called ANSYS. The coordinates of the airfoil cross-section of the turbine blade at the root and the tip are the input data. The input values were fed into the program from a file called **node**. The node file contains the node numbers and the corresponding coordinates of the top and the bottom layers of the turbine blade. The program is versatile enough to discretize both straight, and tapered blade. One can conveniently modify the node file to obtain the discretization for a given type of blade. The purpose of the program was to calculate the geometric properties as discussed in Section 2.2.2.1. This was done by using only the preprocessor module of the finite element package.

Two routines/macros were used:

i) area - calculates the centroid of the individual finite elemental surface area (both pressure and suction sides). The values of these are written in output data files, and is suitably explained in the algorithm.

ii) volume - calculates the volumetric properties such as volume of the each elemental layer of the blade, its moment of inertia, centroid etc.

```
! ANSYS  ALGORITHM

/prep7
/title,  THREE-DIMENSIONAL FINITE ELEMENT DISCRETIZATION OF THE TURBINE
BLADE

/inp,node      ! Nodes for the bottom & top layers are read from file
! Node Filling Between Bottom and Top layers of the blade
*do,m,1,15,1
fill,m,500+m,9,50+m,50
fill,m+30,530+m,9,80+m,50
*enddo
!/view,1,-1,-1,2
!nplo

! Element Definition
et,1,solid90          ! 20-Noded, solid, Isoparametric, serendipity Element
e,1,3,33,31,101,103,133,131
emore,2,18,32,16,102,118,132,116
emore,51,53,83,81
/pnum,enum,1
! eplo

!ELEMENT GENERATION
egen,7,2,1,7,1
egen,2,100,1,8,7
egen,7,2,8,14,1
egen,2,100,8,15,7
egen,7,2,15,21,1
egen,2,100,15,22,7
egen,7,2,22,28,1
```

```
egen,2,100,22,29,7
egen,7,2,29,35,1

! VIEW THE MODEL IN 3_DIMENSION
!/view,1,-1,-1,2
!eplo

! Keypoint Generation from the nodes to calculate the geometric properties
*do,i,1,6,1
j = 100*(i-1)
*do,m,1,15
knode,m+j,m+j
knode,m+30+j,m+30+j
*enddo
*enddo

/inp,area      ! A routine/ macro for calculating the Surface area, and the geometric
                 Centroid.

!/inp,volume   ! Calculates the Volume of each finite element, and the
               ! Moment of Inertia of the elemental layer, and the entire
               ! blade about the blade frame.
/fini
/exit
```

MACROS

i) area

```
!  Determination of Geometric Properties of Finite Surface area of the Blade
*DIM,cs,,40,3        ! centroid of the suction surfaces
*DIM,cp,,40,3        ! centroid of the pressure surfaces
*DIM,as,,40          ! area of the suction surfaces
```

```
*DIM,ap,,40          ! area of the pressure surfaces

! SURFACE AREA GENERATION
ii = 1
*do,j,1,5,1
i = 100*(j-1)
a,i+1,i+31,i+131,i+101
asum
kk = 8*(j-1) + 1
*get,cp(kk,1),area,ii,cent,x        ! X-Coordinate of Centroid of pressure Surface
*get,cp(kk,2),area,ii,cent,y        ! Y-Coordinate of Centroid of pressure Surface
*get,cp(kk,3),area,ii,cent,z        ! Z-Coordinate of Centroid of pressure Surface
*get,ap(kk),area,ii,area
adele,ii

*do,m,1,13,2
a,i+m,i+m+2,i+m+2+100,i+100+m
asum

pp = 8*(j-1) + (m+3)/2
*get,cp(pp,1),area,ii,cent,x
*get,cp(pp,2),area,ii,cent,y
*get,cp(pp,3),area,ii,cent,z
*get,ap(pp),area,ii,area
adele,ii
*enddo

*do,m,1,13,2
a,i+30+m,i+30+m+2,i+30+m+2+100,i+30+100+m
asum
qq = 8*(j-1) + (m+1)/2
*get,cs(qq,1),area,ii,cent,x        ! X-Coordinate of centroid of Suction Surface
```

```
*get,cs(qq,2),area,ii,cent,y      ! Y-Coordinate of centroid of Suction Surface
*get,cs(qq,3),area,ii,cent,z      ! Z-Coordinate of centroid of Suction Surface
*get,as(qq),area,ii,area
adele,ii
*enddo

rr = qq + 1
a,i+15,i+45,i+145,i+115
asum
*get,cs(rr,1),area,ii,cent,x
*get,cs(rr,2),area,ii,cent,y
*get,cs(rr,3),area,ii,cent,z
*get,as(rr),area,ii,area
adele,ii
*enddo
*status,cp
*status,cs
/output,centp                     ! Writing centroid of Pressure Surfaces in file centp
*vwrite,cp(1,1),cp(1,2),cp(1,3)
(f8.4,2x,f8.4,2x,f8.4)
/output,term
/out,cents
*vwrite,cs(1,1),cs(1,2),cs(1,3)   ! Writing Centroid of Suction Surfaces in file cents
(f8.4,2x,f8.4,2x,f8.4)
/out,term
/out,asp
*vwrite,ap(1)
(f8.4)
/out,term
/out,ass
*vwrite,as(1)                     ! Writing the surface area of the suction side in file
                                  ass
```

(f8.4)
/out,term

ii) volume

! Determination of Volumetric Properties of Finite Elements of the Blade
*do,jv,100,500,100
*do,mv,1,13,2
jjv = jv-100
v,jjv+mv,jjv+mv+2,jv+mv+2,jv+mv,jjv+mv+30,jjv+mv+32,jv+mv+32,jv+mv+30
*enddo
vsum **! Summation of volumes of all elements in an elemental layer.**
vdele,1,7
*enddo

NOTE: The value of volumetric properties were interactively read from the program.

APPENDIX C

C.1 PROFILE DATA OF THE AIRFOIL SECTION USED FOR TURBINE BLADE

The airfoil data are detailed in Figs. C.1, and C.2. Fig. C.1 shows the cross section of the turbine blade with x-coordinates of the corner nodes of the finite elements at this section. Fig. C.2 shows the corresponding y-coordinates. The values of the coordinates are in mm. One can also notice the location of the blade frame, B, at the centroid of the airfoil.

C.2 NODE NUMBERING PATTERN OF THE BLADE FINITE ELEMENT AND THEIR CORNER NODES

Fig. C.3 shows a finite element no. 2 of the three dimensional finite element mode of the turbine blade used in the present work. The node numbering of the element number '2' can be seen in this figure.

Fig. C.4 shows the corner nodes of the finite element and the vectorization scheme. Out of a total of 308 nodes, only 96 corner nodes were used for the three dimensional vectorization scheme of the turbine blade.

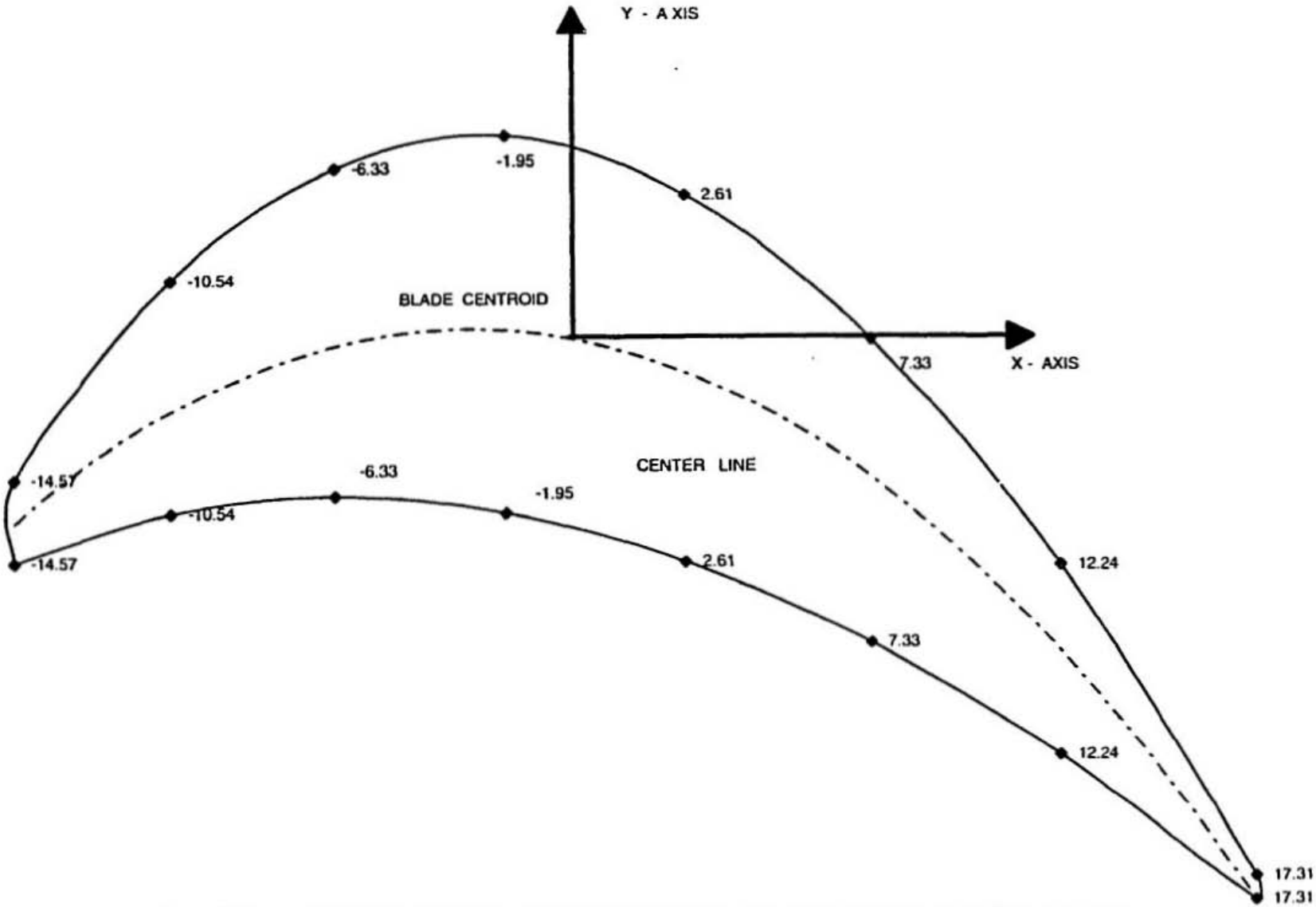

Fig. C.1 BLADE AIRFOIL CROSS-SECTION AT THE ROOT OF THE BLADE SHOWING THE X-COORDINATES OF THE CORNER NODES

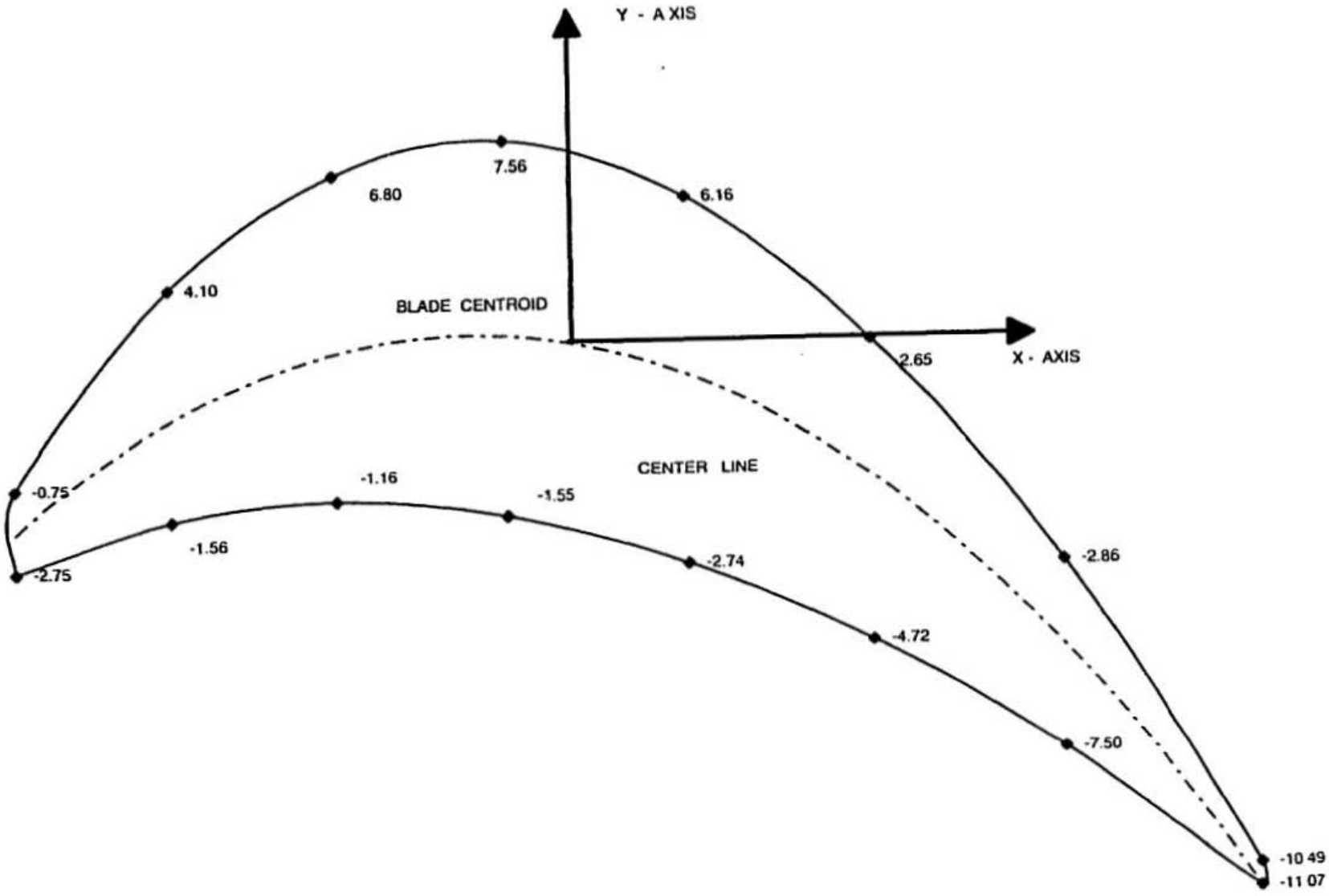

Fig. C.2 BLADE AIRFOIL CROSS-SECTION AT THE ROOT OF THE BLADE SHOWING THE Y-COORDINATES OF THE CORNER NODES

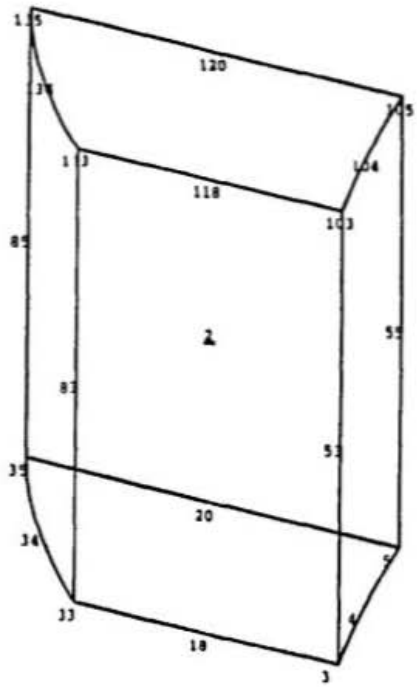

Fig. C.3 A BLADE FINITE ELEMENT (NO. 2) SHOWING THE NODAL ARRANGEMENT

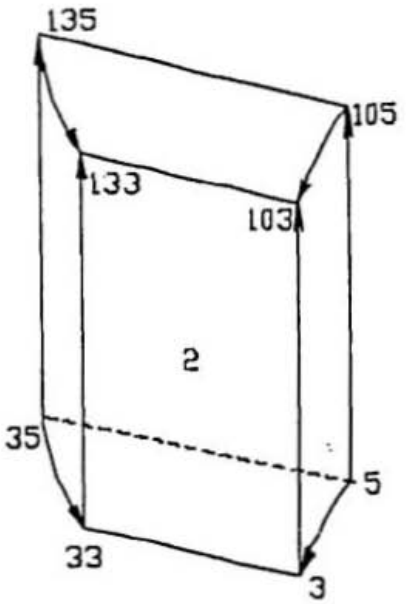

Fig. C.4 A BLADE FINITE ELEMENT (NO. 2) SHOWING THE CORNER NODES

APPENDIX D

PROGRAM LISTINGS

D.1 GEOMETRIC MODELLING AND NOZZLE EXCITATIONS

1. The coordinates of the corner nodes of the entire three - dimensional model were read in the program from suitable data file for a given blade type - viz. straight blade, or tapered blade. The other geometric properties - such as the geometric centroid of each of the finite element surfaces (both pressure side, and suction side), the height of the centroid of the elemental layers from the root of the blade and the mass moment of inertia of the blade, nozzle location etc. were provided as inputs.
2. The results such as force, torque, angular acceleration etc. obtained on simulation of the blade under nozzle excitation were reported in output files.

The results are for the nozzle excitations on a single blade. However, this program is versatile enough to incorporate the effect of the combined mass moment of inertia of the complete sets of blade, and rotor system.

The program was written in FORTRAN 77. The program is listed in D.1.1

D.1.1

```
C     PROGRAM FOR DYNAMIC SIMULATION OF IMPULSE ON A FINITE_ELEMENT
C     DISCRETIZED BLADE.

      DIMENSION K(6,16), CO_ORD(6,4,16), D_CO_ORD(6,4,16), th(50)
      DIMENSION VS(6,3,8), VP(6,3,8), VSH(5,3,8), VPH(5,3,8)
      DIMENSION UVS(6,3,8), UVP(6,3,8),ABSVS(6,8), ABSVP(6,8)
      DIMENSION UVSH(5,3,8), UVPH(5,3,8),ABSVSH(5,8), ABSVPH(5,8)
      DIMENSION USVS(5,3,8), USVP(5,3,8), AVS(5,8), AVP(5,8), RD(5,4,1),
     1 CENT_LAYER(5),OMEGA(3), R_DYN(5,4,1), VB(5,3),VR1(5,3),UVR1(5,3)
      DIMENSION Gamma_s(5,8), Gamma_p(5,8), FACTOR_S(5,8),FACTOR_P(5,8),
     1 DAVS(5,8), DAVP(5,8), QS(5,8), QP(5,8), PROT_GL(5,3,3,8),
     1  SROT_GL(5,3,3,8), TPROT_GL(5,3,3,8), TSROT_GL(5,3,3,8),ABSVR1(5),
     1  UVR2_S(5,3,8), UVR2_P(5,3,8), S_IMP(5,3,8), P_IMP(5,3,8),
     1 A_SIMP(5,8), A_PIMP(5,8), TOT_SIMP(5,3), TOT_PIMP(5,3),
     1 AT_SIMP(5), AT_PIMP(5),TOT_IMP(5,3), TOT_ABSIMP(5),TIMP(3),
     1  CENTP(5,4,8), CENTS(5,4,8), DCENTP(5,4,8), DCENTS(5,4,8),
     1 ALCENTS(5,3), ALCENTP(5,3),ACENTS(3),ACENTP(3),TS(3),TP(3),
     1 T_PIMP(3), T_SIMP(3), APP_IMP(3), TORQUE(3), DDAVS(5,8),
     1  DDAVP(5,8)


      COMMON /DYNAM/CO_ORD, D_CO_ORD, CENTS, CENTP, RR
      COMMON /DYN/ DCENTS, DCENTP
      COMMON /VECT_LAYER/ VS, VP, UVS, UVP, ABSVS, ABSVP
      COMMON /VECT_HEIGHT/ VSH, VPH, UVSH, UVPH, ABSUVSH, ABSUVPH ,Layers
      COMMON/VECT_SURF/USVS,USVP, AVS, AVP
      COMMON /rpm/ OMEGA, RD, R_DYN
      COMMON/PROJ / FACTOR_S , FACTOR_P
      COMMON / ROTATION/ PROT_GL, SROT_GL, TPROT_GL,TSROT_GL
      COMMON/ UNIT_REL_VEL2/ UVR2_S, UVR2_P
      COMMON/IMP_FORCE/ S_IMP, P_IMP, A_SIMP, A_PIMP, TOT_SIMP,
     1 TOT_PIMP, AT_SIMP, AT_PIMP, TOT_IMP,TOT_ABSIMP
      COMMON/ CENTROID / ALCENTS, ALCENTP
      COMMON/VELOCITY/ABSV1, ALPHA
      COMMON /FLOW AREA/ DAVS, DAVP, DDAVS, DDAVP
```

```
      REAL AZ, AINC, th, ABSVS, ABSVP,ABSVPH,ABSVPS, AVS, AVP

      ALIMIT = 0.001

C     ALPHA is the angle of efflux at the Nozzle outlet.
      ALPHA  = 50

C     THETAN is the Nozzle opening angle.
      THETAN = 7.5
      THETAP = THETAN * (3.1415927 / 180.00)

C     START IS THE STARTING VALUE OF ANGLE OF ROTOR MOVEMENT
      START = - 15

C     ANB is the number of Nozzles considered for excitations,
C     ANB = 1 for a signle blade-rotor dynamics.
      ANB = 1

C     ABSV1 is the absolute velocity at Nozzle exit [Dhar, D. pg. 101]
      ABSV1 = 718.05

C     RR is the Rotor radius.
      RR = 0.5

      OPEN (UNIT = 1, FILE = 'CORNER_NOD.DAT', STATUS ='OLD')
      OPEN (UNIT = 2, FILE = 'CP.DAT', STATUS ='OLD')
      OPEN (UNIT = 3, FILE = 'CS.DAT', STATUS ='OLD')
      OPEN (UNIT = 4, FILE = 'CENT.DAT', STATUS ='OLD')

      OPEN (UNIT = 31, FILE = 'qs.dat', STATUS ='NEW')
      OPEN (UNIT = 32, FILE = 'qp.dat', STATUS ='NEW')
      OPEN (UNIT = 33, FILE = 'pappl.dat', STATUS ='NEW')
      OPEN (UNIT = 34, FILE = 'simp.dat', STATUS ='NEW')
      OPEN (UNIT = 35, FILE = 'pimp.dat', STATUS ='NEW')
      OPEN (UNIT = 36, FILE = 'tot_simp.dat', STATUS ='NEW')
      OPEN (UNIT = 37, FILE = 'tot_pimp.dat', STATUS ='NEW')
```

```
      OPEN (UNIT = 38, FILE = 'tot_imp.dat', STATUS ='NEW')
      OPEN (UNIT = 39, FILE = 'timp.dat', STATUS ='NEW')
      OPEN (UNIT = 40, FILE = 't_pimp.dat', STATUS ='NEW')
      OPEN (UNIT = 41, FILE = 't_simp.dat', STATUS ='NEW')
      OPEN (UNIT = 42, FILE = 'lp.dat', STATUS ='NEW')
      OPEN (UNIT = 43, FILE = 'ls.dat', STATUS ='NEW')
      OPEN (UNIT = 44, FILE = 'torque.dat', STATUS ='NEW')
      OPEN (UNIT = 45, FILE = 'omega.dat', STATUS ='NEW')
      OPEN (UNIT = 46, FILE = 'ang_acc.dat', STATUS ='NEW')

C     Layers = no. of blade airfoil cross sections
      Layers = 6

C     ILayers = no of elemental layers = Layers - 1
      ILayers = 5

C     Reading Blade data

      DO 1 L = 1, Layers
      DO 2 N = 1, 16

      READ(1,*) K(L,N), (CO_ORD(L,M,N),M=1,3)

      temp1 = CO_ORD(L,1,N)
      temp2 = CO_ORD(L,2,N)
      temp3 = CO_ORD(L,3,N)

C     Co-ordinate unit correction, and transformation to Global frame.

      CO_ORD(L,1,N) = temp1/1000.00
      CO_ORD(L,2,N) = temp2/1000.00
      CO_ORD(L,3,N) = temp3/100.00 + RR
      CO_ORD(L,4,N) = 1.0

2     CONTINUE
1     CONTINUE
```

```
C       Reading Blade surface centroids

        DO 41 L = 1, ILayers
        READ(4,*) CENT_LAYER(L)

        DO 42 N = 1, 8
        READ(2,*)(CENTP(L,M,N),M=1,3)
        READ(3,*)(CENTS(L,M,N),M=1,3)

        tp1 = CENTP(L,1,N)
        tp2 = CENTP(L,2,N)
        tp3 = CENTP(L,3,N)

        ts1 = CENTS(L,1,N)
        ts2 = CENTS(L,2,N)
        ts3 = CENTS(L,3,N)

C       Centroid unit correction, and transformation to global frame.

        CENTP(L,1,N) = tp1/1000.00
        CENTP(L,2,N) = tp2/1000.00
        CENTP(L,3,N) = tp3/100.00 + RR
        CENTP(L,4,N) = 1.0

        CENTS(L,1,N) = ts1/1000.00
        CENTS(L,2,N) = ts2/1000.00
        CENTS(L,3,N) = ts3/100.00 + RR
        CENTS(L,4,N) = 1.0

42      CONTINUE
41      CONTINUE


        DO 25 L = 1, ILayers

        RD (L,1,1) = 0.0
        RD (L,2,1) = 0.0
```

```
      RD (L,3,1) = CENT_LAYER(L) /100 + RR
      RD (L,4,1) = 1.0

25    continue


      IT = 16

C     Anticlockwise corrections

      ASTART = - START * (3.1415927 / 180.00)
      AINC = 0
      AZ = (2*START/(IT-1))*(3.1415927 / 180.00)

C     Specify the initial rotating speed of the rotor
      OMEGA(1) = 100
      OMEGA(2) = 0
      OMEGA(3) = 0

      DO 10 I = 1,IT,1

      th(I) = th(I) + AINC + ASTART
      AINC = AINC + AZ

      WRITE(45,*) OMEGA(1)

      CALL DYN_CO_ORD (th, I)

      DO 15 L = 1,Layers

      CALL LAYER_VECTOR(D_CO_ORD,L, I)

15    continue


      DO 18 L = 1,ILayers
```

```
      CALL HEIGHT_VECTOR (D_CO_ORD,L,I)

      CALL SURFACE_VECTOR(L,I, VSH, VPH,VS, VP)

      CALL INCIDENT_REL_VEL(L,I,th,VR1, UVR1, ABSVR1)

      CALL INCIDENT_ANGLE(UVR1, USVS, USVP, Gamma_s, Gamma_p, L)

      CALL PROJECT_AREA (AVS, AVP, DAVS, DAVP, L)

      CALL REFLECT_REF_GEN (UVR1, USVS, USVP, L)

      CALL REFLECT_REL_VEL(UVR1,USVS,USVP,Gamma_s, Gamma_p,L)

      CALL VEL_TRIAD (UVR1,D_CO_ORD, L, THETAP)

      CALL MASS_FLOW (ABSVR1, DDAVS, DDAVP,L, QS, QP)

      CALL IMPULSE(UVR1, ABSVR1, QS, QP, L)

18    continue

*****************************************************************************

*     This is analysis section for impulse and torque at different time
      DO 30 M = 1,3

      TIMP(M) = 0
      TP(M) =0
      TS(M) =0
      T_PIMP(M) = 0
      T_SIMP(M) = 0

      DO 31 L = 1, ILayers

      TP(M) = TP(M) + TOT_PIMP(L,M)*ALCENTP(L,M)
      TS(M) = TS(M) + TOT_SIMP(L,M)*ALCENTS(L,M)
```

```
      T_PIMP(M) = T_PIMP(M) + TOT_PIMP(L,M)
      T_SIMP(M) = T_SIMP(M) + TOT_SIMP(L,M)

      TIMP(M) = TIMP(M) + TOT_IMP(L,M)

31    CONTINUE
30    CONTINUE

      WRITE(40,*) (T_PIMP(M),M=1,3)
      WRITE(41,*) (T_SIMP(M),M=1,3)

      IF(ABS(T_PIMP(1)) .LE. ALIMIT .AND. ABS(T_PIMP(2)) .LE. ALIMIT .AND.
     1 ABS(T_PIMP(3)) .LE. ALIMIT) THEN

      ACENTP(1) = 0
      ACENTP(2) = 0
      ACENTP(3) = 0

      ELSE IF (ABS(T_PIMP(3)) .LE. ALIMIT) THEN

      ACENTP(1) = TP(1) /T_PIMP(1)
      ACENTP(2) = TP(2) /T_PIMP(2)
      ACENTP(3) = DCENTP(3,3,5)

      ELSE
      ACENTP(1) = TP(1) /T_PIMP(1)
      ACENTP(2) = TP(2) /T_PIMP(2)
      ACENTP(3) = TP(3) /T_PIMP(3)
      ENDIF


      DO 50 M =1,3

      IF(ABS(T_SIMP(M)) .LE. ALIMIT) THEN
      ACENTS(M) = 0
      ELSE
      ACENTS(M) = TS(M) /T_SIMP(M)
      ENDIF
```

```
50    CONTINUE

      IF (ABS(TIMP(1)) .LE. ALIMIT .AND. ABS(TIMP(2)) .LE. ALIMIT .AND.
     1 ABS(TIMP(3)) .LE. ALIMIT) THEN

      APP_IMP(1) = 0
      APP_IMP(2) = 0
      APP_IMP(3) = 0

      ELSE IF( ABS(TIMP(3)) .LE. ALIMIT) THEN
      APP_IMP(3) = DCENTP(3,3,5)
      APP_IMP(1) = (ACENTP(1)*T_PIMP(1) - ACENTS(1)*T_SIMP(1))/TIMP(1)
      APP_IMP(2) = (ACENTP(2)*T_PIMP(2) - ACENTS(2)*T_SIMP(2))/TIMP(2)

      ELSE
      APP_IMP(1) = (ACENTP(1)*T_PIMP(1) - ACENTS(1)*T_SIMP(1))/TIMP(1)
      APP_IMP(2) = (ACENTP(2)*T_PIMP(2) - ACENTS(2)*T_SIMP(2))/TIMP(2)
      APP_IMP(3) = (ACENTP(3)*T_PIMP(3) - ACENTS(3)*T_SIMP(3))/TIMP(3)
      ENDIF

      AIMP = SQRT(TIMP(1)**2 + TIMP(2)**2 + TIMP(3)**2)

      WRITE(39,*) (TIMP(M),M=1,3), AIMP
      WRITE(33,*) (APP_IMP(M),M =1,3)

      CALL CROSS_PROD(TIMP, APP_IMP,TORQUE)
      WRITE(44,*) (TORQUE(M),M=1,3)

      CALL DYN_PARA (TORQUE, OMEGA, AZ,ANB, I)

10    continue

      close(1)
      close(2)
      close(3)
      close(4)

      close(31)
```

```
      close(32)
      close(33)
      close(34)
      close(35)
      close(36)
      close(37)
      close(38)
      close(39)
      close(40)
      close(41)
      close(42)
      close(43)
      close(44)
      close(46)

      STOP
      END

*-----------------------------------------------------------------
      SUBROUTINE DYN_CO_ORD (th, I)
*-----------------------------------------------------------------
      DIMENSION CO_ORD(6,4,16), D_CO_ORD(6,4,16), TEMP_IN(4,16),
     1 TEMP_OUT(4,16), th(50), OBX(4,4),CENTS(5,4,8), DCENTS(5,4,8),
     1 CENTP(5,4,8), DCENTP(5,4,8),TS_IN(4,8),TS_OUT(4,8),TP_IN(4,8),
     1 TP_OUT(4,8)

      COMMON /DYNAM/ CO_ORD, D_CO_ORD,CENTS,CENTP, RR
      COMMON /DYN/ DCENTS, DCENTP
      REAL th, theta

      CALL TH_XAXIS (th, OBX, 0, I)

      DO 11 L = 1, 6
      DO 10 N = 1, 16
      DO 10 M = 1, 4

10    TEMP_IN(M,N) = CO_ORD(L,M,N)
```

```
      CALL MATMUL (OBX, TEMP_IN, TEMP_OUT,4, 4,16)

      DO 9 N = 1, 16
      DO 9 M = 1, 4

9     D_CO_ORD(L,M,N) = TEMP_OUT(M, N)

11    continue

      DO 15 L = 1, 5

      DO 14 N = 1, 8
      DO 14 M = 1, 4
      TP_IN(M,N) = CENTP(L,M,N)
14    TS_IN(M,N) = CENTS(L,M,N)

      CALL MATMUL (OBX, TP_IN, TP_OUT,4, 4,8)
      CALL MATMUL (OBX, TS_IN, TS_OUT,4, 4,8)

      DO 16 N = 1, 8
      DO 16 M = 1, 4

      DCENTP(L,M,N) = TP_OUT(M,N)
16    DCENTS(L,M,N) = TS_OUT(M,N)

15    continue

      RETURN
     END


C*************************************************************************
      SUBROUTINE LAYER_VECTOR(D_CO_ORD,L,II)
C*************************************************************************
      DIMENSION VS(6,3,8), VP(6,3,8), D_CO_ORD(6,4,16),UVP(6,3,8),
     1 UVS(6,3,8), ABSVP(6,8), ABSVS(6,8),STEMP_IN(3),STEMP_OUT(3),
     1 PTEMP_IN(3), PTEMP_OUT(3)
```

```
      REAL ABSVS, ABSVP, ABSSTEMP, ABSPTEMP
      COMMON /VECT_LAYER/ VS, VP, UVS, UVP, ABSVS, ABSVP
      N = 16

      DO 1 I = 1, N/2 -1
      J = N/2 + I
      DO 2 K = 1, 3

      VP(L,K, I+1) = (D_CO_ORD(L,K,I) - D_CO_ORD(L,K,I+1))
2     VS(L,K, I) = (D_CO_ORD(L,K,J) - D_CO_ORD(L,K,J+1))
1     CONTINUE

      DO 3 K = 1,3
      VS(L,K, N/2) = (D_CO_ORD(L,K,N) - D_CO_ORD(L,K,N/2))
3     VP(L,K,1)    = (D_CO_ORD(L,K,N/2 + 1) - D_CO_ORD(L,K,1))

      DO 4 NN = 1,8
      DO 5 MM = 1,3

      STEMP_IN(MM)= VS(L,MM,NN)
5     PTEMP_IN(MM)= VP(L,MM,NN)

      CALL UNIT_VECT(STEMP_IN,STEMP_OUT, ABSSTEMP)
      CALL UNIT_VECT(PTEMP_IN,PTEMP_OUT, ABSPTEMP)

      DO 6 MM = 1,3
      UVS(L,MM,NN) = STEMP_OUT(MM)
6     UVP(L,MM,NN) = PTEMP_OUT(MM)

      ABSVS(L,NN) = ABSSTEMP
4     ABSVP(L,NN) = ABSPTEMP
      RETURN
     END


**********************************************************************
      SUBROUTINE HEIGHT_VECTOR(D_CO_ORD,L,II)
**********************************************************************
```

```
      DIMENSION D_CO_ORD(6,4,16), VSH(5,3,8), VPH(5,3,8),UVSH(5,3,8),
     1 UVPH(5,3,8), ABSVSH(5,8),ABSVPH(5,8),STEMP_IN(3),STEMP_OUT(3),
     1  PTEMP_IN(3), PTEMP_OUT(3)

      COMMON /VECT_HEIGHT/ VSH, VPH, UVSH, UVPH, ABSUVSH, ABSUVPH , Layers
      REAL ABSUVSH, ABSUVPH, ABSSTEMP, ABSPTEMP


      IF(L .EQ.6) GOTO 9

      DO 1 NN = 1,8
      JJ = NN + 8
      DO 2 MM = 1,3

      VSH(L,MM,NN) =     D_CO_ORD(L+1,MM,JJ) - D_CO_ORD(L,MM,JJ)
2     VPH(L,MM,NN) =  D_CO_ORD(L+1,MM,NN) - D_CO_ORD(L,MM,NN)

1     CONTINUE

      DO 4 NN = 1,8
      DO 5 MM = 1,3

      STEMP_IN(MM)= VSH(L,MM,NN)
5     PTEMP_IN(MM)= VPH(L,MM,NN)

      CALL UNIT_VECT(STEMP_IN,STEMP_OUT, ABSSTEMP)
      CALL UNIT_VECT(PTEMP_IN,PTEMP_OUT, ABSPTEMP)

      DO 6 MM = 1,3
      UVSH(L,MM,NN) = STEMP_OUT(MM)
6     UVPH(L,MM,NN) = PTEMP_OUT(MM)

      ABSVSH(L,NN) = ABSSTEMP
4     ABSVPH(L,NN) = ABSPTEMP

9     RETURN
      END
```

```
************************************************************************
      SUBROUTINE SURFACE_VECTOR(L,I, VSH, VPH,VS, VP)
************************************************************************
      DIMENSION VSH(5,3,8), VPH(5,3,8), VS(6,3,8), VP(6,3,8)
      DIMENSION SVS(5,3,8), SVP(5,3,8), AVS(5,8), AVP(5,8)
      DIMENSION USVS(5,3,8), USVP(5,3,8), STEMP_IN(3), PTEMP_IN(3)
      DIMENSION STEMPH_IN(3), PTEMPH_IN(3), STEMP_OUT(3), PTEMP_OUT(3)
      DIMENSION USTEMP_OUT(3), UPTEMP_OUT(3),SUC_AREA1(5,8), SUC_AREA2(5,8),
     1 PRESS_AREA1(5,8), PRESS_AREA2(5,8), USVS_2(5,3,8), USVP_2(5,3,8)

      REAL USTEMPAREA, UPTEMPAREA, AVS, AVP
      COMMON/VECT_SURF/USVS,USVP, AVS, AVP
      If(L. EQ. 6) GOTO 10

      DO 4 NN = 1,8
      DO 5 MM = 1,3

*     Generating temporary variables

      STEMP_IN(MM)  = VS(L,MM,NN)
      PTEMP_IN(MM)  = VP(L,MM,NN)
      STEMPH_IN(MM) = VSH(L,MM,NN)
5     PTEMPH_IN(MM) = VPH(L,MM,NN)

      CALL CROSS_PROD(STEMP_IN, STEMPH_IN, STEMP_OUT)
      CALL CROSS_PROD(PTEMPH_IN, PTEMP_IN, PTEMP_OUT)

      CALL UNIT_VECT(STEMP_OUT,USTEMP_OUT,USTEMPAREA)
      CALL UNIT_VECT(PTEMP_OUT,UPTEMP_OUT,UPTEMPAREA)

      DO 6 MM = 1,3
      USVS(L,MM,NN) = USTEMP_OUT(MM)
6     USVP(L,MM,NN) = UPTEMP_OUT(MM)

      SUC_AREA1(L,NN) = USTEMPAREA
      PRESS_AREA1(L,NN) = UPTEMPAREA

4     Continue
```

```
*       Corner Surfaces Require Special Treatment

        DO 30 MM = 1,3
        STEMP_IN(MM)  = VS(L+1,MM,8)
        STEMPH_IN(MM) = VPH(L,MM,8)
        PTEMP_IN(MM)  = VP(L+1,MM,1)
30      PTEMPH_IN(MM) = VSH(L,MM,1)

        CALL CROSS_PROD(STEMP_IN, STEMPH_IN, STEMP_OUT)
        CALL CROSS_PROD(PTEMPH_IN, PTEMP_IN, PTEMP_OUT)

        CALL UNIT_VECT(STEMP_OUT,USTEMP_OUT,USTEMPAREA)
        CALL UNIT_VECT(PTEMP_OUT,UPTEMP_OUT,UPTEMPAREA)

*       Corner Surfaces Require Special Treatment

        DO 11 MM = 1,3

        USVS_2(L,MM,8) = USTEMP_OUT(MM)
11      USVP_2(L,MM,1) = UPTEMP_OUT(MM)

        SUC_AREA2(L,8) = USTEMPAREA
        PRESS_AREA2(L,1) = UPTEMPAREA

        DO 7 NN = 2,8
        DO 8 MM = 1,3

        STEMP_IN(MM)  = VS(L+1,MM,NN -1)
        PTEMP_IN(MM)  = VP(L+1,MM,NN)
        STEMPH_IN(MM) = VSH(L,MM,NN)
8       PTEMPH_IN(MM) = VPH(L,MM,NN-1)

        CALL CROSS_PROD(STEMP_IN, STEMPH_IN, STEMP_OUT)
        CALL CROSS_PROD(PTEMPH_IN, PTEMP_IN, PTEMP_OUT)


        CALL UNIT_VECT(STEMP_OUT,USTEMP_OUT,USTEMPAREA)
        CALL UNIT_VECT(PTEMP_OUT,UPTEMP_OUT,UPTEMPAREA)
```

```
      DO 9 MM = 1,3

      USVS_2(L,MM,NN-1) = USTEMP_OUT(MM)
9     USVP_2(L,MM,NN) = UPTEMP_OUT(MM)

      SUC_AREA2(L,NN-1) = USTEMPAREA
      PRESS_AREA2(L,NN) = UPTEMPAREA

7     continue

      DO 20 NN = 1, 8

      AVS(L,NN) = (SUC_AREA1(L,NN) + SUC_AREA2(L,NN))/2
      AVP(L,NN) = (PRESS_AREA1(L,NN) + PRESS_AREA2(L,NN))/2

20    continue
10    RETURN
      END

*************************************************************************
      SUBROUTINE INCIDENT_REL_VEL(L,I,th,VR1, UVR1, ABSVR1)
*************************************************************************
      DIMENSION V1(3), VR1(5,3), VB(5,3), UVR1(5,3), TEMP_IN(3),
     1  TEMP_OUT(3),ABSVR1(5), th(50)

      COMMON/VELOCITY/ABSV1, ALPHA
      REAL ABSV1, ABSVR1, th, TEMPABS

      CN = COS(ALPHA * 3.14159 /180)
      SN = SIN(ALPHA * 3.14159 /180)

      V1(1) =  CN*ABSV1
      V1(2) =  SN*ABSV1
      V1(3) =  0

      IF(L.EQ.6) GOTO 1

      CALL BLADE_VEL(L,I,th,VB)
```

```
      VR1(L,1) = V1(1) - VB(L,1)
      VR1(L,2) = V1(2) - VB(L,2)
      VR1(L,3) = V1(3) - VB(L,3)

      DO 2 NN = 1,3
2     TEMP_IN (NN) = VR1(L,NN)

      CALL UNIT_VECT(TEMP_IN, TEMP_OUT, TEMPABS)
      DO 3 NN = 1,3
3     UVR1(L,NN) = TEMP_OUT(NN)
      ABSVR1(L) = TEMPABS

1     RETURN
      END


*************************************************************************
      SUBROUTINE BLADE_VEL(L,I, th, VB)
*************************************************************************
      DIMENSION VB(5,3), OBX (4,4), OMEGA(3), RD(5,4,1), R_DYN(5,4,1),
     1  TEMP(3), TEMP_IN(4,1) , TEMP_OUT(4,1), VTEMP(3), th(50)

      common /rpm/ OMEGA, RD, R_DYN

      REAL theta, th

      CALL TH_XAXIS(th, OBX, 0,I)

      DO 1 M = 1,4
1     TEMP_IN(M,1) = RD(L,M,1)

      CALL MATMUL (OBX, TEMP_IN, TEMP_OUT, 4,4,1)

      DO 2 M = 1,4
2     R_DYN (L, M, 1) = TEMP_OUT(M,1)

      DO 3 M = 1, 3
3     TEMP(M) = R_DYN (L, M, 1)
```

```
      CALL CROSS_PROD (TEMP,OMEGA, VTEMP)

      DO 4 M = 1, 3
4     VB(L,M) = 2 * 3.14159 * VTEMP(M) /60.
      RETURN
      END

*****************************************************************************
      SUBROUTINE INCIDENT_ANGLE(UVR1, USVS, USVP, Gamma_s, Gamma_p, L)
*****************************************************************************
      DIMENSION UVR1(5,3), USVS(5,3,8), USVP(5,3,8), GAMMA_S(5,8),
     1  GAMMA_P(5,8), STEMP_IN(3), PTEMP_IN(3)
      DIMENSION FACTOR_S(5,8), FACTOR_P(5,8), VTEMP(3)

      COMMON /PROJ/ FACTOR_S, FACTOR_P
      DO 1 M = 1,8
      DO 2 N = 1,3

      STEMP_IN(N)  = USVS(L, N, M)
      PTEMP_IN(N)  = USVP(L, N, M)

2     VTEMP(N) = UVR1(L,N)

      CALL DOT_PROD(VTEMP, STEMP_IN, STEMP_OUT)
      CALL DOT_PROD(VTEMP, PTEMP_IN, PTEMP_OUT)

      Gamma_s(L,M) = ACOS(STEMP_OUT)
      Gamma_p(L,M) = ACOS(PTEMP_OUT)

      FACTOR_S (L,M) = STEMP_OUT
      FACTOR_P (L,M) = PTEMP_OUT

1     continue

      RETURN
      END
```

```
************************************************************************
      SUBROUTINE PROJECT_AREA (AVS, AVP, DAVS, DAVP, L)
************************************************************************
      DIMENSION AVS(5,8), AVP(5,8), DAVS(5,8), DAVP(5,8), FACTOR_S(5,8),
     1  FACTOR_P(5,8)

      REAL AVS, AVP
      COMMON / PROJ/ FACTOR_S, FACTOR_P
      DO 2 M = 1,8

C     CALCULATION OF PROJECTED AREA OF PRESSURE SIDE
      IF (FACTOR_P(L,M) .LT. 0) THEN
      DAVP (L,M) = ABS(FACTOR_P(L,M)) * AVP(L,M)
      ELSE
      DAVP(L,M) = 0
      ENDIF

C     CALCULATION OF PROJECTED AREA OF SUCTION SIDE

      IF (FACTOR_S(L,M) .LT. 0) THEN
      DAVS (L,M) = ABS(FACTOR_S(L,M)) * AVS(L,M)
      ELSE
      DAVS(L,M) = 0
      ENDIF

2     CONTINUE
      RETURN
      END

************************************************************************
      SUBROUTINE  REFLECT_REF_GEN(UVR1, USVS, USVP, L)
************************************************************************
      DIMENSION UVR1(5,3), USVS(5,3,8), USVP(5,3,8), ANS1(5,3,8),
     1  ANS2(5,3,8), ANP1(5,3,8), ANP2(5,3,8), TEMPS1_IN(3), TEMP2_IN(3)
      DIMENSION TEMPP1_IN(3), TEMPS_OUT(3), TEMPP_OUT(3), TEMP_S(3),
     1  TEMP_P(3), UTEMPS_OUT(3), UTEMPP_OUT(3), PROT_GL(5,3,3,8),
     1   SROT_GL(5,3,3,8), TPROT_GL(5,3,3,8), TSROT_GL(5,3,3,8)
```

```
      COMMON / ROTATION/ PROT_GL, SROT_GL, TPROT_GL, TSROT_GL

      REAL AMTEMPS_OUT, AMTEMPP_OUT

C     This subroutine Generates a Local Frame of reference for relative
C     velocity rotation. The Gloabl - Local Refrerence Rotation Matrix
C     for each surface have been calculated as *ROT_GL, and their Transpose
C     have been calculated as T*ROT_GL.

      DO 1 N = 1,8
      DO 2 M = 1,3
      TEMPS1_IN(M) = USVS(L,M,N)
      TEMP2_IN(M)  = UVR1(L,M)
2     TEMPP1_IN(M) = USVP(L,M,N)

      CALL CROSS_PROD (TEMPS1_IN, TEMP2_IN, TEMPS_OUT)

      CALL UNIT_VECT(TEMPS_OUT, UTEMPS_OUT, AMTEMPS_OUT)

C     Making Sure That the Z - AXIS is positive

      IF(UTEMPS_OUT(3) .LE. 0.0) THEN

            do 22 M = 1,3
            UTEMPS_OUT(M) = -1* UTEMPS_OUT(M)
22          continue

      ENDIF

      CALL CROSS_PROD (UTEMPS_OUT, TEMPS1_IN, TEMP_S)

      CALL CROSS_PROD (TEMPP1_IN, TEMP2_IN, TEMPP_OUT)

      CALL UNIT_VECT(TEMPP_OUT, UTEMPP_OUT, AMTEMPP_OUT)


*     Making Sure That the Z - AXIS is positive
      IF(UTEMPP_OUT(3) .LE. 0) THEN
```

```
            do 23 M = 1,3
            UTEMPP_OUT(M) = -1* UTEMPP_OUT(M)
23          continue

      ENDIF

      CALL CROSS_PROD (UTEMPP_OUT, TEMPP1_IN, TEMP_P)

      DO 3 M = 1,3

      ANS1(L,M,N) = UTEMPS_OUT(M)
      ANS2(L,M,N) = TEMP_S(M)
      ANP1(L,M,N) = UTEMPP_OUT(M)
      ANP2(L,M,N) = TEMP_P(M)

*     Generating Rotation Matrix for Pressure Surface

      PROT_GL(L,M,1,N) = USVP(L,M,N)
      PROT_GL(L,M,2,N) = ANP2(L,M,N)
      PROT_GL(L,M,3,N) = ANP1(L,M,N)

*     Generating Rotation Matrix for Suction Surface

      SROT_GL(L,M,1,N) = USVS(L,M,N)
      SROT_GL(L,M,2,N) = ANS2(L,M,N)
      SROT_GL(L,M,3,N) = ANS1(L,M,N)

*     Geneating the Transpose of the Rotation Matrix on Pressure Surface

      TPROT_GL(L,1,M,N) = USVP(L,M,N)
      TPROT_GL(L,2,M,N) = ANP2(L,M,N)
      TPROT_GL(L,3,M,N) = ANP1(L,M,N)

*     Geneating the Transpose of the Rotation Matrix on Suction Surface

      TSROT_GL(L,1,M,N) = USVS(L,M,N)
      TSROT_GL(L,2,M,N) = ANS2(L,M,N)
      TSROT_GL(L,3,M,N) = ANS1(L,M,N)
```

```
3       CONTINUE
1       CONTINUE

        RETURN
        END

*****************************************************************************************************
        SUBROUTINE REFLECT_REL_VEL(UVR1,USVS,USVP,Gamma_S, Gamma_P,L)
*****************************************************************************************************
        DIMENSION UVR1(5,3), USVS(5,3,8), USVP(5,3,8), Gamma_s(5,8),
     1  Gamma_p(5,8), PROT_GL(5,3,3,8), SROT_GL(5,3,3,8)
        DIMENSION TPROT_GL(5,3,3,8), TSROT_GL(5,3,3,8), TTEMP_S(3,3),
     1  TTEMP_P(3,3), AUVR1(3), SBUVR1(3), PBUVR1(3), OBZ(3,3)
        DIMENSION SNBUVR1(3), PNBUVR1(3), TEMP_S(3,3), TEMP_P(3,3),
     1  SNAUVR1(3), PNAUVR1(3), DIFF_S(3), DIFF_P(3), UVR2_S(5,3,8),
     1  UVR2_P(5,3,8)

        COMMON / ROTATION/ PROT_GL, SROT_GL, TPROT_GL,TSROT_GL
        COMMON/ UNIT_REL_VEL2/ UVR2_S, UVR2_P


        BETA = 0.9
        ERR = .0001
*       BETA IS THE VELOCITY FRICTION FACTOR


        DO 1 N = 1, 8
        DO 2 J = 1, 3
        DO 3 M = 1, 3

        TTEMP_P(J,M) = TPROT_GL(L,J,M,N)
        TTEMP_S(J,M) = TSROT_GL(L,J,M,N)
        TEMP_P(J,M) = PROT_GL(L,J,M,N)
3       TEMP_S(J,M) = SROT_GL(L,J,M,N)

2       AUVR1(J) = UVR1(L,J)

        CALL MATMUL(TTEMP_P, AUVR1, PBUVR1, 3, 3, 1)
```

```
      CALL MATMUL(TTEMP_S, AUVR1, SBUVR1, 3, 3, 1)

      phi_s =  Gamma_s(L,N)

      CALL TH_ZAXIS (phi_s, OBZ)

      CALL MATMUL (OBZ, SBUVR1, SNBUVR1, 3,3,1)

      phi_p =  Gamma_p(L,N)

      CALL TH_ZAXIS (phi_p, OBZ)

      CALL MATMUL (OBZ, PBUVR1, PNBUVR1, 3,3,1)

      CALL MATMUL(TEMP_P, PNBUVR1, PNAUVR1, 3, 3, 1)

      CALL MATMUL(TEMP_S, SNBUVR1, SNAUVR1, 3, 3, 1)

      DO 4 M = 1,3

      DIFF_S(M) = ABS(USVS(L,M,N) - SNAUVR1(M))
      DIFF_P(M) = ABS(USVP(L,M,N) - PNAUVR1(M))
4     continue

C     Angle correction and obtaining proper reflected velocity
C     For Suction Side

      IF(ABS((SNAUVR1(1)) - (USVS(L,1,N))).LE. ERR .AND.
     1        ABS((SNAUVR1(2)) - (USVS(L,2,N))).LE. ERR .AND.
     1        ABS((SNAUVR1(3)) - (USVS(L,3,N))).LE. ERR) THEN
        phi_s = 2 * Gamma_s(L,N) -3.141359

      ELSE

        phi_s = 3 * 3.14159 - 2 * Gamma_s(L,N)

      ENDIF
```

```
            CALL TH_ZAXIS (phi_s, OBZ)
            CALL MATMUL (OBZ, SBUVR1, SNBUVR1, 3,3,1)
            CALL MATMUL(TEMP_S, SNBUVR1, SNAUVR1, 3, 3, 1)

C       For Pressure Side

        IF(ABS((PNAUVR1(1)) - (USVP(L,1,N))).LE. ERR .AND.
     1        ABS((PNAUVR1(2)) - (USVP(L,2,N))).LE. ERR .AND.
     1        ABS((PNAUVR1(3)) - (USVP(L,3,N))).LE. ERR) THEN

          phi_p = 2 * Gamma_p(L,N) -3.141359

        ELSE

          phi_p = 3 * 3.14159 - 2 * Gamma_p(L,N)

        ENDIF
            CALL TH_ZAXIS (phi_p, OBZ)
            CALL MATMUL (OBZ, PBUVR1, PNBUVR1, 3,3,1)
            CALL MATMUL(TEMP_P, PNBUVR1, PNAUVR1, 3, 3, 1)

        DO 5 M = 1,3

        UVR2_S(L,M,N) = BETA * SNAUVR1(M)
        UVR2_P(L,M,N) = BETA * PNAUVR1(M)

5       CONTINUE
1       CONTINUE
        RETURN
        END


**************************************************************************
C       This program calculates the flow fraction impinging on the blade
C       element.
        SUBROUTINE VEL_TRIAD( UVR1,D_CO_ORD,L, THETAP)
**************************************************************************
```

```
      DIMENSION UVR1(5,3), UX(3), UY(3) , UZ(3), Frame(4,4), Frameinv(4,4)
      DIMENSION ANZ_DAT(4,4), P_NZDAT(4,4), TEMP(4), TEMP_OUT(4),
     1  D_CO_ORD(6,4,16), TEMP1(4,4), TEMP2(4,4), PTEMP1(4,4),
     1  STEMP2(4,4), DAVS(5,8), DAVP(5,8), DDAVS(5,8), DDAVP(5,8)

      COMMON /FLOW AREA/ DAVS, DAVP, DDAVS, DDAVP

      ANZ_DAT(1,1) =  -0.03
      ANZ_DAT(1,2) =  -0.03
      ANZ_DAT(1,3) =  -0.03
      ANZ_DAT(1,4) =  -0.03

      ANZ_DAT(2,1) =  - tan(THETAP/2) * 0.5
      ANZ_DAT(2,2) =  + tan(THETAP/2) * 0.5
      ANZ_DAT(2,3) =  - tan(THETAP/2) * 0.61
      ANZ_DAT(2,4) =  + tan(THETAP/2) * 0.61

      ANZ_DAT(3,1) = 0.5
      ANZ_DAT(3,2) = 0.5
      ANZ_DAT(3,3) = .61
      ANZ_DAT(3,4) = .61

      ANZ_DAT(4,1) = 1
      ANZ_DAT(4,2) = 1
      ANZ_DAT(4,3) = 1
      ANZ_DAT(4,4) = 1


      OPEN (UNIT = 66, FILE = 'frame.dat', STATUS = 'NEW')
      OPEN (UNIT = 67, FILE = 'triad.dat', STATUS = 'NEW')

C     Eqn of Plane Normal to Rel. vel. vector : [Linear Algebra, Barnett,259]
C     X*UVR1(L,1) + Y*UVR1(L,2) + Z*UVR1(L,3) =
C                          X0.UVR1(L,1) + Y0*uvr1(L,2) + Z0*uvr1(L,3)

      X0 = -30E-3
      Y0 = ANZ_DAT(2,1)
      Z0 = 0.5
```

```
      Y = -7.5e-3
      Z = 0.50

      X = - ((Y-Y0) *UVR1(L,2) + (Z - Z0)*UVR1(L,3))/UVR1(L,1) + X0

      VECTL = SQRT((X - X0)**2 + (Y-Y0)**2 + (Z-Z0)**2)

      UX(1) = (X-X0)/VECTL
      UX(2) = (Y-Y0)/VECTL
      UX(3) = (Z-Z0)/VECTL

      UZ(1) = UVR1(L,1)
      UZ(2) = UVR1(L,2)
      UZ(3) = UVR1(L,3)

      CALL CROSS_PROD(UZ, UX, UY)
      CALL DOT_PROD(UX, UY, VAL)

      Do 1 M = 1,3

      Frame (M, 1) = UX(M)
      Frame (M, 2) = UY(M)
      Frame (M, 3) = UZ(M)
1     Frame (4, M) = 0

      Frame (1, 4) = X0
      Frame (2, 4) = Y0
      Frame (3, 4) = Z0
      Frame (4, 4) = 1

      CALL MINV( Frame, framinv,4,4)

      DO  2 M = 1, 4

      TEMP(1) = ANZ_DAT(1,M)
      TEMP(2) = ANZ_DAT(2,M)
      TEMP(3) = ANZ_DAT(3,M)
      TEMP(4) = ANZ_DAT(4,M)
```

```
      CALL MATMUL (framinv, TEMP, TEMP_OUT, 4, 4, 1)

      P_NZDAT (1,M) = TEMP_OUT(1)
      P_NZDAT (2,M) = TEMP_OUT(2)
      P_NZDAT (3,M) = TEMP_OUT(3)
      P_NZDAT (4,M) = TEMP_OUT(4)

2     CONTINUE

C     Calculation of projected surface of the pressure side

      DO 10 M = 1, 4
      TEMP1(M,2) = D_CO_ORD(L,M, 9)
      TEMP1(M,1) = D_CO_ORD(L,M, 1)
      TEMP1(M,4) = D_CO_ORD(L+1,M,9)
      TEMP1(M,3) = D_CO_ORD(L+1,M,1)
10    CONTINUE

      CALL MATMUL(framinv, TEMP1, PTEMP1, 4,4,4)

      OLD_AREA = DAVP(L,1)

      CALL CALC_AREA (P_NZDAT, PTEMP1,  OLD_AREA, AREA)

      DDAVP(L,1) = AREA

      DO 5 N = 2, 8
      DO 11 M = 1,4

      TEMP1(M,2) = D_CO_ORD(L,M,N-1)
      TEMP1(M,1) = D_CO_ORD(L,M, N)
      TEMP1(M,4) = D_CO_ORD(L+1,M, N-1)
      TEMP1(M,3) = D_CO_ORD(L+1,M, N)

11    CONTINUE

      CALL MATMUL(framinv, TEMP1, PTEMP1, 4,4,4)
```

```
      DO 16 J = 1, 4
16    CONTINUE
      OLD_AREA = DAVP(L,N)
      CALL CALC_AREA (P_NZDAT,PTEMP1, OLD_AREA, AREA)
      DDAVP(L,N) = AREA
5     CONTINUE

C     Calculation of projected surface of the suction side
      DO 6 N = 9, 15
      DO 12 M =1, 4
      TEMP2(M,2) = D_CO_ORD(L,M,N)
      TEMP2(M,1) = D_CO_ORD(L,M, N+1)
      TEMP2(M,4) = D_CO_ORD(L+1,M, N)
      TEMP2(M,3) = D_CO_ORD(L+1,M, N+1)
12    CONTINUE

      CALL MATMUL(framinv, TEMP2, STEMP2, 4,4,4)

      OLD_AREA = DAVS (L, N-8)

      CALL CALC_AREA (P_NZDAT,STEMP2, OLD_AREA, AREA)
      DDAVS(L, N-8) = AREA

6     CONTINUE

      DO 13 M = 1,4
      TEMP2(M,2) = D_CO_ORD(L,M,16)
      TEMP2(M,1) = D_CO_ORD(L,M,8)
      TEMP2(M,4) = D_CO_ORD(L+1,M,16)
      TEMP2(M,3) = D_CO_ORD(L+1,M,8)
13    CONTINUE

      CALL MATMUL(framinv, TEMP2, STEMP2, 4,4,4)
      OLD_AREA = DAVS (L, 8)

      CALL CALC_AREA (P_NZDAT,STEMP2, OLD_AREA, AREA)
      DDAVS(L,8) = AREA
```

```
      DO  3 M = 1, 4
      WRITE(66,*) (P_NZDAT(M,N), N = 1, 4)
      WRITE(67,*) (Framinv(M,N), N = 1, 4)
3     CONTINUE

      RETURN
      END


**********************************************************************
      SUBROUTINE MASS_FLOW (ABSVR1,DDAVS, DDAVP,L, QS, QP)
**********************************************************************
      DIMENSION DDAVS(5,8), DDAVP(5,8), QS(5,8), QP(5,8), ABSVR1(5)

*     RHO is the density of the flow [ Deepak Dhar, pg.101]
      RHO =  2.890

      DO 1 N = 1,8

      QP(L,N) = RHO * ABSVR1(L) * DDAVP(L,N)
      QS(L,N) = RHO * ABSVR1(L) * DDAVS(L,N)

      WRITE(31,*) QS(L,N)
      WRITE(32,*) QP(L,N)

1     CONTINUE

      RETURN
      END

**********************************************************************
      SUBROUTINE IMPULSE(UVR1, ABSVR1, QS, QP,L)
**********************************************************************

      DIMENSION QS(5,8), QP(5,8), ABSVR1(5), UVR1(5,3),
     1  UVR2_S(5,3,8), UVR2_P(5,3,8), S_IMP(5,3,8), P_IMP(5,3,8),
     1 A_SIMP(5,8), A_PIMP(5,8), TOT_SIMP(5,3), TOT_PIMP(5,3),
     1 AT_SIMP(5), AT_PIMP(5),TOT_IMP(5,3), TOT_ABSIMP(5),
```

```
     1  DCENTP(5,4,8), DCENTS(5,4,8), ALCENTP(5,3), ALCENTS(5,3),
     1  TEMPS(5,3), TEMPP(5,3)

        COMMON/IMP_FORCE/ S_IMP, P_IMP, A_SIMP, A_PIMP, TOT_SIMP,
     1  TOT_PIMP, AT_SIMP, AT_PIMP, TOT_IMP,TOT_ABSIMP
        COMMON/ UNIT_REL_VEL2/ UVR2_S, UVR2_P
        COMMON/ DYN / DCENTS, DCENTP
        COMMON/ CENTROID / ALCENTS, ALCENTP

        ALIMIT = .001
        DO 1, N = 1,8
        DO 2, M = 1,3

        S_IMP(L,M,N) = ABSVR1(L)*QS(L,N)* (UVR1(L,M) - UVR2_S(L,M,N))
     2  P_IMP(L,M,N) = ABSVR1(L)*QP(L,N)* (UVR1(L,M) - UVR2_P(L,M,N))

        A_SIMP(L,N)=SQRT(S_IMP(L,1,N)**2+S_IMP(L,2,N)**2+S_IMP(L,3,N)**2)
        A_PIMP(L,N)=SQRT(P_IMP(L,1,N)**2+P_IMP(L,2,N)**2+P_IMP(L,3,N)**2)

        WRITE(34, *) (S_IMP(L,M,N), M =1,3), A_SIMP(L,N)
        WRITE(35, *) (P_IMP(L,M,N), M =1,3), A_PIMP(L,N)

     1  CONTINUE

        DO 3, M = 1,3
        TOT_SIMP(L,M) = 0
        TOT_PIMP(L,M) = 0
        TEMPS(L,M) = 0
        TEMPP(L,M) = 0
        DO 4, N = 1,8

        TOT_SIMP(L,M) = TOT_SIMP(L,M) + S_IMP(L,M,N)
        TOT_PIMP(L,M) = TOT_PIMP(L,M) + P_IMP(L,M,N)

        TEMPS(L,M) = TEMPS(L,M) + S_IMP(L,M,N)*DCENTS(L,M,N)
     4  TEMPP(L,M) = TEMPP(L,M) + P_IMP(L,M,N)*DCENTP(L,M,N)

        TOT_IMP(L,M) = TOT_PIMP(L,M) - TOT_SIMP(L,M)
```

```
3       CONTINUE

        IF (ABS(TOT_PIMP(L,1)) .LE. ALIMIT .AND. ABS(TOT_PIMP(L,2)).LE. ALIMIT
     1  .AND. ABS(TOT_PIMP(L,3)) .LE. ALIMIT ) THEN

        ALCENTP(L,1) = 0
        ALCENTP(L,2) = 0
        ALCENTP(L,3) = 0

       ELSEIF(ABS(TOT_PIMP(L,3)) .LE. ALIMIT ) THEN
        ALCENTP(L,1) = TEMPP(L,1)/TOT_PIMP(L,1)
       ALCENTP(L,2) = TEMPP(L,2)/TOT_PIMP(L,2)
       ALCENTP(L,3) = DCENTP(L,3,5)
        ELSE

        ALCENTP(L,1) = TEMPP(L,1)/TOT_PIMP(L,1)
       ALCENTP(L,2) = TEMPP(L,2)/TOT_PIMP(L,2)
       ALCENTP(L,3) = TEMPP(L,3)/TOT_PIMP(L,3)
       ENDIF

        DO 10 M = 1,3
       IF(ABS(TOT_SIMP(L,M)) .LE. ALIMIT) THEN
       ALCENTS(L,M) = 0
       ELSE
       ALCENTS(L,M) = TEMPS(L,M)/TOT_SIMP(L,M)
       ENDIF
10      continue

        AT_SIMP(L)=SQRT(TOT_SIMP(L,1)**2+TOT_SIMP(L,2)**2+TOT_SIMP(L,3)**2)
        AT_PIMP(L)=SQRT(TOT_PIMP(L,1)**2+TOT_PIMP(L,2)**2+TOT_PIMP(L,3)**2)

        TOT_ABSIMP(L)=SQRT(TOT_IMP(L,1)**2+TOT_IMP(L,2)**2+TOT_IMP(L,3)**2)

        WRITE(36,*) (TOT_SIMP(L,M), M =1,3), AT_SIMP(L)
        WRITE(37,*) (TOT_PIMP(L,M), M =1,3), AT_PIMP(L)
        WRITE(38,*) (TOT_IMP(L,M), M =1,3), TOT_ABSIMP(L)
        WRITE(42,*) (ALCENTP(L,M), M =1,3)
        WRITE(43,*) (ALCENTS(L,M), M =1,3)
```

```
      RETURN
      END

*****************************************************************************
      SUBROUTINE CALC_AREA (P_NZDAT, TEMP, OLD_AREA, AREA)
*****************************************************************************
      DIMENSION P_NZDAT(4,4),TEMP(4,4),PNOZ(2,4),BLADE(2,4)

      DO 1 N = 1, 2
      DO 2 M = 1, 4

      PNOZ(N,M)   = P_NZDAT(N,M)
2     BLADE(N,M) = TEMP(N,M)
1     CONTINUE

C     CALCULATION OF DIFFERENTIAL AREA
C     NEGLECTING ELEMENTS LYING OUTSIDE THE DOMAIN OF THE NOZZLE

      IF (MIN(PNOZ(1,1),PNOZ(1,2),PNOZ(1,3),PNOZ(1,4)) .GE.
     1 MAX(BLADE(1,1), BLADE(1,2), BLADE(1,3), BLADE(1,4)).OR.
     1  MAX(PNOZ(1,1),PNOZ(1,2),PNOZ(1,3),PNOZ(1,4)) .LE.
     1 MIN(BLADE(1,1), BLADE(1,2), BLADE(1,3), BLADE(1,4)).OR.
     1  MIN(PNOZ(2,1), PNOZ(2,2), PNOZ(2,3), PNOZ(2,4)).GE.
     1 MAX(BLADE(2,1), BLADE(2,2), BLADE(2,3), BLADE(2,4)).OR.
     1  MAX(PNOZ(2,1), PNOZ(2,2), PNOZ(2,3), PNOZ(2,4)).LE.
     1 MIN(BLADE(2,1), BLADE(2,2), BLADE(2,3), BLADE(2,4))) THEN

      AREA = 0

      ELSE
      AREA = OLD_AREA

      ENDIF
      RETURN
      End

*****************************************************************************
```

```
      SUBROUTINE DYN_PARA (TORQUE, OMEGA, AZ, ANB,I)
*****************************************************************
      DIMENSION TORQUE(3),OMEGA(3),ANG_ACC(50)

C     ANB is the number of blades used on the wheel
      REAL OMEGA

      AIG = 0.049226*ANB + 24.6925

      ANG_ACC(I) = ANB*(TORQUE(1))/ AIG

      OMEGA(1) = 2*3.14592*OMEGA(1)/60

      OMEGA(1) = SQRT(OMEGA(1)**2 + 2*ANG_ACC(I) *ABS(AZ)*180/3.1345927)
     1 * 30 /3.14592

      OMEGA(2) = 0
      OMEGA(3) = 0

      WRITE(46,*) ANG_ACC(I)

      RETURN
      END

*****************************************************************
*     Subroutine To Calculate The Inverse Of a Matrix
      SUBROUTINE MINV(A, AINV, ND, N)
*****************************************************************

      DIMENSION A(ND, ND), AINV(ND, ND), C(50,50 )

*     N IS THE ACTUAL DIMENSION OF SQUARE MATRIX,
*     AND ND IS THE DIMENSION TO BE PUT IN DIMENSION STATEMENT OF THE
*     MAIN PROGRAM.

*     A IS THE ACTUAL MATRIX AND AINV IS THE INVERSE OF THE MATRIX A
*     C IS A TEMPORARY MATRIX WHICH IS COPIED FROM A
```

```
      REAL A, AINV, DET

      INTEGER ND, N, IPASS, IROW, ICOL

      DET = 1.0

      DO 1 I = 1,N
      DO 1 J = 1,N

      IF(I . EQ. J) THEN
            AINV(I,I) = 1.0
      ELSE
            AINV(I,J) = 0.0
      ENDIF

      C(I,J) = A(I,J)

1     CONTINUE

      DO 9 IPASS = 1,N
      IMX = IPASS
      DO 2 IROW = IPASS, N
      IF(ABS(C(IROW, IPASS)) .GT. ABS(C(IMX, IPASS))) THEN
      IMX = IROW
      ENDIF
2     CONTINUE

      IF(IMX. NE. IPASS) THEN
            DO 3 ICOL = 1,N

      TEMP = AINV(IPASS, ICOL)
      AINV(IPASS, ICOL) = AINV(IMX, ICOL)
      AINV(IMX, ICOL) = TEMP

      IF(ICOL .GE. IPASS) THEN

      TEMP = C(IPASS, ICOL)
      C(IPASS, ICOL) = C(IMX, ICOL)
```

```
      C(IMX, ICOL) = TEMP
      ENDIF
3     CONTINUE
            ENDIF

      PIVOT = C(IPASS, IPASS)

      DET = DET * PIVOT

      IF( DET .EQ. 0.0) THEN
            WRITE(*,10)
            STOP
                  ENDIF

      DO 6 ICOL = 1,N
      AINV(IPASS, ICOL) = AINV( IPASS, ICOL)/PIVOT
      IF(ICOL.GE.IPASS) THEN
      C(IPASS, ICOL) = C(IPASS, ICOL)/PIVOT
      ENDIF
6     CONTINUE

      DO 8 IROW = 1,N
      IF(IROW. NE. IPASS) THEN
      FACTOR = C(IROW, IPASS)
      ENDIF

      DO 7 ICOL = 1,N
      IF(IROW.NE.IPASS) THEN
      AINV(IROW, ICOL) = AINV(IROW, ICOL) - FACTOR*AINV(IPASS, ICOL)
      C(IROW, ICOL) = C(IROW, ICOL) - FACTOR*C(IPASS, ICOL)
      ENDIF
7     CONTINUE

8     CONTINUE

9     CONTINUE

      RETURN
```

```
10      FORMAT(5X,'----ERROR IN MINV---- THE MATRIX IS SINGULAR',/,
     1          10X, ' PROGRAM TERMINATED')

        END

*************************************************************************
        SUBROUTINE TH_XAXIS (theta, OBX, R,I)
*************************************************************************
        DIMENSION OBX(4,4), theta(50)

        REAL theta

       S = SIN(theta(I))
       C = COS(theta(I))

       OBX(1,1) = 1
       OBX(1,2) = 0
       OBX(1,3) = 0
       OBX(1,4) = 0
       OBX(2,1) = 0
       OBX(3,1) = 0
       OBX(4,1) = 0
       OBX(4,2) = 0
       OBX(4,3) = 0
       OBX(4,4) = 1

       OBX(2,2) = C
       OBX(2,3) = -S
       OBX(2,4) = 0
       OBX(3,2) = S
       OBX(3,3) = C
        OBX(3,4) = R

        RETURN
        END

*************************************************************************
        SUBROUTINE TH_ZAXIS (phi, OBZ)
```

```
**********************************************************************
      DIMENSION OBZ(3,3)

      S = SIN(phi)
      C = COS(phi)

      OBZ(1,1) = C
      OBZ(1,2) = -S
      OBZ(1,3) = 0

      OBZ(2,1) = S
      OBZ(2,2) = C
      OBZ(2,3) = 0

      OBZ(3,1) = 0
      OBZ(3,2) = 0
      OBZ(3,3) = 1

      RETURN
      END

C**********************************************************************
      SUBROUTINE MATMUL(E,F,G,ii,jj,kk)
C**********************************************************************
      DIMENSION E(ii,jj), F(jj, kk), G(ii,kk)

*     Matrix multiplication:  G(ii,kk) = E(ii,jj) * F(jj,kk)

      DO 30 L = 1,ii
      DO 30 N = 1,kk
      G(L,N) = 0
      DO 20 M = 1,jj

20    G(L,N) = G(L,N) + E(L,M) * F(M,N)
30    continue

      RETURN
      END
```

```
************************************************************************
*       DOT PRODUCT
        SUBROUTINE DOT_PROD(A,B,CD)
************************************************************************
        DIMENSION A(3),B(3),C(3)

        DO 1 J = 1,3
1       C(J) = A(J) * B(J)

        CD =  C(1) + C(2) + C(3)
        RETURN
        END

************************************************************************
*       CROSS PRODUCT
        SUBROUTINE CROSS_PROD(A, B, C)
************************************************************************
        DIMENSION A(3),B(3),C(3)

        C(1) = A(2)*B(3) - A(3)*B(2)
        C(2) = A(3)*B(1) - A(1)*B(3)
        C(3) = A(1)*B(2) - A(2)*B(1)

        RETURN
        END


************************************************************************
        SUBROUTINE UNIT_VECT(VECTA, UVECTA, ABSVECTA)
************************************************************************
        DIMENSION VECTA(3), UVECTA(3)

        REAL ABSVECTA

        ABSVECTA = SQRT( VECTA(1) **2 + VECTA(2)**2 + VECTA(3)**2)
        DO 1 II = 1,3
1       UVECTA(II) = VECTA(II) / ABSVECTA
```

```
RETURN
END
```

D.2 CALCULATION OF THE TOTAL FORCES, AND THE TORQUE ON THE ENTIRE BLADE-ROTOR ASSEMBLY SYSTEM

1. The forces obtained due to the nozzle excitations on a single blade due to the combined mass moment of inertia of the whole system was fed in as input. The corresponding va'ues of the point of application of the forces were also fed into this program.

2. The program resolves the forces on the twelve such blades, and calculates the resultant forces, and the torques on the rotor system.

The program is listed in D.2.1

D.2.1

```
C     PROGRAM TO CALCULATE THE TOTAL FORCES, AND TORQUES DUE TO
      SIMULTANEOUS EXCITATIONS ON ALL THE BLADES

      DIMENSION F(3), R(3), DT(3), DF(3), DR(3), FTOT(3), TTOT(3),
     1 OBX(3,3)
      OPEN(UNIT = 1, FILE = 'timp.dat', STATUS = 'OLD')
      OPEN(UNIT = 2, FILE = 'pappl.dat', STATUS = 'OLD')
      OPEN(UNIT = 3, FILE = 'ftot.dat', STATUS = 'NEW')
      OPEN(UNIT = 4, FILE = 'ttot.dat', STATUS = 'NEW')
      WRITE(*,*) ' GIVE  IT '
      READ (*,*) IT
      AINC = 30
      DO 1 I = 1,IT
      READ(1,*) (F(M), M = 1, 3)
      READ(2,*) (R(M), M = 1, 3)
      FTOT(1) = 0
      FTOT(2) = 0
      FTOT(3) = 0
      TTOT(1) = 0
      TTOT(2) = 0
      TTOT(3) = 0
      TH = 0
      AAINC = 0

      DO 2 J = 1, 12
      TH = TH + AAINC
      AAINC = AINC * 3.14159/180
      CALL TH_XAXIS (TH, OBX)
      CALL MATMUL (OBX, F, DF, 3, 3, 1)
      FTOT (1) = FTOT(1) + DF(1)
      FTOT (2) = FTOT(2) + DF(2)
      FTOT (3) = FTOT(3) + DF(3)
      write(8,*)( DF(M), M=1,3)
      CALL MATMUL(OBX, R, DR, 3, 3, 1)
      CALL CROSS_PROD(DF, DR, DT)
      TTOT(1) = TTOT(1) + DT(1)
```

```
      TTOT(2) = TTOT(2) + DT(2)
      TTOT(3) = TTOT(3) + DT(3)
2     CONTINUE

      WRITE(3,*) (FTOT(M) , M = 1, 3)
      WRITE(4,*) (TTOT(M) , M = 1, 3)
1     CONTINUE
      CLOSE (1)
      CLOSE (2)
      CLOSE (3)
      CLOSE (4)
      STOP
      END

*****************************************************************
      SUBROUTINE TH_XAXIS (theta, OBX)
*****************************************************************
      DIMENSION OBX(3,3)

      REAL theta

     S = SIN(theta)
     C = COS(theta)

     OBX(1,1) = 1
     OBX(1,2) = 0
     OBX(1,3) = 0
     OBX(2,1) = 0
     OBX(3,1) = 0

     OBX(2,2) = C
     OBX(2,3) = -S
     OBX(3,2) = S
     OBX(3,3) = C

      RETURN
      END
```

```
C*************************************************************************
      SUBROUTINE MATMUL(E,F,G,ii,jj,kk)
C*************************************************************************
      DIMENSION E(ii,jj), F(jj, kk), G(ii,kk)
C       Matrix multiplication:  G(ii,kk) = E(ii,jj) * F(jj,kk)
      DO 30 L = 1,ii
      DO 30 N = 1,kk
      G(L,N) = 0
      DO 20 M = 1,jj
20     G(L,N) = G(L,N) + E(L,M) * F(M,N)
30     continue
      RETURN
      END


**************************************************************************
C       CROSS PRODUCT
      SUBROUTINE CROSS_PROD(A, B, C)
**************************************************************************
      DIMENSION A(3),B(3),C(3)
      C(1) = A(2)*B(3) - A(3)*B(2)
      C(2) = A(3)*B(1) - A(1)*B(3)
      C(3) = A(1)*B(2) - A(2)*B(1)
      RETURN
      END
```